Ferdowsi University of Mashhad

Print ISSN 2008-9147
Online ISSN 2717-3364
Numbers: 26

JCMR

Journal of Cell and Molecular Research

Volume 13, Number 2, (Winter) 2022

بسم الله الرحمن الرحیم

Issuance License No. 124/902-27.05.2008 from Ministry of Culture and Islamic Guidance
Scientific Research Issuance License No. 161675 from the Ministry of Science, Research and Technology, Iran

Journal of Cell and Molecular Research (JCMR)

Volume 13, Number 2, (Winter) 2022

JCMR Office: Department of Biology, Faculty of Sciences, Ferdowsi University of Mashhad, Mashhad, Iran.
Postal Code: 9177948953
P.O. Box: 917751436
Tel: +98-513-8804063/+98-9156996326
Fax: +98-513-8795162
E-mail: jcmr@um.ac.ir
Online Submission: https://jcmr.um.ac.ir

Table of Contents

Research Article

The Effect of Cartilage and Bacteria-derived Glycoproteins as a Biological Dressing on Wound Healing

Fatemeh Naseri[1], Gholamreza Hashemitabar[1], Nasser Mahdavi Shahri[2], Hossein Nourani[3], Amin Tavassoli[1]

[1]*Division of Biotechnology, Faculty of Veterinary Medicine, Ferdowsi University of Mashhad, Mashhad, Iran*
[2]*Department of Biology, Faculty of Science, Ferdowsi University of Mashhad, Mashhad, Iran*
[3]*Department of Pathobiology, Faculty of Veterinary Medicine, Ferdowsi University of Mashhad, Mashhad, Iran*

Received 25 September 2021 Accepted 06 October 2021

Abstract

Immediate intervention with minimal side effects is the most significant factor in the enhancement of wound healing. However, a majority of drugs used for this purpose are chemical-based containing various compounds, such as sulfite, which sometimes causes allergic reactions in a number of patients, or anti-inflammatory agents that cause elevated blood sugar and weight gain. Hence, many researchers look for natural compounds, such as glycoproteins, not only to reduce the side effects but also to improve the speed of healing. In this study, we have created a natural biological dressing using the combination of extracellular matrix (ECM) derived from articular cartilage and DH5α bacterial ghost (BG). Both articular cartilage and BG contain high amounts of collagen and glycoproteins, and proteoglycans, respectively. The experimental wound on the rabbit pinna was treated by the biological dressing. Then microbial, scanning electron microscopy and microscopic analyses measured the wound healing parameters, including the number of fibroblast cells, the collagen contents, percentage of wound closure, and the number of colonies. The results confirmed ECM (OC), BG (OG) and their mixture (OGC) groups have better effects than control groups. Histological parameters, such as number of fibroblast cells and the amount of collagen fibers, represented a greater degree of wound healing in OGC group compared with OC, OG, and control groups. Our findings proved that ECM and bacterial ghost effectively increased the rate of wound healing. The mixture of ECM and BG provides a biological dressing that could be used in wound repair in the future.

***Keywords*:** Decellularization; Biological dressing; Bovine articular cartilage; Extracellular matrix; Bacterial ghost

Introduction

Chronic wounds are considered as a health burden and may cause physical disability and infectious diseases; so, rapid treatment of injuries with minimum adverse effects is urgent (Caporusso et al. 2019). Failure in wound healing can lead to microbial infection, increased morbidity, and imposed financial hardship, and emotional stress on health systems (Brigham and McLoughlin 1996). However, our knowledge about the wound healing process has markedly advanced in recent years. Wound healing is a critical process for maintaining tissue homeostasis leading to restitution of tissue integrity and barrier function (Hackam and Ford 2002). The healing process reflects the interactions among different cell types, growth factors, cytokines, blood components, and the ECM. The process of wound healing is complex in mammals, including three interrelated phases, namely inflammation, proliferation, and tissue remodeling (Greaves et al. 2013).

The first phase is inflammation, which begins shortly after the injury. In this phase, macrophages and neutrophils are recruited to protect the site of injury against invasive microbes. Also, capillaries, blood platelets, and active cytokines are increased. In the proliferation phase that occurs 1 to 3 weeks after a wound in humans, angiogenesis is a hallmark characterized by the increased proliferation of fibroblasts and re-epithelialization. The third phase is tissue remodeling, in which fibroblasts produce collagen by stimulating macrophages. At this phase, the synthesis and accumulation of collagen are propagated, and other cellular matrix proteins improve the strength and integrity of the damaged area (Broughton et al. 2006; Gantwerker and Hom 2011).

Due to the increased prevalence of wounds and its impact on high-cost treatment, the need for effective, safe, and affordable wound healing promoters would be needed.

*Corresponding author's e-mail address: *hashemit@um.ac.ir*

Alternative or complementary medicine has been extensively used for wound healing. From the past to the present, natural compounds, such as plant-derived materials and naturally occurring compounds such as honey, as an alternative and complementary medicine, are used for wound healing (Agyare et al. 2019). Although biological wound dressings, including natural-derived substances, have long been employed for wound healing, clinical trials are still in their early stages. These products have many advantages, such as possessing antioxidant, anti-inflammatory, antimicrobial agents, as well as enhancers for re-epithelialization and collagen synthesis (Ibrahim et al. 2018).

Cell-secreted compounds, including proteins and glycoproteins, play a positive role in wound healing. In multicellular organisms, the extracellular matrix (ECM) is considered a rich source of these compounds. ECM is composed of glycosaminoglycans (GAGs), proteoglycans (PGs), and collagens (Ghatak et al. 2015). ECM plays a physical role in tissue maintenance and acts as scaffold support for tissues. It can also control cellular signaling and behavior, such as proliferation, differentiation, and migration during the complex wound healing process. The surface macromolecules of bacteria are another source of glycoproteins. These compositions can be obtained using the bacterial ghost technique (Paukner et al. 2006; Kawano et al. 2021).

This study aims to assay the wound healing potential of biological dressing that was composed of ECM derived from decellularized bovine articular cartilage and bacterial ghost in the form of ointment in wound healing. In this study, wound healing parameters showed that compounds obtained from ECM and bacterial ghost could expedite the healing process in an experimental wound created on the rabbit pinna.

Materials and Methods

Isolation of ECM derived from Decellularized Cartilage

The entire experimental procedures carried out were approved by the Animal Research Ethics Committee of the Ferdowsi University of Mashhad (ethics code: IR.UM.REC.1398.122). In this experimental study, bovine articular cartilage was harvested from the sacrificed animals immediately after slaughtering. The articular cartilage was stored at -4°C before decellularization. Frozen samples were then thawed at room temperature and washed with sterile phosphate-buffered saline (PBS); these freeze-thaw cycles were repeated five times. In the next step, samples were then incubated with 0.25% trypsin at 37°C for 1 hour. After that, specimens were rinsed in 5% SDS and 2.5% Triton x-100 (Merck, Germany) solutions for 3 hours, followed by gentle agitation to achieve maximum elimination of cell debris while maintaining the ECM compositions. Eventually, in order to remove residual detergents from ECM derived from articular cartilage, samples were washed with sterile distilled water, 70% ethanol, and sterile PBS in a shaker incubator.

Histological Analyses

Specimens were fixed in Bouin's solution, dehydrated through a graded series of ethanol, embedded in paraffin (Lab-O-Wax, Italy), cross-sectioned at a thickness of 7 µm by a microtome apparatus (Leits, Austria), deparaffinized by xylene, rehydrated, and finally stained with hematoxylin and eosin (H&E) to determine the construct cellularity. Toluidine blue (Merck, Darmstadt, Germany) staining was performed to qualitatively measure the amount of GAGs in ECM derived from decellularized cartilage. The sections were observed under a polarizing microscope (Olympus, IX70, Japan) stained with Picrosirius red (Merck, Darmstadt, Germany) served as a specific stain to identify the collagen structure. The DNA content of ECM derived from decellularized cartilage was determined by a fluorescent dye, 4, 6 diamidino-2-phenylindole (DAPI; Sigma-Aldrich, Taufkirchen, Germany) (Kapuscinski 1995).

Wound Microbiology

Wound microbiology was conducted to analyze the effect of biological dressing on wound bacterial burden. Samples were obtained from the wound region with a swab on days 0, 3, 7, 10, 15, and 21 after the creation of injury. Afterward, samples were cultured on the agar medium and incubated at 37 °C for 24 hours. Finally, the resulting colonies were counted (Park et al. 2008).

Generation of Bacterial Ghost

The pmET32c plasmid was previously generated at our laboratory (Soleymani et al. 2020). The *E. coli* DH5α (was generously donated by Research Institute of Biotechnology, Ferdowsi University of Mashhad, Mashhad, Iran) was transfected by the pmET32c plasmid, and bacterial ghosts were prepared as previously described. Briefly, to generate the *E. coli* DH5α bacterial ghost, the expression of E-lysis and staphylococcal nuclease (SNUC) genes were induced by the thermal inactivation of λ repressor at 42 °C and the addition

of isopropyl β- d-1-thiogalactopyranoside (IPTG) to the culture medium, respectively. For the production of BG, a single transfected colony was added to the SOB^{++} medium and cultured overnight in a shaker incubator at 28 °C temperature. After that, 1 ml of the culture medium was used to inoculate 200 mL of SOB^{++} medium and then incubated at 28 °C with shaking (150 rpm) to achieve an optical density at 600 nm (OD_{600nm}). IPTG (5 mM) was added to the culture medium (OD_{600nm} of 0.2–0.3) to induce SNUC expression. After 45 min, with an increase in the temperature from 28 to 42 °C, the expression of E-lysis was induced. The culture was monitored for 4 hours at a wavelength of 600 nm. Finally, the *E. coli* DH5α bacterial ghost was centrifuged, washed three times with 0.9% NaCl solution, and finally stored at 80 °C for subsequent analyses.

Preparation of Biological Dressings

The ointment base consisted of two oil and aqueous phases were prepared as previously described by Mashreghi et al (Mashreghi et al. 2013). Briefly, the biological dressing containing bacterial ghost and ECM derived from cartilage was prepared by pulverizing the ECM using a Mixer Mill device and lyophilizing the bacterial ghost. Next, the resulting mixture was added to the ointment base and mixed.

Animal Handling, Induction of Experimental Wound Model, and Histological Evaluations

In this study, 12 male New Zealand white rabbits with an approximate weight of 2,500 gr and an age range of 2–3 months were purchased from the Razi Institute of Mashhad, Iran. We created an experimental wound on the rabbit pinna using a punching apparatus. For this purpose, the hairs of the ear pinna were shaved and sterilized with ethanol (70%). Afterward, by means of lidocaine spray, the entire surface of the ears was locally anesthetized. After that, 3 holes with a diameter of 2 mm were created in each pinna at the medial region of the ears, located between peripheral veins and central arteries. The ointment base was applied for the O group, a mixture of BG and the ointment base for the OG group, a mixture of ECM and the ointment base for the OC group, a mixture of ECM and bacterial ghost, as well as the ointment base for the OCG group. A swab saturated with topical ointment was rubbed on each wound, while the control group (C) was left untreated.

Wound closure was analyzed in each group using images taken by a digital camera. Then, to evaluate the wound healing parameters, sampling was performed at 0, 3, 7, 10, 15, and 21 days post-injury (Schallberger et al. 2008). The animals were sacrificed, and the wound region and surrounded parts were isolated with a scalpel. The obtained specimens were fixed in Bouin's solution. The number of fibroblast cells was determined by H&E staining. For each wound region, four sections were specified, and three regions in each section were selected to be visualized at 100X magnitude. Masson's trichrome staining was utilized to detect collagen fibers, resulting in blue-colored fibers that contain collagen. The stained regions are ranked based on the color intensity as follows 1: very rare, 2: rarely, 3: moderate, 4: very, and 5: very much.

Scanning Electron Microscopy (SEM)

In order to prepare DH5α BG for electron microscopy, samples were fixed in 2.5% glutaraldehyde (TAAB Laboratories, UK) for 24 h, followed by three 15-min washing steps in 0.1 M sodium cacodylate buffer (pH 7.4, TAAB Laboratories, UK). Next, samples were treated with 1% osmium tetroxide (TAAB Laboratories, UK) for 1 h, rinsed again in 0.1 M sodium cacodylate buffer, and dehydrated through a graded series of ethanol. Finally, samples were fixed on metal stubs coated with gold-palladium by the sputtering method (Sputter coater, SC7620, East Sussex, UK). Consequently, specimens were observed using SEM (LEO 1450VP, Germany).

Statistical Analysis

The variables included the percentage of wound closure, the number of colonies, the number of fibroblast cells, the collagen contents, and the number of colonies. Statistical analyses were performed using GraphPad Prism software (8.0) . Kruskal–Wallis test followed by Dunn's multiple comparisons analysis was used to find statistically significant differences. Differences were considered significant when the p value was ≤ 0.05. The significant differences between the C group and the other groups are shown as $^{****}p \leq 0.0001$, $^{***}p \leq 0.001$, $^{**}p \leq 0.01$ and $^{*}p \leq 0.05$.

Results

Histological Examination of ECM derived from Bovine Articular Cartilage

Articular cartilage was decellularized with enzymatic and physicochemical experiments using 1) 0.25% trypsin, 2) snap freeze-thaw, and 3) treatment with detergents.

As shown in Figure 1, decellularized cartilage is devoid of chondrocytes compared with naïve cartilage. Also, toluidine blue and Picrosirius-red

staining methods demonstrated GAGs. Also, collagen-rich contents remained intact in the ECM. Therefore, the nuclei of cartilage stained with DAPI are visualized as bright spots and indicate the presence of chondrocytes in the cartilage matrix (Figure 1). However, the image of decellularized cartilage exhibits the matrix completely dark due to the absence of any nucleus.

BG Generation

In order to assess the generation of BG, the samples were analyzed by SEM (Figure 2). The surface morphological structure of *E. coli* bacterial ghost indicates the number of pores, implying the efficiency of the lysis process.

ECM derived from bovine articular cartilage as well as BG were ground and mixed with the ointment base. The resulting mixture was utilized as a biological dressing to alleviate the pinna in a rabbit model (Figure 3).

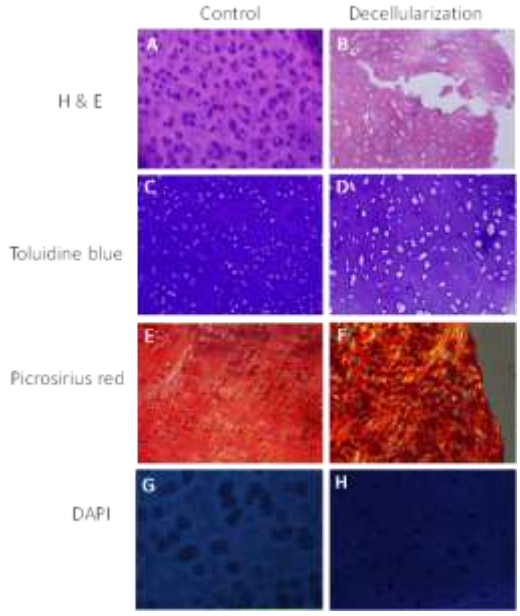

Figure 1. Control and decellularized articular cartilage samples. A & B) H&E staining demonstrated that treatment with trypsin and physicochemical methods led to the complete removal of chondrocytes. Toluidine blue and Picrosirius Red staining methods displayed the intactness of GAGs and collagen contents (C-F). Bovine articular cartilage is stained with DAPI before and after the decellularization process (G and H) (100X magnification).

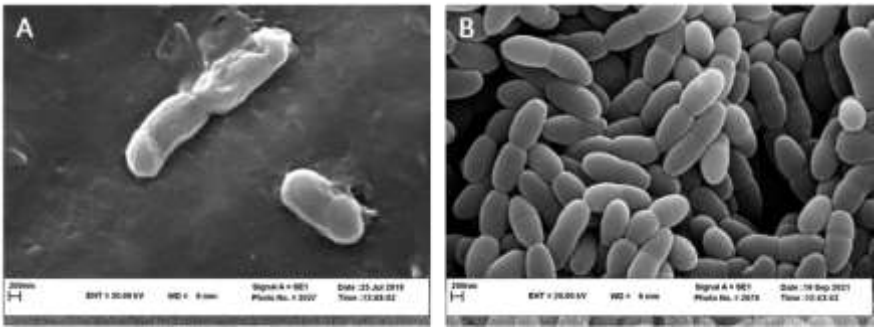

Figure 2. SEM of bacterial ghost. A) *E. coli* bacteria. B) After BG production process, the cytoplasmic contents are released through the pores.

Figure 3. Preparation of biological depressing; A) Decellularized bovine articular cartilage, B) ECM derived from bovine articular cartilage, C) Biological dressing that contains ECM derived from bovine articular cartilage and BG mixed with the ointment base.

Wound closure

In order to evaluate the wound healing ability of biological depressing, the percentage of wound closure was measured on different days through monitoring the wound region and comparison with control wound size. On day 3, there was a significant difference in the percentage of wound closure when OG, OC, and OGC groups were compared with the control groups (C and O). However, on days 7 and 10 post-injury, the differences between the treatment and control groups were not statistically significant. On day 15 post-injury, the differences in the percentage of wound closure were significantly increased in the OGC compared with other groups. On day 21 post-injury, the process of wound closure was completed in OGC in comparison to other groups (Figure. 4). On this day, OG and OC groups had higher degrees of wound closure than control groups. Also, figure 5 displays the extent of closure of the rabbit pinna affected by the OGC treatment group (Figure 5).

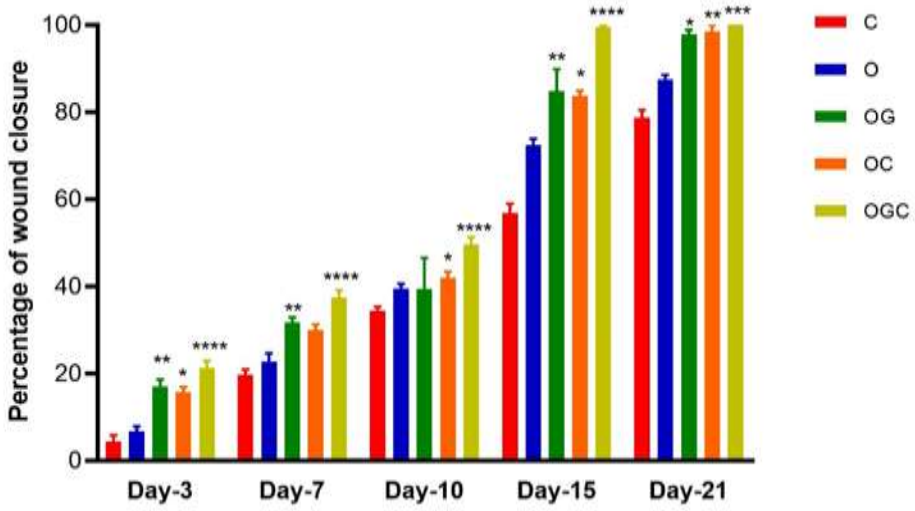

Figure 4. Wound closure; the wound healing process was more pronounced in treatment groups than control groups, C: control group without any treatment, O: groups receiving only the ointment base, OG: the ointment base with bacterial ghost, OC: the ointment base mixed with ECM, OGC: The ointment base mixed with bacterial ghost and ECM. ****$p \leq 0.0001$, ***$p \leq 0.001$, **$p \leq 0.01$ and *$p \leq 0.05$ compared with control group.

Figure 5. Representative pictures of the wound closure on different days on the OGC group.

Microbiology Test

Evaluation of microbial contamination at the site of injury demonstrated that treatments caused a remarkable decrease in bacterial load. The number of colonies in the treatment groups was significantly decreased compared with control groups (Figure 6).

Number of Fibroblast Cells

An increase in the number of fibroblast cells indicates marked acceleration of wound healing. On day 3, the frequency of fibroblast cells was remarkably higher in treatment groups, especially in the OGC group, compared with control groups (Figure 7). On days 7 and 10 post-injury, a significant difference was found in the number of fibroblast cells between treatment and control groups.

Collagen Content

The analysis of collagen content was performed using the measurement of the intensity of blue-colored fibers. As shown in Figure 8, on days 3-10 post-injury, the collagen content was increased in the OGC group compared with other groups, while on day 15, the collagen fibers in the OGC group were comparable with the amounts of collagen fiber seen in normal rabbits (Figure 8). Also, on day 21 post-injury, the collagen content of the OC group was the same as the OGC group.

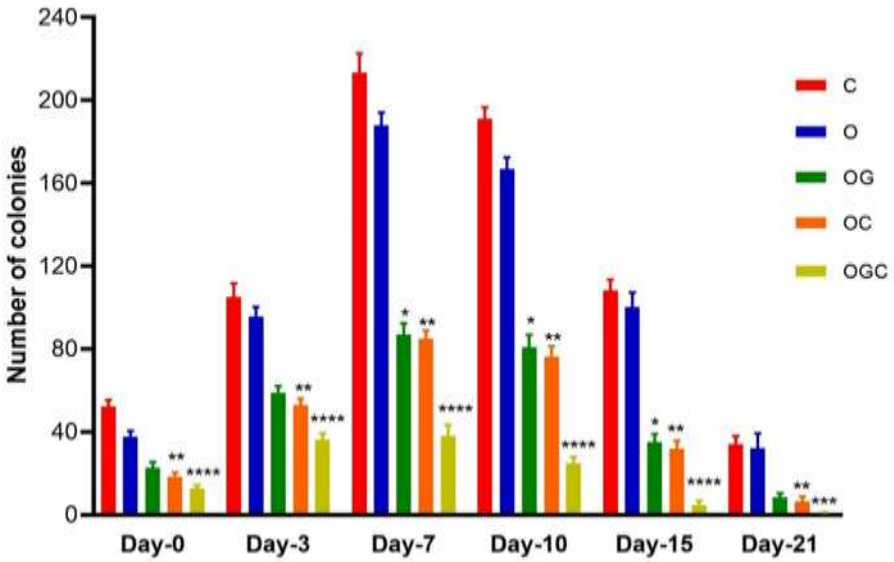

Figure 6. Microbiology of wound healing; on all days, the number of colonies in the treatment groups is decreased compared with control groups. ****$p \leq 0.0001$, ***$p \leq 0.001$, **$p \leq 0.01$ and *$p \leq 0.05$ compared with control group.

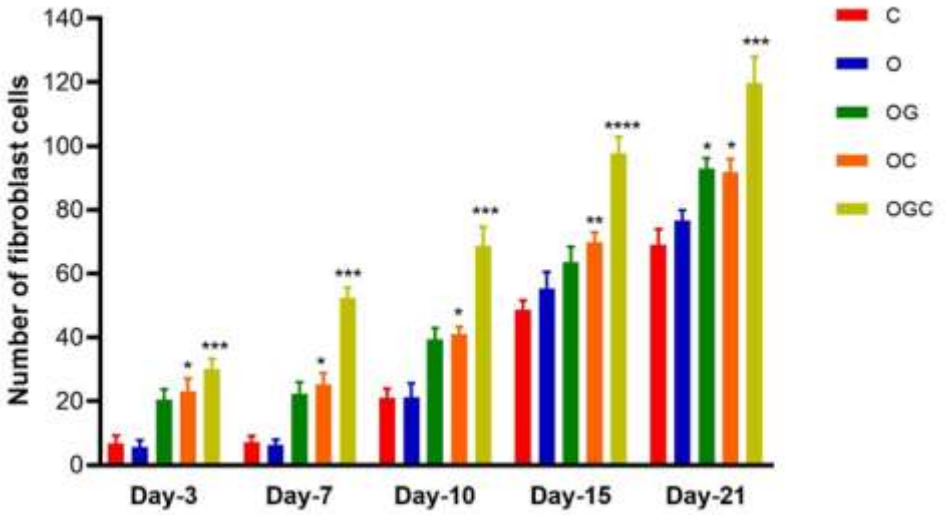

Figure 7. The number of fibroblast cells in control and treatment samples; a significant increase was found in the number of fibroblast cells in treatment groups compared with control groups when the treatment course was ended. ****$p \leq 0.0001$, ***$p \leq 0.001$, **$p \leq 0.01$ and *$p \leq 0.05$ compared with control group.

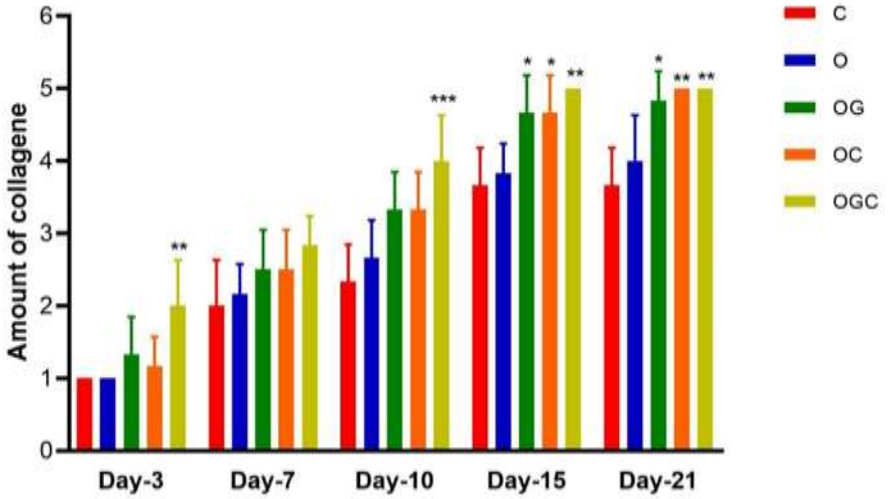

Figure 8. The collagen content; the amount of collagen is substantially higher in treatment groups compared with control groups. ****$p \leq 0.0001$, ***$p \leq 0.001$, **$p \leq 0.01$ and *$p \leq 0.05$ compared with control group.

Discussion

The skin is the first and most crucial defense barrier in mammals; therefore, any damage to this organ must immediately be healed and repaired. Hence, seeking effective treatments with minimum treatment course and side effects would be ideal for the treatment of wounds (Broughton et al. 2006; Velnar et al. 2009). Any rupture in the integrity of skin layers or subcutaneous tissue is called a wound that might be caused by physical or chemical factors. Despite significant advances in wound healing, studies continue to find effective wound healing methods with minimum complications. Therefore, numerous investigations have been conducted on the impact of drugs and wound dressings on accelerating the healing process, such as using calcium, copper, zinc ions, as well as physical factors, such as ultraviolet radiation, electrical stimulation, and laser waves (Reddy et al. 2013; Stanford et al. 1969; Barnett and Varley 1987; Kumar and Jagetia 1995; Brown et al. 1988). The effect of some chemicals, including hydrocortisone, vitamins, phenytoin ointment, saline (Bitar 1997), as well as natural compounds, such as herbs and honey (Al-Waili et al. 2011), was also studied in the literature.

In this study, for the first time, the impact of ECM and BG as novel natural-derived materials on wound healing was assessed. This research aimed to determine whether these natural-derived materials have positive roles in the mitigation of injuries and could be used as a novel biological dressing in the clinic.

Previous studies highlighted the importance of ECM in wound healing (Ghatak et al. 2015). ECM could be obtained from natural tissues. Different types of ECM derived from various tissues have been used as biological scaffolds, such as skin (Brouki Milan et al. 2020), skeletal muscles (Cartmell and Dunn 2000), tendons (Piccoli et al. 2018), small intestinal submucosa (Ji et al. 2019), and liver (Shirakigawa and Ijima 2018). Due to the high amount of GAGs and collagen in the ECM of articular cartilage, bovine articular cartilage was prepared using the decellularization method. Our results have shown that the combination of enzymatic with physicochemical treatments shows a synergistic effect on the complete removal of cellular components as well as the perseveration of ECM contents (Figure 1).

On the other hand, one of the important sources of natural glycoproteins is bacterial cell walls. Bacterial glycoproteins are expressed at the bacterial cell surface and provide natural substances for clinical applications. These compounds play a significant role in interacting with pathogens and identifying their glycan structures (Haidinger et al. 2003). Bacterial ghost contains a variety of surface compounds, such as glycoproteins. The preservation of the natural structure of cell wall components and lack of any genomic or cytoplasmic contents are among exemplary properties of bacterial ghost (Lubitz et al. 2009). In the present study, bacterial ghost was created using the transfection of *E.coli* with the pmET32b plasmid, as previously established at our laboratory (Soleymani et al. 2020). Our findings were confirmed by SEM analysis in which pores in bacterial cell walls were observable (Figure 2, B). After preparing the ECM and bacterial ghost and the mixture of the two compounds with the ointment base (Figure 3), the effect of ECM and bacterial ghost on wound healing of injured rabbit pinna as an experimental model was evaluated at different day intervals.

Wound closure depends on the ability of the type of tissue, animal, and the size of the injury. In the current research, a New Zealand white rabbit was used because the ear pinna of the rabbit wound is an accepted model for the study of wound healing. The pinna tissue is mainly composed of blastema tissue, which is responsible for its capacity in tissue repair (Hashemzadeh et al. 2015).

Due to the microbial load and the initial inflammation on days 3 and 7 post the injury, we did not see a proper wound healing. On the other, our findings showed that the size of the wound was remarkably decreased in the OGC group compared with other groups. On day 15 post-injury, the wound closure was completed in the OGC group, while this process lasted 21 days in the OC group (Figures 4 & 5). Therefore, it seems that the mixture of ECM and bacterial ghost was more effective than other formulations in wound closure. Also, a decrease in bacterial load was inversely correlated with wound closure in treatment groups; in a way, the lowest bacterial load was detected in treatment groups with the highest wound closure (Figure 6).

Fibroblast cells are the most competent cells in wound repair and are considered the main supplier of collagen. The number of fibroblast cells in treatment groups was significantly higher than in control groups (Figure 7). This phenomenon might be due to the presence of PGs and collagen, which possess chemotactic effects on cell polarity and migration. An increase in the number of fibroblast cells led to elevated amounts of collagen in tissues. Collagen is responsible for the tendency of endothelial cells and their physical force to the damaged region. Therefore, as expected, the collagen content was remarkably higher than in the control groups (Figure 8).

Regarding the high amounts of GAGs and collagen in ECM derived from cartilage as well as high amounts of glycoproteins in bacterial ghost, the use of both compounds for wound healing would be beneficial for patients with chronic wounds. Further studies are warranted to delicately unravel the in-vivo effects of biological dressings on wounds in mammals.

Ethics Approval and Consent to Participate

The ethical approval for this study was issued by the Committee on Research Ethics of Ferdowsi University of Mashhad, based on the Ethical Guidelines of Research from the Ministry of Science, Research and Technology of Iran, and following the Declaration of Helsinki.

Consent for Publication

No identifying patient information is included in this report.

Availability of Data and Material

The data used and/or analyzed during the current study are available from the corresponding author on request.

Competing Interests
The authors declare that they have no conflict of interest.

Funding
This study was financially supported by Ferdowsi University of Mashhad.

Authors' contributions
Conceived and designed the experiments: FN, GRH and NMS. Performed the experiments: FN. Analyzed the data: FN, GRH, AT, HN and NMS. Supervised the experiments: GRH and NMS. Wrote the manuscript: FN, GRH and AT. All authors read and approved the final manuscript.

Acknowledgments
Authors would like to thank Dr. Soleymani for technical assistance and her help throughout the project.

References

Agyare, C., A. J. Akindele, and V. Steenkamp. 2019. Natural Products and/or Isolated Compounds on Wound Healing. *Evid Based Complement Alternat Med* 2019:4594965.

Al-Waili, N., K. Salom, and A. A. Al-Ghamdi. 2011. Honey for wound healing, ulcers, and burns; data supporting its use in clinical practice. *ScientificWorldJournal* 11:766-787.

Barnett, S. E., and S. J. Varley. 1987. The effects of calcium alginate on wound healing. *Ann R Coll Surg Engl* 69 (4):153-155.

Bitar, M. S. 1997. Insulin-like growth factor-1 reverses diabetes-induced wound healing impairment in rats. *Horm Metab Res* 29 (8):383-386.

Brigham, P. A., and E. McLoughlin. 1996. Burn incidence and medical care use in the United States: estimates, trends, and data sources. *J Burn Care Rehabil* 17 (2):95-107.

Broughton, G., 2nd, J. E. Janis, and C. E. Attinger. 2006. Wound healing: an overview. *Plast Reconstr Surg* 117 (7 Suppl):1e-S-32e-S.

Brouki Milan, P., A. Pazouki, M. T. Joghataei, M. Mozafari, N. Amini, S. Kargozar, M. Amoupour, N. Latifi, and A. Samadikuchaksaraei. 2020. Decellularization and preservation of human skin: A platform for tissue engineering and reconstructive surgery. *Methods* 171:62-67.

Brown, M., M. K. McDonnell, and D. N. Menton. 1988. Electrical stimulation effects on cutaneous wound healing in rabbits. A follow-up study. *Phys Ther* 68 (6):955-960.

Caporusso, J., R. Abdo, J. Karr, M. Smith, and A. Anaim. 2019. Clinical experience using a dehydrated amnion/chorion membrane construct for the management of wounds. *Wounds* 31 (4 Suppl):S19-s27.

Cartmell, J. S., and M. G. Dunn. 2000. Effect of chemical treatments on tendon cellularity and mechanical properties. *J Biomed Mater Res* 49 (1):134-140.

Gantwerker, E. A., and D. B. Hom. 2011. Skin: histology and physiology of wound healing. *Facial Plast Surg Clin North Am* 19 (3):441-453.

Ghatak, S., E. V. Maytin, J. A. Mack, V. C. Hascall, I. Atanelishvili, R. Moreno Rodriguez, R. R. Markwald, and S. Misra. 2015. Roles of Proteoglycans and Glycosaminoglycans in Wound Healing and Fibrosis. *Int J Cell Biol* 2015:834893.

Greaves, N. S., K. J. Ashcroft, M. Baguneid, and A. Bayat. 2013. Current understanding of molecular and cellular mechanisms in fibroplasia and angiogenesis during acute wound healing. *J Dermatol Sci* 72 (3):206-217.

Hackam, D. J., and H. R. Ford. 2002. Cellular, biochemical, and clinical aspects of wound healing. *Surg Infect (Larchmt)* 3 Suppl 1:S23-35.

Haidinger, W., U. B. Mayr, M. P. Szostak, S. Resch, and W. Lubitz. 2003. Escherichia coli ghost production by expression of lysis gene E and Staphylococcal nuclease. *Appl Environ Microbiol* 69 (10):6106-6113.

Hashemzadeh, M. R., N. Mahdavi-Shahri, A. R. Bahrami, M. Kheirabadi, F. Naseri, and M. Atighi. 2015. Use of an in vitro model in tissue engineering to study wound repair and differentiation of blastema tissue from rabbit pinna. *In Vitro Cell Dev Biol Anim* 51 (7):680-689.

Ibrahim, N., S. K. Wong, I. N. Mohamed, N. Mohamed, K. Y. Chin, S. Ima-Nirwana, and A. N. Shuid. 2018. Wound Healing Properties of Selected Natural Products. *Int J Environ Res Public Health* 15 (11).

Ji, Y., J. Zhou, T. Sun, K. Tang, Z. Xiong, Z. Ren, S. Yao, K. Chen, F. Yang, F. Zhu, and X. Guo. 2019. Diverse preparation methods for small intestinal submucosa (SIS): Decellularization, components, and structure. *J Biomed Mater Res A* 107 (3):689-697.

Kapuscinski, J. 1995. DAPI: a DNA-specific fluorescent probe. *Biotech Histochem* 70 (5):220-233.

Kawano, Y., V. Patrulea, E. Sublet, G. Borchard, T. Iyoda, R. Kageyama, A. Morita, S. Seino, H. Yoshida, O. Jordan, and T. Hanawa. 2021. Wound Healing Promotion by Hyaluronic Acid: Effect of Molecular Weight on Gene Expression and In Vivo Wound Closure. *Pharmaceuticals (Basel)* 14 (4).

Kumar, P., and G. C. Jagetia. 1995. Modulation of wound healing in Swiss albino mice by different doses of gamma radiation. *Burns* 21 (3):163-165.

Lubitz, P., U. B. Mayr, and W. Lubitz. 2009. Applications of bacterial ghosts in biomedicine. *Adv Exp Med Biol* 655:159-170.

Mashreghi, M., M. Rezazade Bazaz, N. Mahdavi Shahri, A. Asoodeh, M. Mashreghi, M. Behnam Rassouli, and S. Golmohammadzadeh. 2013. Topical effects of frog "Rana ridibunda" skin secretions on wound healing and reduction of wound microbial load. *J Ethnopharmacol* 145 (3):793-797.

Park, M., S. Kim, I. S. Kim, and D. Son. 2008. Healing of a porcine burn wound dressed with human and bovine amniotic membranes. *Wound Repair Regen* 16 (4):520-528.

Paukner, S., T. Stiedl, P. Kudela, J. Bizik, F. Al Laham, and W. Lubitz. 2006. Bacterial ghosts as a novel advanced targeting system for drug and DNA delivery. *Expert Opin Drug Deliv* 3 (1):11-22.

Piccoli, M., C. Trevisan, E. Maghin, C. Franzin, and M. Pozzobon. 2018. Mouse Skeletal Muscle Decellularization. *Methods Mol Biol* 1577:87-93.

Reddy, K. K., L. Grossman, and G. S. Rogers. 2013. Common complementary and alternative therapies with potential use in dermatologic surgery: risks and benefits. *J Am Acad Dermatol* 68 (4):e127-e135.

Schallberger, S. P., B. J. Stanley, J. G. Hauptman, and B. A. Steficek. 2008. Effect of porcine small intestinal submucosa on acute full-thickness wounds in dogs. *Vet Surg* 37 (6):515-524.

Shirakigawa, N., and H. Ijima. 2018. Decellularization of Liver and Organogenesis in Rats. *Methods Mol Biol* 1577:271-281.

Soleymani, S., A. Tavassoli, G. Hashemi Tabar, G. A. Kalidari, and H. Dehghani. 2020. Design, development, and evaluation of the efficacy of a nucleic acid-free version of a bacterial ghost candidate vaccine against avian pathogenic E. coli (APEC) O78:K80 serotype. *Vet Res* 51 (1):144.

Stanford, W., B. W. Rappole, and C. L. Fox, Jr. 1969. Clinical experience with silver sulfadiazine, a new topical agent for control of pseudomonas infections in burns. *J Trauma* 9 (5):377-388.

Velnar, T., T. Bailey, and V. Smrkolj. 2009. The wound healing process: an overview of the cellular and molecular mechanisms. *J Int Med Res* 37 (5):1528-1542.

Short Communication

In silico Study to Identification of Potential SARS-CoV-2 Main Protease Inhibitors: Virtual Drug Screening and Molecular Docking with AutoDock Vina and Molegro Virtual Docker

Mohammad Amin Manavi

Department of Medicinal Chemistry, Faculty of Pharmacy, Tehran University of Medical Sciences, Tehran, Iran

Received 17 July 2021 Accepted 7 December 2021

Abstract

Coronavirus disease 2019 (COVID-19) has emerged in Wuhan, China, and because of fast transmission, it has led to its extensive prevalence in almost all countries, which has made it a global crisis. Drug repurposing is considered a fast way to discover new applications of the current drugs. This study aims to recognize a possible small molecule as a primary protease inhibitor versus the main protease protein of SARS-CoV-2 by computational programs. Virtual screening procedures like using Molegro Virtual Docker, AutoDock Tool, and AutoDock Vina, were done for more than 1600 FDA-approved medicines downloaded from the ZINC database, were employed to characterize new implied molecule inhibitors for the recently published crystal structure of the main protease protein of SARS-CoV-2. Virtual screening results indicated, many drugs including ARBs, cephalosporins, some kinase inhibitors, HMG CoA reductase, and leukotriene receptor antagonist, may inhibit the main protease of SARS-COV-2. Velpatasvir, Molnupiravir, and Ivermectin were selected by virtual screening methods for further studies to find an efficient ligand for the treatment of COVID-19. Due to some other beneficial features, including anti-infectious, anti-inflammatory properties, and ADME profile, they could be a promising drug nominee for repurposing to the treatment of COVID-19. Velpatasvir was selected by some virtual screening methods for further studies to find a suitable ligand for the treatment of COVID-19. Furthermore, more studies need to approve this data and finally clinical trial needs to be done to examine the efficacy of Velpatasvir for the treatment of covid-19 as an anti-viral agent.

Keywords*: *Velpatasvir, Virtual screening, COVID-19, Molecular Docking, Repurpose, Main Protease Inhibitor

Introduction

The appearance of the new coronavirus (new CoV-19) has influenced human health and also human lifestyle on a global scale. Discovery of the novel targeted drug(s) is needed quickly and has taken the main step in combating the coronavirus disease-19 (COVID-19) pandemic. The SARS-CoV-2 caused an efficacious supplementary strange global public health warning, with comparably high mortality and high transmission speed. The SARS-CoV-2 main protease is necessary for viral replication and could be an important drug target (Soga et al., 2021). It's more than 1 year since WHO announced that COVID-19 has become a pandemic, and to date, there are more than 260,000,000 Confirmed cases, more than 5,230,000 Confirmed deaths and, 223 Countries, areas, or territories are involved in this crisis (Akl et al., 2013).

The SARS-CoV-2 main protease is one of the most critical proteins for transcription and replication of the virus, which cleaves the polyproteins into smaller fragments. Drug repurposing is considered as a way to discover new applications of the current drugs in handling several diseases. The main protease of a virus, like the new coronavirus, plays an essential role in reproduction and expansion (Osipiuk et al., 2021). *In silico* drug repurposing is an alternative efficacious approach to neutralize COVID-19 (Choudhury et al., 2021). This procedure may speed up the process of determining the therapeutic compounds for the newly emerged sicknesses (Polamreddy and Gattu, 2019).

Under the current emergency situation, it operated virtual screening tools to search for drugs and natural products that have been deposited in the Drug data Bank to accelerate drug discovery. This research was performed to estimate and determine whether FDA-approved medicines might be considered as COVID-19 main protease inhibitors. The aim of this study was to explore whether FDA-approved drugs could help manage COVID-19 by

*Corresponding author's e-mail address: *ma-manavi@student.tums.ac.ir*

directly affecting the virus particle, as, a rapid and relatively highly accurate method for screening a large number of ligands is *in silico* methods such as molecular docking.

Materials and Methods

To identify the suitable ligand with the desirable interaction with the main protease of SARS-CoV-2, all FDA-approved drugs, containing 1615 medicines, were obtained from the ZINC database. Drugs were screened through molecular docking simulations over the main protease binding site of SARS-CoV-2. The crystal structure of the main protease of SARS-CoV-2 which has been published recently, was downloaded as a PDB file from a website related to the protein data bank (http://www.rcsb.org) with PDB ID: 6wtt (Sharun et al., 2020).

First, databases such as ZINC were used to download the SDF file format of small molecules for searching the DrugBank database and followed by molecular docking. Auto Dock Tool (ADT, Ver.1.5.6) was used to prepare the input files and analyze the result (Morris et al., 2009). 3D structures of FDA-approved drugs were downloaded from the ZINC database (Sterling and Irwin, 2015) in structure-data file (SDF) format. Molegro Virtual Docker (MVD) ver. 6, was used for the first step of molecular docking. The docking was performed with these steps: 1) importing SDF file of ligands and PDB file format of the protein; 2) searching for all probable cavities on the protein surface which led to the selection of five cavities; 3) setting the binding site and grid space to 0.3Å; 4) setting the search algorithm on the energy-minimization; and 5) hydrogen bonds optimization, then run the software and saving the docking results for the following analysis. Docking scores represent calculated ligand-receptor (protein) interaction energy; hence, more negative scores indicate better binding bias (Jadhav and Karuppayil, 2021).

In the next step, all FDA-approved drugs that included 1615 drugs, or in other words, ligands, were screened. Every ligand was docked ten times with each cavity. After *in silico* screening of drug spaces, they were sorted based on their affinity to main protease and 18 drugs, as potential SARS-CoV-2 main protease inhibitor, were selected to be examined for further analyses. In the next step, the selected ligands by Molegro Virtual Docker, were prepared for docking with AutoDock Tool. Some investigated medications of COVID-19 such as Ivermectin, Molnupiravir and Remdesivir were also chosen to be examined as positive controls.

For protein input file preparation, all water molecules, ligands, and ions were removed from the PDB file. Then polar hydrogens were added, the Kollman-united charge was used to determine the partial atomic charge, and the prepared file was saved in PDBQT format for use in the following steps. Ligand with structure data file (SDF) format should be converted to PDB format, so Open Babel (version 2.3.1) was used to do so (Nosrati et al., 2018). Protein with PDB format was chosen as a macromolecule and was saved as a PDBQT file. Later, 90×90× 90Å (x, y, and z) grid box was centered on the protease binding pocket with 0.375 nm spacing for each dimension and a grid center at dimensions of -15.845, 30.799 and 11.939 was determined for x, y, and z, respectively.

Result and Discussion

Initially, a screening procedure was used to screen 1615 ligands. After docking, those ligands with a mol MolDock score lower than 160 were selected and chosen for the next steps. therefore 18 compounds were found and chosen for next step. AutoDock tool was run, and compounds were sort based on their binding energy.

Pharmacophore studies have been indicated that, some amino acids are more responsible for interaction between ligands and active site of main protease, such as: Tyr 237, Glu 288, Lue287, Ile 249, Arg4 and Phe 294. Trypan Blue, Venetoclax, Indocyanine green (Pourhajibagher and Bahador, 2020) had the highest scores among the chosen drugs, but others could be better choices because of the side effects and lower availability of these three drugs.

Some statins like atorvastatin have been suggested as useful drugs in COVID-19 patients mainly. In addition to the different helpful effects of atorvastatin, its high ability to inhibit the main protease enzyme made it an ideal choice for further studies. (Li et al., 2021) Many cephalosporins indicated high affinity to 6wtt protein. These medicines have an excellent anti-upper respiratory infection and could be considered as satisfactory prophylaxis and treatment for pneumonia caused by covid-19, although because of possible antibiotic resistance it could not be a good option for inhibition of virus loading, but could be used as an adjuvant therapy (Kumar et al., 2021).

Some ARBs like losartan and Azilsartan, and Candesartan indicated a high affinity to the main protease of new coronavirus which made them a potential medicine for managing this crisis. Many studies discussed about interaction between ARBs

and COVID-19 (Bavishi et al., 2021) and there was no significant difference in hospitalization or death rate, So, these drugs could not be a good choice. Although other studies should be done to find ARB-like drugs that inhibit the main protease of new coronavirus. Velpatasvir also indicated a good affinity to main protease of new coronavirus. It is an NS5A inhibitor, which is used in combination with Sofosbuvir in the treatment of hepatitis C. It is just shown that this drug could be useful for treatment of COVID19 through *in silico* study before (Bharti and Shukla, 2021). As it has been shown in figure 1, there are 4 amino acids that have a role in interaction between Velpatasvir and the main protease, including: GLY 275, MET 276, LEU 286 and ALA 285.

Furthermore, the investigated medication of COVID-19 has been utilized in this study. Some particular medicines have been studied in various clinical trials for the treatment of COVID-19. The affinity of Remdesivir to the main protease of new coronavirus is higher than other drugs which are under investigation in clinical trials, and the FDA has recently emergency approved this drug for this illness (Elfiky, 2020)

It is recognized that Remdesivir targets SARS-CoV-2 RNA-dependent RNA polymerase (RDRP). It acts as an RNA nucleotide structure scaffold and can be incorporated into the replicating strand, therefore terminating RNA chain stretching out interfered by the SARS-CoV-2 RDRP complex (Mei and Tan, 2021).

Ivermectin is also another option which is investigation for the treatment of the COVID-19 infection. It can be a potent inhibitor for SARS-CoV-2 to enter into the human cell and even inhibits RNA duplication of that. Ivermectin is a broad-spectrum antiparasitic agent, that has inhibitory potential on many viral infections. It has also been found that ivermectin could prevent SARS-CoV-2 replication *in vitro*. Binding Affinity in AutoDock Tool for ivermectin was Interestingly high (-15.8) but in Molegro Virtual Docker ligand and receptor indicated no affinity. (Perišić, 2020).

In one study it was revealed that Molnupiravir (EIDD-2801) could be useful for the treatment of COVID-19 infection and also, its inhibitory activity has also been demonstrated against coronaviruses including SARS, MERS and SARS-CoV-2. Moreover, it was shown that EIDD-2801 exhibits some level of efficiency in the inhibition of SARS-CoV-2 mRNA replication. (Cox et al., 2021)

In figure 2, it has been shown that Ivermectin, Molnupiravir, Remdesivir and also Velpatasvir could inhibit the main protease of SARS-COV-2.

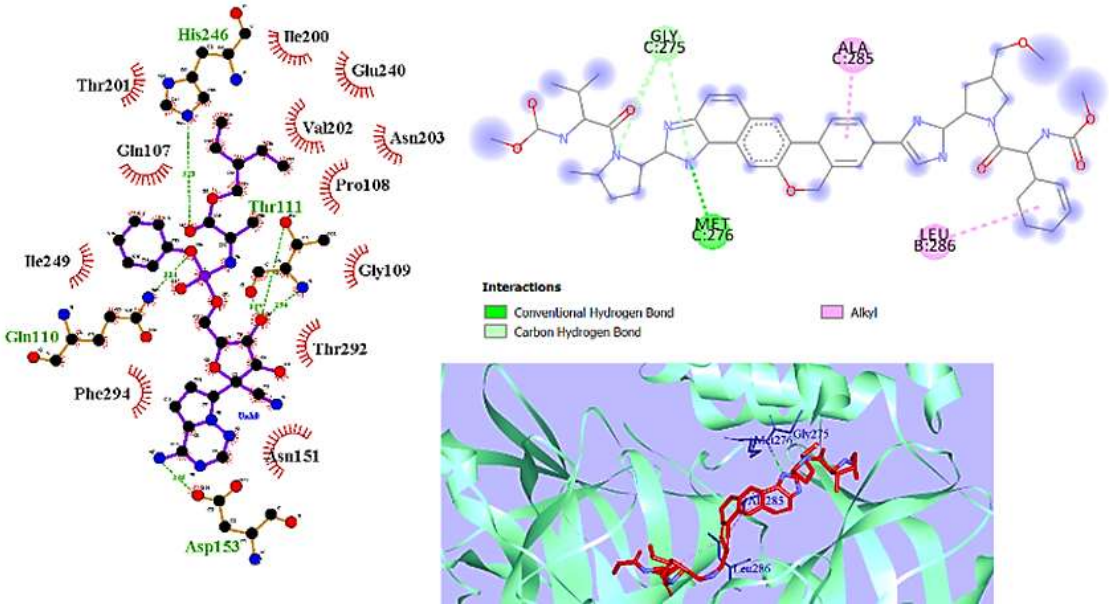

Figure 1. 2D ligand-protein interactions: integration of 6wtt with Velpatasvir designed by LigPlus+ (Left), by Discovery Studio (right-UP). 3D ligand-protein integrations of 6wtt with Velpatasvir designed by Discovery Studio (right-down).

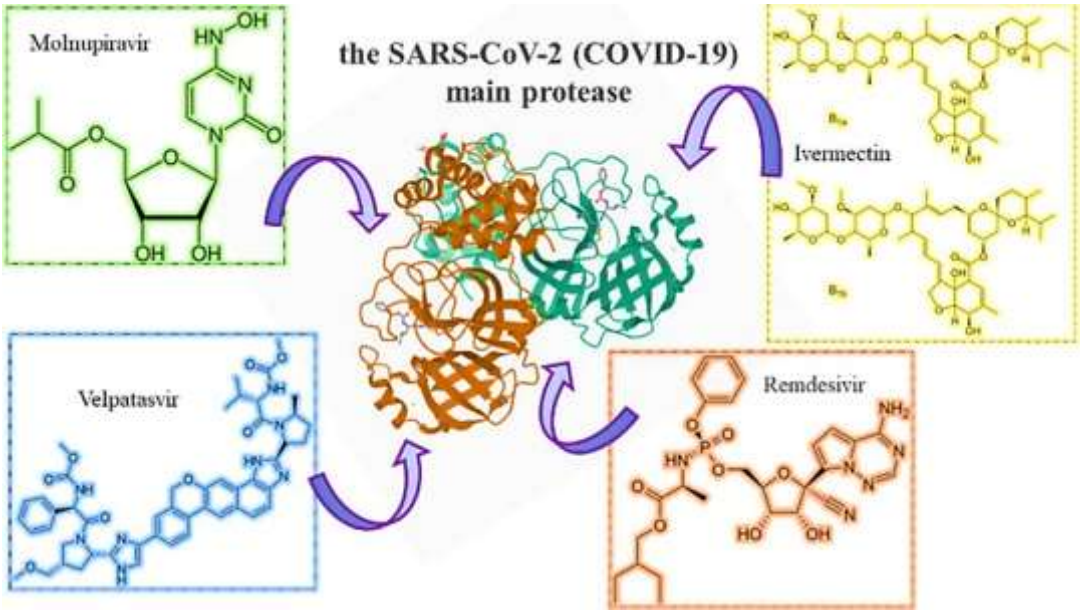

Figure 2. Ivermectin, Molnupiravir, Remdesivir and Velpatasvir as of SARS-COV-2 main protease inhibitors.

Conclusions

In this study, an *in silico* molecular docking experiment was performed on the interaction of FDA-approved drugs with the SARS-CoV-2 main protease enzyme. The virtual screening result consisted of many drugs include 3 ARBs, 5 cephalosporins, a kinase inhibitor and an HMG CoA reductase and leukotriene receptor antagonist, and some other medicines. Velpatasvir is the recommended drug in this study that could be useful for treatment of COVID-19 infection. Moreover, it could be mentioned that the limitation of this study is related to the reliability of *in silico* studies. In this regard, further experimental investigations are needed to confirm the potential of these compounds as treatment for COVID-19 infection.

References

Akl E. A., Jawad M., Lam W. Y., Co C. N., Obeid R. and Irani J. (2013) Motives, beliefs and attitudes towards waterpipe tobacco smoking: a systematic review. Harm Reduction Journal 10:12

Bavishi C., Whelton P. K., Mancia G., Corrao G. and Messerli F. H. (2021) Renin-angiotensin-system inhibitors and all-cause mortality in patients with COVID-19: a systematic review and meta-analysis of observational studies. J Hypertens 39:784-794.

Bharti R. and Shukla S. K. (2021) Molecules against Covid-19: An *in silico* approach for drug development. Journal of Electronic Science and Technology:100095.

Choudhury S., Moulick D., Borah A., Saikia P. and Mazumder M. K. (2021) In search of drugs to alleviate suppression of the host's innate immune responses against SARS-CoV-2 using a molecular modeling approach. *In Silico* Pharmacol 9:26.

Cox R. M., Wolf J. D. and Plemper R. K. (2021) Therapeutically administered ribonucleoside analogue MK-4482/EIDD-2801 blocks SARS-CoV-2 transmission in ferrets. Nat Microbiol 6:11-18.

Elfiky A. A. (2020) Ribavirin, Remdesivir, Sofosbuvir, Galidesivir, and Tenofovir against SARS-CoV-2 RNA dependent RNA polymerase (RDRP): A molecular docking study. Life Sci 253:117592.

Jadhav A. K. and Karuppayil S. M. (2021) Topoisomerase II as a target for repurposed antibiotics in Candida albicans: an *in silico* study. *In Silico* Pharmacol 9:24.

Kumar R., Kumar V. and Lee K. W. (2021) A computational drug repurposing approach in identifying the cephalosporin antibiotic and anti-hepatitis C drug derivatives for COVID-19 treatment. Comput Biol Med 130:104186.

Li Y., Duche A., Sayer M. R., Roosan D., Khalafalla F. G., Ostrom R. S., Totonchy J. and Roosan M. R. (2021) SARS-CoV-2 early infection signature identified potential key infection mechanisms and drug targets. BMC Genomics 22:125.

Mei M. and Tan X. (2021) Current Strategies of Antiviral Drug Discovery for COVID-19. Front Mol Biosci 8:671263.

Morris G. M., Huey R., Lindstrom W., Sanner M. F., Belew R. K., Goodsell D. S. and Olson A. J. (2009) AutoDock4 and AutoDockTools4: Automated docking with selective receptor flexibility. J Comput Chem 30:2785-2791.

Nosrati M., Shakeran Z. and Shakeran Z. (2018) Frangulosid as a novel hepatitis B virus DNA polymerase inhibitor: a virtual screening study. *In Silico* Pharmacol 6:10.

Osipiuk J., Azizi S.A., Dvorkin S., Endres M., Jedrzejczak R., Jones K. A., Kang S., Kathayat R. S., Kim Y., Lisnyak V. G., Maki S. L., Nicolaescu V., Taylor C. A., Tesar C., Zhang Y.A., Zhou Z., Randall G., Michalska K., Snyder S. A., Dickinson B. C. and Joachimiak A. (2021) Structure of papain-like protease from SARS-CoV-2 and its complexes with non-covalent inhibitors. Nature Communications 12:743.

Perišić O. (2020) Recognition of Potential COVID-19 Drug Treatments through the Study of Existing Protein-Drug and Protein-Protein Structures: An Analysis of Kinetically Active Residues. Biomolecules 10.

Polamreddy P. and Gattu N. (2019) The drug repurposing landscape from 2012 to 2017: evolution, challenges, and possible solutions. Drug Discov Today 24:789-795.

Pourhajibagher M. and Bahador A. (2020) Computational Biology Analysis of COVID-19 Receptor-Binding Domains: A Target Site for Indocyanine Green Through Antimicrobial Photodynamic Therapy. J Lasers Med Sci 11:433-441.

Sharun K., Tiwari R. and Dhama K. (2020) Protease inhibitor GC376 for COVID-19: Lessons learned from feline infectious peritonitis. Annals of medicine and surgery (2012) 61:122-125.

Soga M., Evans M. J., Cox D. T. C. and Gaston K. J. (2021) Impacts of the COVID-19 pandemic on human–nature interactions: Pathways, evidence and implications. People and Nature 3:518-527.

Sterling T. and Irwin J. J. (2015) ZINC 15 Ligand Discovery for Everyone. Journal of Chemical Information and Modeling 55:2324-2337.

Research Article

Production and Purification of Recombinant B Subunit of *Vibrio cholerae* Toxin in *Escherichia coli*

Ali Khastar[1], Majid Jamshidian-Mojaver[1*], Hamidreza Farzin[1], Masoumeh Jomhori Baloch[1], Iman Salamatian[1], Kaveh Akbarzadeh-Sherbaf [2]

[1] *Department of Biotechnology Research, Mashhad Branch, Razi Vaccine and Serum Research Institute, Agriculture Research, Education and Extension Organization (AREEO), Mashhad, Iran*
[2] *Department of Computer Engineering, Imam Reza International University, Mashhad, Iran*

Received 24 August 2021 Accepted 10 January 2022

Abstract

Cholera toxin B subunit (CTB) is a non-toxic and immunostimulatory component of *Vibrio cholera* toxin. CTB is one of the most studied protein compounds for adjuvant design. This study aimed to produce and purify recombinant CTB (rCTB) by pET-22a plasmid in *Escherichia coli* BL21(DE) strain, focusing on cost-effectiveness and ease of use. The target gene was identified in the genome of *Vibrio cholerae* biotype *El Tor* through the NCBI database, and its specific primers were designed. The gene fragment was amplified by PCR and cloned into pET-22a plasmid by *Nco*I and *Sac*I restriction enzymes and transformed into *E. coli*. Transformed bacteria were inoculated into a 2×YT medium. Stimulation of recombinant protein production was performed by adding IPTG with a final concentration of 0.4 mM. Finally, recombinant protein was purified by a Ni-IDA column. The concentration of recombinant protein was determined by GM1-ELISA and Bradford tests. The Western blotting technique verified recombinant CTB, So results showed the expected bands at a molecular weight of about 12.76 kDa (denatured) and 63 kDa (non-denatured). GM1-ELISA and Bradford tests showed the final protein concentrations of 11 and 9.57 mg/L, respectively. GM1-ELISA confirmed the biological activity of rCTB in the presence of GM1 ganglioside receptor. Recombinant CTB produced by the method proposed in this research has high purity and appropriate concentration and can be used in immunological studies, especially adjuvant design.

***Keywords*:** Cholera toxin B subunit, *Escherichia coli*, Molecular cloning, *Vibrio cholerae*

Introduction

Cholera toxin is one of the most studied bacterial toxins of the AB5 family, which is widely used as a potent mucosal adjuvant in various studies due to its ability to increase the immune response to the antigen injected with it. This toxin is an important virulence factor of *Vibrio cholerae* that causes severe diarrhea in infected people and consists of two proteins, subunit A, which is a monomer in the complex and has a molecular weight of 28 kDa, subunit B (CTB) is a Pentamer with a molecular weight of 11.6 kDa (Lebens and Holmgren, 1994). CTB is a circular structure consisting of five CTB monomers; Each monomer interacts with two adjacent molecules through hydrogen bonding and salt bridges, without covalent bonding. Centre of this pentameric structure accepts a tunnel-like structure whose inner wall is composed of 5 alpha-helical structures, each belonging to a monomer (Sixma et al., 1993).

Each CTB monomer consists of 124 amino acids, including 21 residues of leader peptide and mature form contains 103 amino acids. After producing CTB in the cytoplasm, it is directed to the periplasmic space; Here, CTB monomers come together to form a pentameric structure that may be secreted separately or in association with CTA as holotoxin AB5(Lebens and Holmgren, 1994).

The B subunit of the cholera toxin is the non-toxic part of this toxin. Its tendency to monosialotetrahexosylganglioside(GM1) receptor, which is widely distributed in cell types, including intestinal epithelial cells, antigen-presenting cells (APCs), macrophages, dendritic cells, and B cells, allows optimal access to the immune system. The identification of its cellular receptor regulates the cellular uptake of cholera toxin; CTB interacts with this receptor via the pentasaccharide fragment of GM1 (Baldauf et al., 2015).

*Corresponding author's e-mail address: *m.jamshidian@rvsri.ac.ir*

Because CTB is a non-toxic part of the cholera holotoxin, interest in it has grown over the past few decades. This subunit can form stable pentamers and exhibit multifaceted biological activity (Holmgren et al., 2005). For this reason, CTB has been considered as a potential vaccine and adjuvant scaffold (Boustanshenas et al., 2013a). In addition, CTB has been shown to have potent anti-inflammatory and immunomodulatory effects (Baptista et al., 2014). Since many non-recombinant CTB on the market contains small amounts of cholera toxin and its A subunit, high purity recombinant CTB are essential for immunological research.

Non-toxicity combined with stability and relative ease of expression of CTB makes it easy to use as a flexible adjuvant. The possibility of expressing this protein in many types of organisms expands its application potential(Lebens et al., 2016). Due to its effective binding to APCs and epithelial surfaces, its ability to reduce antigen amounts up to 100 times for immunization creates a valuable and cost-effective adjuvant(Stratmann, 2015).

One of the essential applications of CTB is its use in biotechnology and immunology studies, especially the development of effective adjuvants for commercial vaccines. Past studies(Alam et al., 2013; Baptista et al., 2014; Boustanshenas et al., 2013a; Charles et al., 2014; Khastar et al., 2021) have shown the widespread use of CTB as a vaccine adjuvant (co-administration or conjugation), cholera vaccine immunogen and immunomodulator. These studies have led to various rCTB expression systems for more efficient access to this protein. Given that CTB appears to be more effective for killed bacterial-based vaccines(Charles et al., 2014), the development of alternative methods of producing and transmitting recombinant CTB could play a significant role in preventing and controlling cholera. Due to its ability to stimulate mucosal humoral immune responses, the antigen-CTB combination provides a promising strategy for vaccination against enteric pathogens and mucosal diseases(Baldauf et al., 2015).

Unfortunately, many researchers cannot access this protein due to international sanctions related to bioterrorism and the very high cost of commercially recombinant CTB. So this study aimed to produce rCTB by focusing on cost-effectiveness and ease of production by a pET-based expression system in *Escherichia coli*.

Materials and Methods

Culture of Vibrio cholerae and DNA Extraction

Vibrio cholerae serotype *Inaba* and biotype *El Tor* were purchased from the Iranian research organization for science and technology (IROST) with PTCC.No 1611. Bacteria were inoculated in 100 cc of Craig's medium (Atlas, 2010) containing 3 g/L of casein hydrolyzate (Merck®, Germany), 0.4 g/L of yeast extract (Merck®, Germany), 0.05 g/L of K_2HPO_4 (SAFC®, USA), and 2mL of 20% glucose(Merck®, Germany) solution (w/v) based on Khastar and colleagues (Khastar et al., 2020) described. The inoculated culture medium was incubated at 48 °C without shaking. After culture, bacterial DNA was extracted by a genomic DNA extraction kit (Denazist®, Iran) according to the manufacturer's instructions and stored for further studies.

Gene Amplification by PCR

The nucleotide sequence of the Cholera toxin B subunit gene was extracted from the Gene Bank of the United States National Center for Biotechnology Information (NCBI, GenBank accession no. AY307389.1), with a size of 321 base pairs. Forward(5′-CATGACACACCTCAAAATATTACTGA-3′)and Reverse (5′CGAGCTCGGTACCATTTGCCATACT-3′) primers were designed based on the above sequence and synthesized by BioNEER Company of South Korea.

The target gene fragment was amplified by *pfu* DNA polymerase (G-biosciences, USA). DNA amplification was performed at a final volume of 25µL, which included 12.5µL of Mastermix solution, 0.5µL of each primer (10 picomols), 2µL DNA template, and 9.5 µL of molecular-grade nuclease-free water. The heat cycle of the reaction mixture was set for 35 cycles, beginning with a period of initial denaturation at 95°C for 10 min. Temperature and time profiles of each cycle were as follows: 95 ºC for 30 seconds (denaturation), 48ºC for 20 seconds (annealing), 72ºC for 20 seconds (extension).

According to the manufacturer's instructions, the target gene was removed from the agar gel by PCR extraction kit (Pioneer Gene Transfer Co, Iran) and stored for further studies.

Gene Cloning in pET-22a

The target gene was cloned into pET-22a by the *Sac* I (Thermofisher®, USA) and *Nco* I (Thermofisher®, USA) restriction enzymes and T4 DNA ligase (Thermofisher®, USA). Finally, the cloned plasmid was transformed into *Escherichia coli* BL21 (DE3) strain, cultured on 2xYT plates (containing 100µg/mL ampicillin), and incubated overnight at

37 °C. Plasmid-free bacteria will not be able to grow in this medium.

In order to investigate the entry of the gene fragment into the plasmid, PCR was performed randomly from several colonies using universal specific primers of the T7 promoter and terminator (Sigma-Aldrich®, Germany). Typically, the distance between these two regions is about 310 bp, which is expected to reach 631 bp if the gene fragment enters.

Expression of Recombinant Proteins

In this study, a 2xYT bacterial culture medium containing 16g/L of tryptone (Merck®, Germany), 10g/L of yeast extract (Merck®, Germany), and 5g/L of NaCl (Fakhr Razi®, Iran) was used to culture the transformed bacteria., Initially, 10cc of the culture medium (containing 100 µg/mL ampicillin) was inoculated with a colony of bacteria and incubated for 16h at 37°C with a 150×g shaker (starter culture). Finally; the starter culture was added to 1 liter of culture medium (containing 100µg /mL ampicillin) and incubated under the same conditions. When the OD_{600} reached 0.7 (range between 0.6 to 1), Isopropyl β- d-1-thiogalactopyranoside (IPTG) with a final concentration of 0.4mM was added to the culture medium and incubated for 3 hours under the conditions described above. Then the culture medium was placed on ice for 5min and centrifuged at 13000×g at 4°C (SIGMA®, Germany), and the precipitate was stored in a -20°C freezer for further investigation.

Extraction of Recombinant Protein from Periplasmic Space

In order, to lysis the cells and extract the recombinant protein, a lysis buffer containing 50 mM potassium phosphate, 400mM NaCl, 100mM KCl, 10% (v/v) glycerol, 0.5% (v/v) Triton ×100, and 10mM imidazole was used at a final pH of 7.8. First, the Frozen cell precipitate of the previous step was slowly melted and dissolved well in a lysis buffer, then transferred to a liquid nitrogen tank to freeze again. After freezing, the sample was melted at 42°C. This process was repeated three times. Finally, the samples were centrifuged at maximum speed for 1 minute at 4°C. The supernatant containing soluble proteins was stored for further evaluation.

Purification of rCTB by Ni-IDA Column

Due to six histidine residues in the C-terminal of the rCTB and the affinity of histidine for nickel metal, it can be easily purified by nickel-containing chromatographic columns. The above column was purchased from Pars Tous Biotechnology Company. The purification process was performed according to the manufacturer's instructions with some changes. After passing the previous stage solution from the nickel column, the column was washed with a washing solution containing 500mM NaCl, 50mM sodium phosphate, and 10mM imidazole at a final pH of 7.8. In order to purify the rCTB from nickel seed, the column was washed three times with an elution solution containing 500mM NaCl, 50mM sodium phosphate, and 150mM imidazole at a final pH of 7.8, and the column output was stored each time.

Confirmation of rCTB by SDS-PAGE and Western Blotting

SDS-PAGE method was used to evaluate the quality of purified protein. 15µL of the purified protein was combined with a suitable ratio of loading buffer (Cytomatingene® co, Iran) and, after boiling, was loaded on 15% acrylamide gel. After electrophoresis, the gel was stained with silver nitrate(panreac®, Spain) as the silvering agent.

Also, to ensure the proper production of recombinant protein by *Escherichia coli*, the Western blotting technique was used. After washing the nitrocellulose paper with TBS (Novagen®, USA) and TBS/TT (Novagen®, USA) solutions, the paper was blocked with bovine serum albumin (BSA, Sigma-Aldrich®, Germany) at room temperature for one hour. In this study, a conjugated anti-polyhistidine antibody with HRP (Sigma-Aldrich®, Germany) in a ratio of 1: 1000 was used. For staining the paper, 3,3 ', 5,5'-Tetramethylbenzidine (TMB) solution (Suitable for Western blot, Cytomatingene® co, Iran) was used according to the manufacturer's instructions.

Determination of Purified rCTB Concentration by GM1-ELISA and Bradford Methods

The GM1-ELISA technique, previously described by Khastar and colleagues (Khastar et al., 2020), was used to determine the amount of the rCTB with slight modifications. The microtiter plates were coated with GM1gangloside receptor in a ratio of 1:500. 100 µL of purified rCTB, which was well combined with a potent protease inhibitor (Thermofisher®, USA), was added to the plate wells. HRP-conjugated anti-polyhistidine antibody (Sigma-Aldrich®, Germany- diluted in PBS solution containing 0.1% BSA) was used in a ratio of 1:1000. The estimated time for blocking the wells with BSA (Sigma-Aldrich®, Germany) and using anti-his-tag antibody was 30-60 min, respectively. TMB solution was used to stain the substrate. Finally, the microtiter plate was read at 450 nm.

The study also used the standard Bradford protocol (Kruger, 2009) to calculate the concentration of

purified protein. BSA was used as a protein standard in this technique.

Results

PCR and Cloning of Gene Fragments

The results of the PCR technique based on the specific primers showed a band with the expected size (321bp) on the agarose gel (Figure 1). The presence of about 631 bp bands from PCR of the T7 promoter and terminator region from some of the colonies grown in 2xYT plates on the agarose gel indicates that the target gene has entered the plasmid quite correctly (Figure 1).

Qualitative and Quantitative Evaluation of rCTB

The results of SDS-PAGE showed that the rCTB was produced by *Escherichia coli* BL21(DE3) strain (Figure 2). In this study, the culture medium before adding IPTG was considered as negative control. If the bacterium produced the protein, a protein band of about 12.76kDa (due to the addition of six histidine residues to the C-terminal of the rCTB) in denature form and 63kDa in non-denature form was expected to be observed in the acrylamide gel (Figure 2). After staining the nitrocellulose paper, a protein blot of about 12.76kDa was observed, indicating the correct expression of the recombinant B subunit of the cholera toxin (Figure 3). Table 1 shows the results of measuring the concentration of purified rCTB.

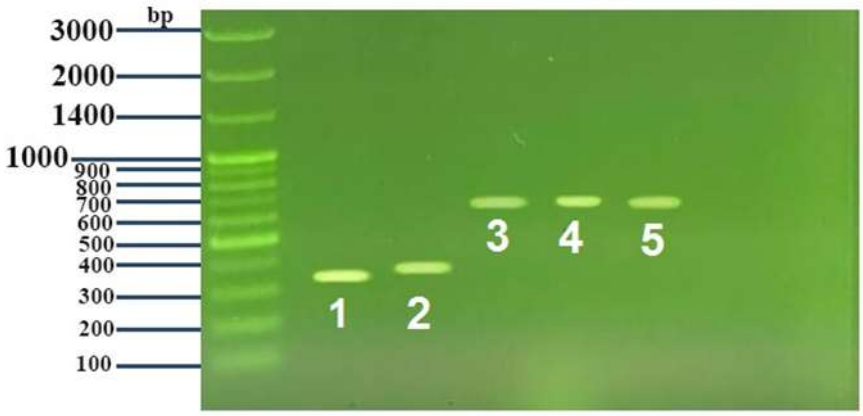

Figure 1. Results of amplification of gene fragments. Columns 3 to 5 result from amplification of the region between the T7 promoter and terminator from three random colonies. Column 1 shows the distance between the T7 promoter and terminator without the insertion of the target gene, and column 2 shows the result of amplification of the desired gene by the primers.

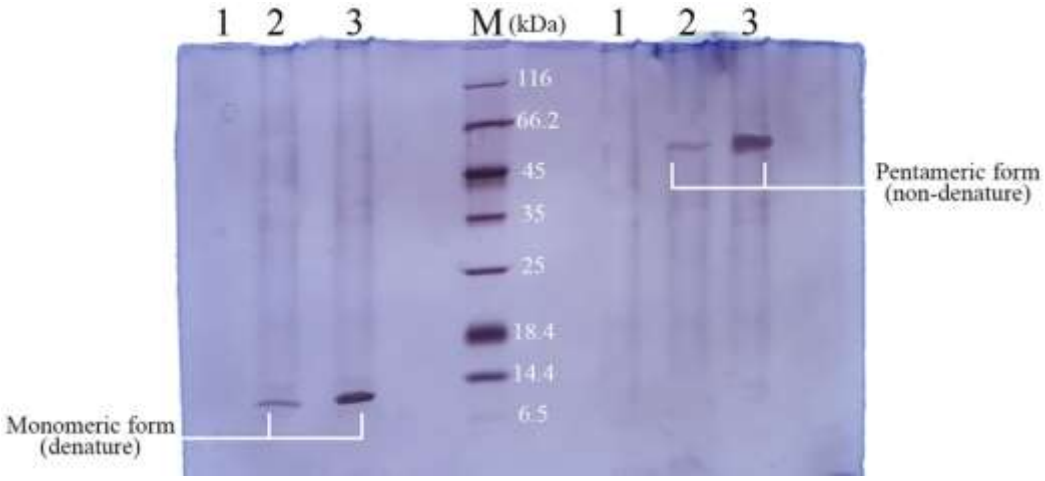

Figure 2. Results of quality assay of recombinant protein by SDS-PAGE. Column 1: Culture medium before induction by IPTG. Column 2: Culture medium after induction with IPTG. Column 3: Recombinant protein purified

using Ni-IDA column. The molecular weight in denatured and non-denatured forms is about 12.76 and 63 kDa, respectively.

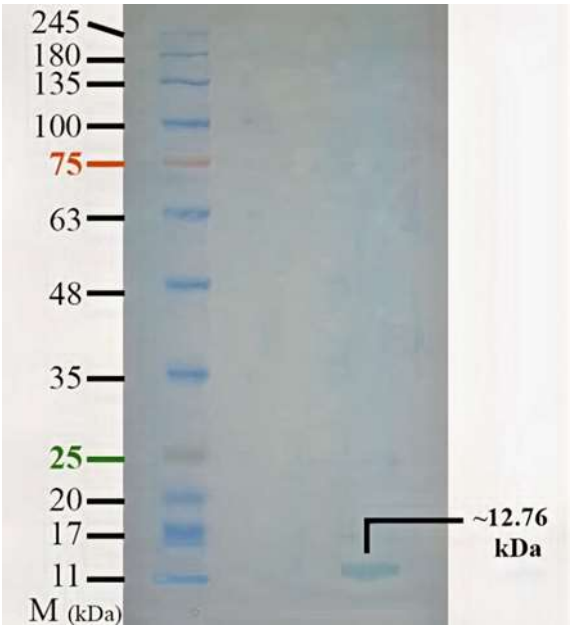

Figure 3. The result of the Western blot technique confirms the correct production of rCTB.

Table 1. Results from quantitative rCTB assays

Assessment method	First wash	Second wash	Third wash
GM1-ELISA	11 µg/mL	0.33 µg/mL	-
Bradford	9.57 µg/mL	0.1 µg/mL	-

Discussion

The main virulence factor of Vibrio cholerae is cholera toxin (CT), which consists of two subunits: subunit A (CTA) and subunit B (CTB) (Kim et al., 2009). CTB is a non-toxic protein with a high affinity for the GM1 ganglioside receptor on the surface of mammalian cells (Chinnapen et al., 2007). Today, CTB is recombinantly produced and is part of an internationally licensed cholera vaccine. This protein can build potent humoral immunity, which neutralizes the cholera toxin in the body (Alam et al., 2013; Charles et al., 2014; Clemens et al., 1986; Schaetti et al., 2012). In addition, many studies show that CTB administration can play an anti-inflammatory role in the body (Baldauf et al., 2015).

In this study, first; a gene fragment related to the synthesis of the B subunit of cholera toxin was identified, and its specific primers were designed. After amplification, the target gene was cloned into plasmid pET22a by *Sac* I and *Nco* I restriction enzymes. Recombinant CTB can be produced in various expression systems, including plants, yeast and fungi (Arakawa et al., 1998; Hamorsky et al., 2013; Hiramatsu et al., 2014; Li et al., 2014; Meng et al., 2011; Okuno et al., 2013). Nevertheless, the most efficient and cost-effective way is to use a pET-based expression system. In addition, this expression plasmid contains the T7 promoter, which is known for its high expression of recombinant proteins and reduced costs and increased efficiency of protein

synthesis. This plasmid has a His-tag coding sequence at the C-terminal, allowing the recombinant protein to be efficiently purified by affinity chromatography with a nickel ion column and using the selective AmpR (ampicillin resistance) marker. Also, The pelB leader sequence in pET-based vectors prevents the inclusion bodies formation and allows the extraction of recombinant proteins from the periplasmic space of *E. coli*, which reduces the cost of protein synthesis. In this study, we tried to provide the most optimal method for rCTB production in *Escherichia coli*. Recombinant CTB can be used as a potent Immunostimulant and non-toxic adjuvant in various commercial vaccines. As Figures 2 and 3 and the quantification results (Table 1) show, the recombinant CTB produced by our method is of high purity.

Due to the strong mucosal immunogenicity of CTB, its recombinant production by various techniques has been considered by many researchers. This recombinant protein is currently used in the WHO-approved cholera vaccine. CTB can be produced in many hosts, including prokaryotes such as *Lactobacillus*, *Escherichia coli*, and even genetically modified *Vibrio cholerae* strains. Other hosts for the production of the CTB are simple eukaryotic cells such as yeast or more complex organisms such as silkworms and plants (Bakhshi et al., 2014; Boustanshenas et al., 2013b; Gong et al., 2005; Hiramatsu et al., 2014; Jani et al., 2002; Kim et al., 2006; Kim et al., 2009; Li et al., 2014; Meng et al., 2011; Nochi et al., 2007; Oszvald et al., 2008; Yasuda et al., 1998; Yuki et al., 2013). However, due to the use of bioreactors or controlled culture chambers and unique greenhouses, the production of CTB in eukaryotic cells is not cost-effective. Okuno and colleagues (Okuno et al., 2013) produced recombinant CTB protein in *Lactobacillus casei* and *Lactobacillus reuteri* at a concentration of 0.05 to 1 mg /L, respectively. Their study used the pHIL253 shuttle vector, which can produce maximum recombinant protein in lactic acid bacteria. The immunization of rCTB was also confirmed in female mice with a lifespan of 4 weeks and binding of the recombinant protein to the GM1 receptor. In another study performed to produce recombinant CTB in *Lactobacillus casei* by Hiramatsu and colleagues(Hiramatsu et al., 2014), recombinant CTB protein was purified at a 1 mg/L concentration. In this study, rCTB was fused with the anti-inflammatory YVAD tetrapeptide (tyrosine, valine, alanine, aspartic acid), which inhibits explicitly caspase-1, which catalyzes the production of interleukin (IL) -1 from its inactive precursor. Their results showed that this fused rCTB can inhibit interleukin-1 in intestinal epithelial cells with high efficiency and can be used as a carrier to deliver fused compounds such as vaccine antigen. Other research has been done to produce this protein in different expression systems such as plants and silkworms (*Bombyx mori*), which can be found in the research of Li and colleagues(Li et al., 2014), As well as Meng and colleagues (Meng et al., 2011). They produced 0.5 mg/g of silkworm pupae and 0.23 mg/g of silkworm larvae, respectively. In order to produce CTB in plant expression systems, Hamorsky and colleagues(Hamorsky et al., 2013) were able to produce this protein at a concentration of more than 1 g/kg of fresh leaves of tobacco (*Nicotiana benthamiana*) leaves. Miyata and colleagues were able to produce a recombinant CTB fused to a protein matrix in the yeast *Pichia pastoris*, which dramatically increased the efficiency of the immune response to the antigen in mice. Although they did not specify the final production rate of this recombinant CTB, it is possible to obtain up to 50 mg / L in this expression system(Stratmann, 2015). One of the advantages of the yeast-based expression system is its similarity to bacterial culture without the production of endotoxins. Due to the need for better folding of proteins fused with CTB, yeast-based systems have a tremendous advantage over other systems(Miyata et al., 2012; Song et al., 2004). However, using eukaryotic expression systems is expensive and complicated.

The present study could produce CTB at an 11 mg/L concentration in a very inexpensive 2xYT medium. As Table 1 shows, the accuracy of the GM1-ELISA technique for quantitative CTB assays is higher due to the higher sensitivity of CTB to the GM1 ganglioside receptor. Small molecular size and low weight, along with the high similarity of this protein to the *Escherichia coli* heat-sensitive enterotoxin B subunit, facilitate the expression of this protein in *Escherichia coli*.

Conclusion

In recent years, extensive studies have been conducted on the immunological effects of the cholera toxin B subunit on the effective stimulation of the immune system. Non-toxicity combined with stability and relative ease of expression of CTB makes it easy to use as a flexible adjuvant. The possibility of expressing this protein in many types of organisms expands its application potential. CTB is a combination with diverse applications and promises a practical approach to evolving vaccine development. Therefore, in this study, we aimed a

convenient method for the recombinant production of this protein for use in vaccine design.

Acknowledgements
The authors of this article appreciate all the personnel of the Biotechnology Research Department of the Razi Vaccine and Serum Research Institute (Mashhad branch).

Conflict of Interest
The authors declare no conflict of interest.

References

Alam M. M., Leung D. T., Akhtar M., Nazim M., Akter S., Uddin T., et al. (2013) Antibody avidity in humoral immune responses in Bangladeshi children and adults following administration of an oral killed cholera vaccine. Clinical and Vaccine Immunology 20:1541-1548.

Arakawa T., Yu J., Chong D. K., Hough J., Engen P. C. and Langridge W. H. (1998) A plant-based cholera toxin B subunit–insulin fusion protein protects against the development of autoimmune diabetes. Nature Biotechnology 16:934-938.

Atlas R. M. 2010. Handbook of Microbiological Media. CRC Press, Washington D. C. 288-482 pp.

Bakhshi B., Boustanshenas M. and Ghorbani M. (2014) A single point mutation within the coding sequence of cholera toxin B subunit will increase its expression yield. Iranian Biomedical Journal 18:130.

Baldauf K. J., Royal J. M., Hamorsky K. T. and Matoba N. (2015) Cholera toxin B: one subunit with many pharmaceutical applications. Toxins 7:974-996.

Baptista A., Donato T., Garcia K., Gonçalves G., Coppola M., Okamoto A. S., et al. (2014) Immune response of broiler chickens immunized orally with the recombinant proteins flagellin and the subunit B of cholera toxin associated with Lactobacillus spp. Poultry Science 93:39-45.

Boustanshenas M., Bakhshi B. and Ghorbani M. (2013a) Investigation into immunological responses against a native recombinant CTB whole-cell Vibrio cholerae vaccine in a rabbit model. Journal of Applied Microbiology 114:509-515.

Boustanshenas M., Bakhshi B., Ghorbani M. and Norouzian D. (2013b) Comparison of two recombinant systems for expression of cholera toxin B subunit from Vibrio cholerae. Indian Journal of Medical Microbiology 31:10-14.

Charles R. C., Hilaire I. J., Mayo-Smith L. M., Teng J. E., Jerome J. G., Franke M. F., et al. (2014) Immunogenicity of a killed bivalent (O1 and O139) whole cell oral cholera vaccine, Shanchol, in Haiti. PLoS Neglected Tropical Diseases 8:e2828.

Chinnapen D. J.-F., Chinnapen H., Saslowsky D. and Lencer W. I. (2007) Rafting with cholera toxin: endocytosis and trafficking from plasma membrane to ER. FEMS Microbiology Letters 266:129-137.

Clemens J., Harris J., Khan M. R., Kay B., Yunus M., Svennerholm A.-M., et al. (1986) Field trial of oral cholera vaccines in Bangladesh. The Lancet 328:124-127.

Gong Z.-H., Jin H.-Q., Jin Y.-F. and Zhang Y.-Z. (2005) Expression of cholera toxin B subunit and assembly as functional oligomers in silkworm. BMB Reports 38:717-724.

Hamorsky K. T., Kouokam J. C., Bennett L. J., Baldauf K. J., Kajiura H., Fujiyama K., et al. (2013) Rapid and scalable plant-based production of a cholera toxin B subunit variant to aid in mass vaccination against cholera outbreaks. PLoS Neglected Tropical Diseases 7:e2046.

Hiramatsu Y., Yamamoto M., Satho T., Irie K., Kai A., Uyeda S., et al. (2014) Recombinant fusion protein of cholera toxin B subunit with YVAD secreted by Lactobacillus casei inhibits lipopolysaccharide-induced caspase-1 activation and subsequent IL-1 beta secretion in Caco-2 cells. BMC Biotechnology 14:1-9.

Holmgren J., Adamsson J., Anjuère F., Clemens J., Czerkinsky C., Eriksson K., et al. (2005) Mucosal adjuvants and anti-infection and anti-immunopathology vaccines based on cholera toxin, cholera toxin B subunit and CpG DNA. Immunology Letters 97:181-188.

Jani D., Meena L. S., Rizwan-ul-Haq Q. M., Singh Y., Sharma A. K. and Tyagi A. K. (2002) Expression of cholera toxin B subunit in transgenic tomato plants. Transgenic Research 11:447-454.

Khastar A., Farzin H. and Jamshidian-Mojaver M. (2021) Evaluation of Cholera toxin Adjuvanticity Effect on the Production of Specific Antibodies Induced by Avian Infectious Bronchitis Vaccine in Chickens. Archives of Razi Institute:-.

Khastar A., Jamshidian-mojaver M. and Ghalandari B. (2020) Evaluation and optimization of cholera toxin production by Vibrio cholerae in different time

periods. Journal of Veterinary Microbiology 16:137-148.

Kim Y.-S., Kim B.-G., Kim T.-G., Kang T.-J. and Yang M.-S. (2006) Expression of a cholera toxin B subunit in transgenic lettuce (Lactuca sativa L.) using Agrobacterium-mediated transformation system. Plant Cell, Tissue and Organ Culture 87:203-210.

Kim Y.-S., Kim M.-Y., Kim T.-G. and Yang M.-S. (2009) Expression and assembly of cholera toxin B subunit (CTB) in transgenic carrot (Daucus carota L.). Molecular Biotechnology 41:8-14.

Kruger N. J. 2009. The Bradford method for protein quantitation. 17-24 pp.

Lebens M. and Holmgren J. (1994) Structure and arrangement of the cholera toxin genes in Vibrio cholerae O139. FEMS Microbiology Letters 117:197-202.

Lebens M., Terrinoni M., Karlsson S. L., Larena M., Gustafsson-Hedberg T., Källgård S., et al. (2016) Construction and preclinical evaluation of mmCT, a novel mutant cholera toxin adjuvant that can be efficiently produced in genetically manipulated Vibrio cholerae. Vaccine 34:2121-2128.

Li S., Wei Z., Chen J., Chen Y., Lv Z., Yu W., et al. (2014) Oral administration of a fusion protein between the cholera toxin B subunit and the 42-amino acid isoform of amyloid-β peptide produced in silkworm pupae protects against Alzheimer's disease in mice. PloS One 9:e113585.

Meng Q., Wang W., Shi X., Jin Y. and Zhang Y. (2011) Protection against autoimmune diabetes by silkworm-produced GFP-tagged CTB-insulin fusion protein. Clinical and Developmental Immunology 2011.

Miyata T., Harakuni T., Taira T., Matsuzaki G. and Arakawa T. (2012) Merozoite surface protein-1 of Plasmodium yoelii fused via an oligosaccharide moiety of cholera toxin B subunit glycoprotein expressed in yeast induced protective immunity against lethal malaria infection in mice. Vaccine 30:948-958.

Nochi T., Takagi H., Yuki Y., Yang L., Masumura T., Mejima M., et al. (2007) Rice-based mucosal vaccine as a global strategy for cold-chain-and needle-free vaccination. Proc. Natl. Acad. Sci 104:10986-10991.

Okuno T., Kashige N., Satho T., Irie K., Hiramatsu Y., Sharmin T., et al. (2013) Expression and secretion of cholera toxin B subunit in lactobacilli. Biological and Pharmaceutical Bulletin 36:952-958.

Oszvald M., Kang T.-J., Tomoskozi S., Jenes B., Kim T.-G., Cha Y.-S., et al. (2008) Expression of cholera toxin B subunit in transgenic rice endosperm. Molecular Biotechnology 40:261.

Schaetti C., Weiss M. G., Ali S. M., Chaignat C.-L., Khatib A. M., Reyburn R., et al. (2012) Costs of illness due to cholera, costs of immunization and cost-effectiveness of an oral cholera mass vaccination campaign in Zanzibar. PLoS Neglected Tropical Diseases 6:e1844.

Sixma T. K., Kalk K. H., van Zanten B. A., Dauter Z., Kingma J., Witholt B., et al. (1993) Refined structure of Escherichia coli heat-labile enterotoxin, a close relative of cholera toxin. Journal of Molecular Biology 230:890-918.

Song H., Zhou L., Fang W., Li Y., Wang X., Fang H., et al. (2004) High-level expression of codon optimized foot-and-mouth disease virus complex epitopes and cholera toxin B subunit chimera in Hansenula polymorpha. Biochemical and Biophysical Research Communications 315:235-239.

Stratmann T. (2015) Cholera toxin subunit B as adjuvant—an accelerator in protective immunity and a break in autoimmunity. Vaccines 3:579-596.

Yasuda Y., Matano K., Asai T. and Tochikubo K. (1998) Affinity purification of recombinant cholera toxin B subunit oligomer expressed in Bacillus brevis for potential human use as a mucosal adjuvant. FEMS Immunol. Med. Microbiol 20:311-318.

Yuki Y., Mejima M., Kurokawa S., Hiroiwa T., Takahashi Y., Tokuhara D., et al. (2013) Induction of toxin-specific neutralizing immunity by molecularly uniform rice-based oral cholera toxin B subunit vaccine without plant-associated sugar modification. Plant Biotechnology Journal 11:799-808.

Research Article

Association of HLA-A*03/A*31 and HLA-A*24/A*31 Haplotypes with Multiple Sclerosis

Seyed Javad Rajaei[1], Mostafa Shakhsi-Niaei[1,2*], Masoud Etemadifar[3,4]

[1]*Department of Genetics, Faculty of Basic Sciences, Shahrekord University, Shahrekord, Iran*
[2]*Institute of Biotechnology, Shahrekord University, Shahrekord, Iran*
[3]*Department of Neurology, Faculty of Medical School, Isfahan University of Medical Sciences, Isfahan, Iran*
[4]*Research Committee of Multiple Sclerosis (IRCOMS), Isfahan, Iran*

Received 26 September 2021 Accepted 6 February 2022

Abstract

Multiple sclerosis (MS) is an autoimmune disease of the central nervous system with unknown etiology. Recent evidences suggest the HLA contribution to Multiple sclerosis (MS) pathogenicity as they may present neuropeptides to cytotoxic lymphocytes. We aimed to investigate the association of some related HLA-A alleles and haplotypes with MS and compare the results with other Universal reports to shed light on some aspects of this universally expanded disease. In this investigation, alleles were genotyped by polymerase chain reaction with sequence-specific primers (PCR-SSP) in 50 MS patients, and 50 unrelated healthy individuals. The analysis was carried out using SPSS V.19 statistical software. The results of this study showed a significant association of HLA-A*03 and HLA-A*24 alleles with MS ($P<0.0001$), but HLA-A*02 and other alleles did not show any significant association ($P>0.05$). However, other alleles were not significantly associated ($P>0.05$). Interestingly, in our study, the HLA-A*31 allele was often in combination with HLA-A*03 and HLA-A*24 as risk haplotypes in MS patients. In the present study, not only HLA-A*03 and HLA-A*24 were highly associated with the risk of MS susceptibility, but also their combinations with HLA-A*31 allele were more frequent in patients. Therefore, HLA-A*31 may be introduced as a new complementary risk factor in MS pathogenesis.

***Keywords*:** Association Study, HLA-A, HLA-A*31, PCR-SSP, MHC class I, Multiple Sclerosis

Introduction

Multiple sclerosis (MS), a chronic inflammatory condition of the central nervous system (CNS), leads to demyelination and dysfunction of neurons. Further disseminated and focal damage of myelin and axons that ends up to movement disability (Weissert, 2013). The prevalence of MS has been reported from 2 up to 160 per 100,000 in different populations worldwide.

In 2013, the world health organization (WHO) reported that 2.3 million people suffer from MS worldwide (Browne et al. 2014). The prevalence of this disease has been increasing in Iran, especially since a decade ago. The prevalence of MS varies from 5.3 to 74.28 per 100,000 in various regions of Iran (Etemadifar et al. 2006, Tolou-Ghamari, 2015). Particularly, it has been shown that there has been an increase in the prevalence of MS between 2008 and 2013 (Radmehr et al, 2015). Isfahan, in central part of Iran, is one of the largest and most populous provinces. The incidence rate of 9.1 per 100,000 in 2009 was reported for this city, standardized prevalence 71.6 per 100,000 which was about two times of 2007 (Etemadifar and Maghzi, 2011). This dramatic increase in the prevalence of MS puts Isfahan amongst the regions with the highest prevalence of MS in Asia and Oceania (Etemadifar et al. 2006).

Epidemiologists have reported that MS pathogenesis is the result of genetic and environmental factors interplay (Weiner, 2008). Genetic evidences show associated loci in the human Major Histocompatibility complex (MHC) or human leukocyte antigen (HLA) region on chromosome 6p21.3 with MS. The MHC region spans 3.5 Mb, including the class I, II, and III subregions (Horton et al. 2004). The MHC region encompasses about 7.6 Mb and consists of at least 252 expressed genes, which the main proportion of which are related to different immune mechanisms (Ramagopalan et al. 2009). The severity of this disease is affected by

*Corresponding author's e-mail addresses:
Shakhsi-niaei.M@sku.ac.ir
Niaee_m@yahoo.com

genes in the MHC region, but the MHC association with MS seems not as direct as scientists thought before (Natio et al. 1972). The best-established associated MHC class II alleles with MS are HLA-DRB1*15:01, DRB5*01:01, DQA1*01:02, and DQB1*06:02 (Amirzargar et al. 1998). Also, there are evidences for independent effects of markers, form MHC class I, close to HLA-A and HLA-B/HLA-C (Rioux et al. 2009). Associations between HLA class I subtypes and MS has been reported by a number of studies. For example, among Swedish patients, the HLA-A*03 allele increased the risk of MS independently of the HLA-DR15 haplotype, whereas the HLA-A*02 allele was found to decrease the risk of MS (Fogdell-Hahn et al. 2000, Brynedal et al. 2007, Link et al. 2012). Among Italian patients, HLA-A*02 is reported as a protective allele with MS (Bergamaschi et al. 2010, Bergamaschi et al. 2011). In Norwegian sporadic MS cases and Nordic and British affected sibling pairs, HLA-A*03 in contribution with HLA class II alleles was found as associated haplotypes with MS (Harbo et al. 2004). Among Iranian MS patients, the HLA-A*03 (Lotfi et al. 1978, Galehdari et al. 2018) and HLA-A*24 (Kalanie et al. 2000) alleles were found to increase the risk of MS independent from the HLA-DR15 allele, whereas the HLA-A*02 (Amirzargar et al. 2005, Ghanavati et al. 2018) and HLA-A*11 (Amirzargar et al. 2005) alleles decreased the risk of MS. Also, *in silico* studies showed HLA-A*31 allele as a potential important allele in MS susceptibility (Mohammadi-Milasi et al. 2020).

As mentioned above, this disease has been associated with significant rise over the past decade in Isfahan of Iran, as well as other regions worldwide. Accordingly, this study examined the frequency of some important HLA-A alleles with MS patients in Isfahan province and compared the results with other regional or Universal reports to shed light on some aspects of this universally expanded and complex disease.

Materials and Methods

MS Patients and Control Subjects

During one year (2017 to 2018), we conducted this study on 50 patients from Isfahan MS center with Mean SD age of 39.04±0.54 and 50 healthy individuals referred to the al-Zahra hospital, which did not show any autoimmune disease, no history of MS in their close relations, and with mean age of 38.5±10.6 years, with normal laboratory analysis were selected as control group. The patients were diagnosed by a neurologist according to diagnostic criteria described by Mc Donald and a primary progressive (PP), secondary progressive (SP), or relapsing-remitting (RR) disease course (McDonald et al. 2001). To be eligible, patients with RRMS had to havetwo or more attacks in the previous two years. Fifty Controls were originally from the same geographical region and were matched with cases in ethnicity. All the participants were informed about our study and completed a consent form.

DNA Extraction and Genotyping

Peripheral blood samples (5 ml) were collected in EDTA tubes, and DNAs were extracted from whole blood using S3P PCR MASTER MIX (RNA Biotech Co, Isfahan, Iran) according to the manufacturer's manual.

HLA Typing was achieved by Nested PCR and Sequence-Specific PCR (SSP-PCR) methods. Nested PCR involves the use of two primer sets and two successive PCR reactions (Haff et al. 1994) to improve sensitivity and specificity of the test. On the other hand, in PCR-SSP method, specificity is determined by the use of sequence specific primers in which a 3' single-base mismatch inhibits the priming of unspecific reactions. In this research, a combination of both methods has been employed. In the beginning, a long PCR product was amplified by using a primer pair for HLA-A gene in general with a fragment of about 2478 bp. Sequences of primers were as follow: Forward 5'-GATCATTCAGGGGTTACC-3'; Reverse 5'-CATGGCAGGTGTATCTCT-3'. The PCR amplification program was 4 min for initial denaturation at 95ºC, followed by 35 cycles of melting at 94ºC for 30s, annealing at 59ºC for 30s, and elongation at 72ºC for 30s; followed by 7 min of final elongation at 72ºC. Then with the specific designed primers for the alleles of HLA-A*02, HLA-A*03, HLA-A*11 and HLA-A*24 each allele amplified by the PCR-SSP method. A pair of control primers were designed to be present in all HLA-A alleles. Then using the products of this PCR reaction PCR-SSP, the considered alleles were genotyped. Their sequence, length, melting temperature (Tm) and position of the primers are given in Table 1.

Table 1. Oligonucleotide primer properties

Gene	Primer	Primer sequence 5 to 3	Length (mer)	Tm	Location (Exon)
HLA-A02	Sense	GACGGGGAGACACGGAAA	18	58	2
	Antisense	CGTCCAGAGGATGTATGG	18	58	3
HLA-A03	Sense	GAGACACGGAATGTGAAGGCCCAG	24	58	2
	Antisense	CTTGGTGATCTGAGCCGC	18	58	3
HLA-A11	Sense	GAGACACGGAATGTGAAGGCCCAG	24	62	2
	Antisense	GGGCCGGTGCGTGGAGTGG	19	62	3
HLA-A24	Sense	GCGGCTCAGATCACCAAG	18	59	3
	Antisense	GGCAGCTGTGGTGGTACCTTCTG	19	59	4
HLA-A31	Sense	GCCTTGAACGAGGACCTG	19	54	3
	Antisense	CATATGCGTCTTGGGGGGG	18	54	4
Internal control	Sense	CTGGAGAACGGGAAGGAG	19	58	3
	Antisense	CATGGCAGGTGTATCTCT	18	58	4

In summary, 35 cycles carried out comprising: initial denaturation at 95ºC for 4 min, denaturation at 94°C for 30 sec, the SSPs was melting temperatures in the range of 58°C to 64”C for 50 sec, and extension at 72°C for 50 sec, with a final 7-min extension at 72°C. The IMGT/HLA database (http://www.ebi.ac.uk/) was used for the design of all primers and then were evaluated in ncbi/primer blast (www.ncbi.nlm.nih.gov). Finally, the results were validated by sequencing of several random samples.

Statistical Analysis

HLA analysis was performed by comparing the dominant allele frequencies between the MS patients and control subjects using Statistical Package for Social Sciences (SPSS / version 19) software. The high-frequency alleles were analyzed for association with clinical features, by calculating odds ratios (ORs) with 95% confidence intervals (CIs). The relationships between the MS cases and controls were calculated with Pearson’s chi-square test. Statistical significance was considered for $p<0.05$. These values were then corrected by Bonferroni method according to the number of analyzed alleles.

Results

Demographic Data

Summarized characteristics of patients and controls are shown in Table 2. As shown in Table 3, there was a significant increase in the frequency of HLA-A*03 and HLA-A*24 in patients with MS in comparison with those of the healthy controls; and a positive association between HLA-A*03 and MS ($P<0.0001$, odds ratio (OR)=23.059) and HLA-A*24 ($P<0.00001$, odds ratio (OR)=17.379) was also observed. The results showed an increase in the risk of MS and HLA-A*03 and HLA-A*24 frequency in Isfahan province. The results of our study did not replicate the negative association of HLA alleles with MS, but a protective role of HLA-A*02 for some of the clinical symptoms was observed. All four patients who were positive for the HLA-A*02 subtype had no sphincter problems and spasticity. Figure 1 presents the more frequent HLA-A alleles in MS and control subjects.

Table 2. Demographics of the MS patients and control subjects

Variable	Age (year)		Gender		EDSS 1-5	Disease duration (year)		Disease course			Familial history
	Rang	Mean ± SD	Females	Males	Median	Rang	Mean ± SD	RRMS	SPMS	PRMS	
MS patients N=50	14-70	39.04± 0.54	21	29	1.98±1.79	1-20	4.46±4	48 (96 %)	1 (2%)	1 (2%)	10 (20%)
Controls N=50	19-62	385±10.6	23	27	NA	NA	NA	NA	NA	NA	NA

MS: multiple sclerosis; EDSS: expanded disability status scale; RR: relapse remitting; PP: primary progressive; SP: secondary progressive; SD: standard deviation; NA: not applicable.

Table 3. Frequencies of HLA-A alleles in MS patients and control subjects.

HLA-A alleles	MS group frequency, %, n=50	Control group frequency, %, n=50	P-value	Odds ratio	95% confidence interval	P^c
***A02**	4	2	0.6777	2.087	0.307-17.361	NS
***A03**	16	1	0.0001	23.059	2.957-488.362	0.01
***A11**	5	5	1	1	0.230-4352	NS
***A24**	21	2	0.00001	17.379	3.522-186.087	0.001
***A31**	19	10	0.0769	2.452	0.917-6.650	NS
Others	35	80	-	-	-	-

MS: multiple sclerosis; pc: probability after Bonferroni correction for $p < 0.05$. NS: Not Significant.

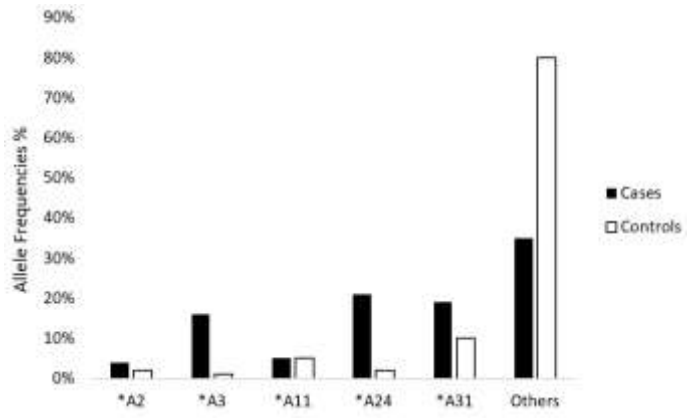

Figure 1. Frequency of HLA-A alleles in MS patients and control subjects. The results revealed that HLA-A24, A3 andA31 were the highest frequency alleles in MS patients, and HLA-A31 the highest frequency allele in control subjects. HLA, human leukocyte antigen.

Discussion

In this study, some HLA-A alleles and haplotypes were found highly associated with multiple sclerosis disease. The genetic associations of variations in MHC genes and MS have been robustly reported in different populations. Some case–control studies have proposed independent associations of HLA class I with MS (Fogdell-Hahn et al. 2000, Harbo et al. 2004, Silva et al. 2009). By using microsatellite markers in the MHC locus, a study on Sardinian families with MS disease found a telomeric region of HLA class I associated with MS but independent of HLA class II variations (Yeo et al. 2007). Parallel findings were reported by a Tasmanian study, which used microsatellite markers to study the class I region believed to play an independent role in susceptibility to and protection from MS (Rubio et al. 2002). In the recent two decades, susceptibility loci for MS, through the HLA region, were replicated in numerous populations, and HLA-A*03 has been described for increasing the risk of MS.

On the one hand, some studies have suggested independent **HLA class I** association with MS (Brynedal et al. 2007, Silva et al. 2009), and on the other hand, there are other studies that have suggested modifying effects of HLA class I alleles beside HLA-DRB1 allele as different haplotypes (Brynedal et al. 2007, Harbo et al. 2004).

Our results revealed an increased susceptibility to MS for people carrying **HLA-A*03** (P<0.0001, OR=23.059) in Isfahan province. This result is consistent with a previous study on MS patients of Tehran (Iran) (P<0.001) (Lotfi et al. 1978), Khuzistan (Iran) (P < 0.001) (Galehdari et al. 2018), Sweden (P=0.0008) (Fogdell-Hahn et al. 2000) and ($2.7*10^{-3}$) (Brynedal et al. 2007) but not with the result of a study in Tehran on samples referred from different regions of Iran (P>0.05) (Kalanie et al. 2000), Bahrain (Al-Nashmi et al. 2018), Norway (Harbo et al. 2004) and Brazil (Werneck et al. 2016), despite a positive trend in some studies.

Our results also revealed an increased susceptibility to MS for people carrying **HLA-A*24** (P<0.0001, OR=17.379) in Isfahan province. This result is consistent with a previous study on MS samples referred from different regions of Iran (P<0.05) (Kalanie et al. 2000) and Kuwait MS patients who carrying A9 (P=0.031) (Al-Shammri et al. 2004), but not with the results of MS patients from Mumbai (India) (P=0.032) (Kankonkar et al. 2012), Sweden (Brynedal et al. 2007), Tehran who carrying A9 (HLA-A*23 and A*24) (Lotfi et al. 1978), and Bahraini MS patients carrying A9 (Al-Nashmi et al. 2018).

Previous studies in different populations have suggested the protective effect of **HLA-A*02** allele for MS. The HLA-A*02 associations among Portuguese (OR=0.54, p=0.001) (Silva et al. 2009), Italian (OR=0.61 $P=5.28*10^{-9}$) (Bergamaschi et al. 2010), Swedish (OR=0.52, P=0.0015) (Fogdell-Hahn et al. 2000) and (2007) (4.4*10-11) (Brynedal et al. 2007), African American (OR=0.72, p=0.013) (Isobe et al. 2013) and (in the absence of Cw*05 and B*44/12) in Italian (OR=0.63 P=0.0007), UK (OR=0.8 P=0.509), and UK combined case-control and family trios (OR=0.65 P=0.0099) (Bergamaschi et al. 2011), showed different levels of associations, but this allele, in all of these studies showed a protective influence. However, in our study, only a low number of MS patients and controls (2 out of 50 patients and 4 out of 50 controls) carrying this allele and maybe is the reason for not significant association of this allele with MS risk and opposite OR. This issue is consistent with the lack of significant association of HLA-A*02 and MS in Iran (Lotfi et al. 1978) and Bahrain (Al-Nashmi et al. 2018).

HLA-A*11 was not significant in our study (P>0.05), similar to Sweden (Brynedal et al. 2007) , but, its association with MS is reported in Tehran (P<0.001) (Lotfi et al. 1978) and Mumbai (India) (P=0.032) (Kankonkar et al. 2012).

Interestingly as **HLA-A*31** allele was reported in an *in silico* study as a potential important allele in MS susceptibility (Mohammadi-Milasi et al. 2020), it was found more frequently in combination with highly associated HLA-A*03 and HLA-A*24 alleles in MS patients than controls (Table 4). This issue may reflect a role for this allele when combined with other risk alleles. However, further studies with a higher number of cases are required to show its effect more precisely.

Table 4. Observed HLA-A haplotypes in MS patients and controls and their attribution to EDSS.

	Other HLA-A allele	MS group frequency, %, n=50	Control group frequency, %, n=50	EDSS Mean
A*31	A*24	6	1	3.2
	A*03	5	1	2.7
	A*11	1	0	1
	others	7	8	1.5
A*24	A*03	3	0	2
	A*02	1	0	3
	A*11	1	0	1
	others	10	2	2
A*03	A*11	1	0	1
	A*02	1	0	1
	others	6	1	2

Recently, has been reported that deeper genotypes, 4-digit genotypes of HLA alleles, may show different behavior. For example, Kloverpris et al. (2011) showed that in HIV C-clade-infected subjects, HLA-*5703 was associated with a lower viral-load set point than HLAB*5702 (Kloverpriset al. 2011). Therefore, according to the controversial association of MS with different HLA-A alelles in different studies, one may suggest that this level of genotyping (2-digit resolution) may not be enough for association study of HLA alleles with MS or other related diseases, especially in heterogeneous populations. Therefore, as antigen presentation is carried out by different MHC class I and MHC class II alleles, comprehensive studies of 4-digit HLA genotyping seem necessary in diseases of interest.

To sum up, in this study HLA-A*03 and HLA – A*24 were highly associated alleles with MS, especially when combined with HLA-A*31 allele. Therefore, combinatory effects of different HLA alleles as HLA haplotypes may be considered as an informative strategy in HLA genotyping studies, either for MHC class I or MHC class II alleles.

Funding statement
This work was partially supported by the University of Shahrekord (Grant No. 141.349)

Conflict of interest
Authors declare no conflict of interest.

Acknowledgements
We would like to thanks Mahdi Khozaei and technicians at the RNA Biotechnolgy Laboratory (Isfahan, Iran). The authors wish to appreciate Isfahan Multiple Sclerosis center for collaboration and Al-Zahra Hospital of Isfahan for providing control samples.

References

Al-Nashmi M., Taha S., Salem A. H., Alsharoqi I. and Bakhiet M. (2018) Distinct HLA class I and II genotypes and haplotypes are associated with multiple sclerosis in Bahrain. Biomedical reports 9:531-539.

Al-Shammri S., Nelson R. F., Al-Muzairi I. and Akanji A. O. (2004) HLA determinants of susceptibility to multiple sclerosis in an Arabian Gulf population. Multiple Sclerosis Journal 10:381-386.

Amirzargar A. A., Tabasi A., Khosravi F., Kheradvar A., Rezaei N., Naroueynejad M. et al. (2005) Optic neuritis, multiple sclerosis and human leukocyte antigen: results of a 4-year follow-up study. European journal of neurology 12:25-30.

Amirzargar, A., Mytilineos, J., Yousefipour, A., Farjadian, S., Scherer, S., Opelz, G. et al. (1998) HLA class II (DRB1, DQA1 and DQB1) associated genetic susceptibility in Iranian multiple sclerosis (MS) patients. European journal of immunogenetics, 25: 297-301.

Bergamaschi L., Ban M., Barizzone N., Leone M., Ferrante D., Fasano M. E. et al. (2011) Association of HLA class I markers with multiple sclerosis in the Italian and UK population: evidence of two independent protective effects. Journal of medical genetics 48:485-492.

Bergamaschi L., Leone M. A., Fasano M. E., Guerini F. R., Ferrante D., Bolognesi E. et al. (2010) HLA-class I markers and multiple sclerosis susceptibility in the Italian population. Genes & Immunity 11:173-180.

Browne P., Chandraratna D., Angood C., Tremlett H., Baker C., Taylor B. V., et al. (2014) Atlas of multiple sclerosis 2013: a growing global problem with widespread inequity. Neurology 83:1022-1024.

Brynedal B., Duvefelt K., Jonasdottir G., Roos I. M., Åkesson E., Palmgren, J. et al. (2007) HLA-A confers an HLA-DRB1 independent influence on the risk of multiple sclerosis. PloS One 2:664.

Etemadifar M., Janghorbani M, Shaygannejad V. and Ashtari, F. (2006) Prevalence of multiple sclerosis in Isfahan, Iran. Neuroepidemiology 27:39-44.

Etemadifar, M. and Maghzi, A.H. (2011) Sharp increase in the incidence and prevalence of multiple sclerosis in Isfahan, Iran. Multiple Sclerosis Journal 17:1022-1027.

Fogdell-Hahn A., Ligers A., Grønning M., Hillert J. and Olerup O. (2000) Multiple sclerosis: a modifying influence of HLA class I genes in an HLA class II associated autoimmune disease. Tissue antigens 55:140-148.

Galehdari H., Mohaghegh M., Majdinasab N., Khatami S. R. and Hosseini Behbahani M. (2018) Analysis of HLA-A*03 in Multiple Sclerosis Patients in Khuzestan Province, Iran. Gene, Cell and Tissue 2018; 5.

Ghanavati R., Shafiei M. and Galehdari H. (2018) Association Between HLA-A*02 Genotype and Multiple Sclerosis in Khuzestan Province, Iran. Jundishapur Journal of Health Sciences 10.

Haff LA. (1994) Improved quantitative PCR using nested primers. Genome Research 3: 332-7.

Harbo HF, Lie BA, Sawcer S, Celius EG, Dai KZ, Oturai A, et al. (2004) Genes in the HLA class I region may contribute to the HLA class II-associated genetic susceptibility to multiple sclerosis. Tissue antigens 63: 237-47.

Horton R., Wilming L., Rand V., Lovering R. C., Bruford E. A., Khodiyar V. K. et al. (2004) Gene map of the extended human MHC. Nature Reviews Genetics 5:889-899.

Isobe N., Gourraud P. A., Harbo H. F., Caillier S. J., Santaniello A., Khankhanian P. et al. (2013) Genetic risk variants in African Americans with multiple sclerosis. Neurology 81:219-227.

Kalanie H., Kamgooyan M., Sadeghian H. and Kalanie A. R. (2000) Histocompatibility antigen (HLA) associations with multiple sclerosis in Iran. Multiple Sclerosis Journal, 6:317-319.

Kankonkar S., Singhal B. S. and Shankarkumar U. (2012) HLAA, B, Cw. DRB1 and DQB1 Alleles in Multiple Sclerosis Patients in India. International Journal of Human Genetics 12:37-40.

Kloverpris H. N., Stryhn A. and Harndahl M. (2012) HLA-B*57 Micropolymorphism Shapes HLA Allele-Specific Epitope Immunogenicity, Selection Pressure, and HIV Immune Control. Journal of virology 86:919–929.

Link J., Kockum I., Lorentzen Å. R., Lie B. A., Celius E. G., Westerlind H. et al. (2012) Importance of human leukocyte antigen (HLA) class I and II alleles on the risk of multiple sclerosis. PloS One 7:367-379.

Lotfi J., Nikbin B., Derakhshan I., Aghai Z. and Ala F. (1978) Histocompatibility antigens (HLA) in multiple sclerosis in Iran. Journal of Neurology, Neurosurgery & Psychiatry 41:699-701.

McDonald W. I., Compston A., Edan G., Goodkin D., Hartung H. P., Lublin F. D. et al. (2001) Recommended diagnostic criteria for multiple sclerosis: guidelines from the International Panel on the diagnosis of multiple sclerosis. Annals of Neurology: Official Journal of the American Neurological Association and the Child Neurology Society 50:121-127.

Mohammadi-Milasi F., Mahnam K. and Shakhsi-Niaei M. (2020) In silico study of the association of the HLA-A* 31:01 allele (human leucocyte antigen allele 31: 01) with neuroantigenic epitopes of PLP (proteolipid protein), MBP (myelin basic protein) and MOG proteins (myelin oligodendrocyte glycoprotein) for studying the multiple sclerosis disease pathogenesis. Journal of Biomolecular Structure and Dynamics 39: 2526-2542.

Naito S., Namerow N., Mickey M. R. and Terasaki P. I. (1972) Multiple sclerosis: association with HL—A3. Tissue antigens 2:1-4.

Radmehr M, Meghdadi S, Bahmanzadeh M. and Sabbagh S. (2015) Prevalence, demographics and clinical characteristics of multiple sclerosis in North of Khuzestan Province, Iran. Jentashapir. Journal of Cellular and Molecular Biology 6:e23831.

Ramagopalan S. V., Knight J. C. and Ebers G. C. (2009) Multiple sclerosis and the major histocompatibility complex. Current opinion in neurology 22:219-225.

Rioux J.D., Goyette P., Vyse T. J., Hammarström L., Fernando M. M., Green T. et al. (2009) Mapping of multiple susceptibility variants within the MHC region for 7 immune-mediated diseases. Proceedings of the National Academy of Sciences 106:18680-18685.

Rubio J. P., Bahlo M., Butzkueven H., van Der Mei I. A., Sale M. M., Dickinson J. L. et al. (2002) Genetic dissection of the human leukocyte antigen region by use of haplotypes of Tasmanians with multiple sclerosis. The American Journal of Human Genetics 70:1125-1137.

Silva A. M., Bettencourt A., Pereira C., Santos E., Carvalho C., Mendonça D. et al. (2009) Protective role of the HLA–A*02 allele in Portuguese patients with multiple sclerosis. Multiple Sclerosis Journal 15:771-774.

Tolou-Ghamari Z. (2015) Preliminary Study of Differences Between Prevalence of Multiple Sclerosis in Isfahan and its' Rural Provinces. Archives of Neuroscience 2:e60043.

Weiner H. L. (2008) A shift from adaptive to innate immunity: a potential mechanism of disease progression in multiple sclerosis. Journal of Neurology 255:3-11.

Weissert R. (2013) The immune pathogenesis of multiple sclerosis. Journal of Neuroimmune Pharmacology 8:857-866.

Werneck L. C., Lorenzoni P. J., Arndt R. C., Kay C. S. K. and Scola R. H. (2016) The immunogenetics of multiple sclerosis. The frequency of HLA-alleles class 1 and 2 is lower in Southern Brazil than in the European population. Arquivos de neuro-psiquiatria 74:607-616.

Yeo TW, De Jager PL, Gregory SG, Barcellos LF, Walton A, Goris A, et al. (2007) A second major histocompatibility complex susceptibility locus for multiple sclerosis. Annals of Neurology: Official Journal of the American Neurological Association and the Child Neurology Society 61: 228-36.

Research Article

Alternative Splicing Novel lncRNAs and Their Target Genes in Ovine Skeletal Muscles

Saad Badday Betti[1,2], Mojtaba Tahmoorespur[1*], Ali Javadmenesh[1,3]

[1]*Department of Animal Science, Faculty of Agriculture, Ferdowsi University of Mashhad, Iran*
[2]*Chief of Agricultural Engineers, Ministry of Agriculture, Baghdad, Iraq*
[3]*Stem Cell Biology and Regenerative Medicine Research Group, Research Institute of Biotechnology, Ferdowsi University of Mashhad, Mashhad, Iran*

Received 9 January 2022 Accepted 18 February 2022

Abstract

Long non-coding RNAs (lncRNAs) compose a plentiful category of transcripts that have gained increasing importance because of their roles in different biological processes. Although the function of most lncRNAs remains unclear. They are implicated in epigenetic regulation of gene expression, including muscle development and differentiation. We aimed to identify the effect of novel lncRNAs (Alternatively spliced) and their target genes on two stages of sheep skeletal muscle growth and development. FastQC files have been used to examine the quality control and the Trimmomatic program for trimming low-quality reads from twelve longissimus dorsal muscle tissue samples (including six young and six old from Texel sheep). Hisat2, Cufflink, Cuffmerge, and Cuffdiff investigated the expression levels. Novel lncRNAs (Alternative spliced) were distinguished using NONCODE databases and Cuffcompare software. In addition, the lncRNA–mRNA interactions and regulatory network visualization were identified via RIsearch and Cytoscape software, respectively. Those 139 novel lncRNA (Alternative spliced) transcripts had been recognized, probably 65 lncRNAs interacted with their target genes and regulated sheep skeletal muscle growth and development. Three novel lncRNA transcripts (TCONS_00041386, TCONS_00050059, and TCONS_00056428) showed a strong association and five transcripts (TCONS_00055761, TCONS_00055762, TCONS_00055763, TCONS_00055764, and TCONS_00055770) had made complex network correlations with mRNAs. Our research provided more knowledge of the associated mechanisms with novel lncRNAs, which could play a role in regulating sheep skeletal muscle tissue development and growth.

Keywords: *Regulatory network, Novel lncRNAs, Skeletal muscle, Alternative splicing, Gene expression*

Introduction

Enhanced knowledge of the myogenesis molecular mechanisms of the livestock (especially ram and lamb) may help raise meat production (Relaix and Zammit, 2012, Rashidian et al., 2020). Texel is a breed of domestic sheep that originates from the island of Texel in the Netherlands. It is a well-muscled sheep, produces a lean meat carcass, and will pass on this quality to its offspring. It is currently the popular sheep in Europe, Australia, New Zealand, and the United States. The most notable feature of Texel is its significant muscle growth and mass (double muscling phenotype) (Clark et al., 2018). Texel Lambs show the advantage of having a full leg score among breed comparisons and less total carcass fat especially contact fat (Kinka and Young, 2019).

RNA-seq (RNA-sequencing) is a technique that can examine RNA quantity and sequences via next-generation sequencing (NGS). It analyzes the transcriptome profile of the cells (or gene expression patterns) in different groups or treatments to understand the related biological processes, such as skeletal muscle growth and development (Badday betti et al., 2022). Some genes can have several promoter regions a tissue-specific expression pattern (Ghanipoor-Samami and Javadmanesh, 2018). Alternative spliced (class-code"j") is a multi-exon with at least one junction match (Pertea and Pertea, 2020). Non-coding RNAs less than 200 bp are known as small ncRNAs and consist of small nuclear RNAs (snRNA), ribosomal RNA (rRNA), transfer RNA (tRNA), small nucleolar RNAs (snoRNA), Piwi-interacting RNAs (piRNAs), small interfering RNAs (siRNAs) and microRNAs (miRNAs). Non-

* Corresponding author's e-mail address: *tahmoores@um.ac.ir*

coding RNAs with more than 200 bp length have been classified as long non-coding RNAs (Neguembor et al., 2014). The gene expression profiling and in situ hybridization investigations have discovered that lncRNA expression is developmentally controlled, can be cell- and tissue-type specific, and can differ temporally, spatially, or in response to the stimulants (Derrien et al., 2012). To date, only some lncRNAs have been identified in detail (Badday Betti et al., 2022).

Nevertheless, lncRNAs are believed to have a broad range of cellular and developmental functions and have been introduced as significant gene expression regulators. LncRNAs may perform either gene expression inhibition or activation via different mechanisms, complicating our understanding of genomic regulation. It is predestined that 25 – 40% of coding genes have overlapping antisense transcriptions. LncRNAs are differentially expressed through three developmental muscle periods in sheep, which might have vital functional roles in myogenic differentiation (Chao et al., 2016). LncRNAs such as H19 play a role in multiple biological processes, including negative regulation of body weight, cell proliferation, and embryonic growth control (Gabory et al., 2009; Gabory et al., 2010). LncRNAs have different classifications based on gene conservation or functions and play a role in chromatin modeling and genomic localization (Ramakrishnaiah et al., 2020). LncRNAs can regulate muscle growth and differentiation through cis-regulatory, trans-regulatory, or competitive endogenous RNAs, indicating that lncRNAs could be important muscle growth regulatory factors and potential valuable molecular marker regions for mutton sheep breeding (Ballarino et al., 2015). Ovine lncRNAs may be involved in skeletal muscle development in Texel and Ujumqin. These results revealed that lncRNAs like TCONS_00044801, TCONS_00008482, and TCONS_00102859 participate in muscle development (Li et al., 2018).

A total of 39 differentially expressed lncRNAs were detected in mutton sheep. Subsequent bioinformatics analyses revealed that 29 lncRNAs were associated with muscle development, metabolism, cell proliferation, and apoptosis. Six lncRNAs noticed as hub lncRNAs, and four lncRNAs showed potential regulatory relationships (Chao et al., 2018). Consequently, in our study, we aimed to identify the effect of novel lncRNAs (Alternative spliced) and their target genes to improve knowledge of their roles in sheep skeletal muscle growth and development at early and adult stages. Also, it might provide a vision about the regulatory genes and put the foundation for selection programs to improve the meat production policies in sheep.

Materials and Methods

Data Collection

We retrieved the RNA raw reads (paired-end) with accession numbers ERR4891 and ERR4892 for analysis based on the Ensemble database. Twelve samples represented at two diverse functional stages: six muscle tissue (longissimus dorsal) samples (ERR489116_1_fastqc to ERR489121_2_fastqc) of Texel juvenile 6-10 months, and six samples (ERR489188_1_fastqc to ERR489189_2_fastqc and from ERR489242_1_fastqc to ERR489245_2_fastqc) for adults (above one year). The sanger/Illumina 1.9 platform had been used for sequencing these samples. Sheep reference genome (Oar_v3.1) and annotated the GTF file (Oar_v3.1.96) based on the Ensemble database had been downloaded.

RNA Sequences Data Analysis

141079400 raw reads were generated by Illumina 1.9 platform with 2×151 bp paired-end reads before trimming was used, and the quality was analyzed by FastQC (v0.11.5) software (Andrews, 2010). Accordingly, we obtained clean data by removing contamination reads, including bases below quality reads, adapters, and low-quality reads using Trimmomatic software (v.0.36) (Bolger et al., 2014). Finally, reads with a minimum Phred quality score of 20 and 36 bp as a minimum length retained.

LncRNA Identification Pipeline

We used the pipeline in Figure S1 (in the supplementary part) to distinguish the candidate lncRNAs. The sheep genome (Oar_v3.1) was indexed in the first step, and the clean reads were aligned via Hisat2-build (Kim et al.,2015). We converted output SAM files from Hisat2 software to BAM files and sorted all BAM files using Samtools software v.1.9 (Li et al.,2009). The mapped reads had assembled using Cufflinks software (v2.2.1.OSX_x86_64) (Trapnell et al., 2010). All GTF files for 12 samples have merged, and the expression level of transcripts (Alternative spliced) had detected by using Cuffmerge software(v2.2.1) (Trapnell et al., 2012).

In the second step, candidate transcripts were identified with class code (Alternative spliced = j) using Cuffcompare software (v2.2.1) (Trapnell et al., 2010), based on related annotation GTF file (Oar_v3.1.96). The pipeline with the following criteria used to detect the potential novel lncRNAs

(Alternative spliced):

1-The transcripts with length ≥ 200 bp retained.
2-The transcripts with exon number < 2 had been removed.
3-The protein-coding potential of transcripts was filtered using two tools CPC2 (score > 0.5) (Kang et al., 2017) and PLEK (score > 0) (Li et al., 2014). The transcripts predicted as non-coding potential using the two tools above have remained.
4-We predicted the open reading frame (ORF) using the TransDecoder tool (v5.5.0) (https://transdecoder.github.io/), and ORF < 300 aa retained.
5-Novel lncRNAs (Alternative spliced) were distinguished using NONCODE databases (v.5) (Fang et al., 2018) http://www.noncode.org/.

Interactions of Novel lncRNAs with Potential Target Genes

The mRNA stability can be modulated by lncRNA (Ramakrishnaiah et al., 2020). We considered each "gene_biotype = mRNA" group in the annotation GTF file (Oar_v3.1.96) as potential target mRNAs. Interaction between lncRNAs–mRNAs had performed to investigate the target mRNA genes, which may organize by the novel lncRNAs using the RIsearch software (RNA Interaction search) (Wenzel et al., 2012) under base-pairing free energy no more than -50 agreement with (Yuan et al., 2020).

Construction of lncRNA-mRNA Network

Cytoscape software v.3.7.2 (Shannon et al., 2003) had been used to visualize the lncRNAs-mRNAs regulatory network

Result

RNA Sequencing and Mapping

Possible functional lncRNAs in parallel to alternatively spliced novel lncRNAs that may implicate the growth and development of sheep skeletal muscle tissue had been identified. Results for quality control, trimming, and mapping for 12 samples had been mentioned in (Table 1).

Table 1. The results for Quality control trimming and mapping had gained per 12 samples

Name of samples	stage	Raw reads before trimming	Raw reads after trimming	GC content (%)	Aligned concordantly exactly %	Overall alignment rate %
ERR489116_1_fastqc / ERR489116_2_fastqc	young	8647125	6622025	44	42.20	83.14
ERR489117_1_fastqc / ERR489117_2_fastqc	young	13368944	10132560	45	51.08	94.46
ERR489118_1_fastqc / ERR489118_2_fastqc	young	13756065	10454415	45	51.17	94.38
ERR489119_1_fastqc / ERR489119_2_fastqc	young	8685734	6641245	44	43.72	84.72
ERR489120_1_fastqc / ERR489120_2_fastqc	young	13374250	10156487	45	51.11	94.52
ERR489121_1_fastqc / ERR489121_2_fastqc	young	13831915	10539372	45	50.79	94.49
ERR489188_1_fastqc / ERR489188_2_fastqc	adult	19697023	15023092	46	63.77	94.04
ERR489189_1_fastqc / ERR489189_2_fastqc	adult	19792913	10350142	46	63.94	94.22

ERR489242_1_fastqc / ERR489242_2_fastqc	adult	9016506	7220274	45	50.03	91.87
ERR489243_1_fastqc / ERR489243_2_fastqc	adult	5771315	4633682	45	48.80	89.71
ERR489244_1_fastqc / ERR489244_2_fastqc	adult	9285314	7445816	45	50.25	91.85
ERR489245_1_fastqc / ERR489245_2_fastqc	adult	5852296	4703164	45	48.11	89.99

Total raw reads before trimming =141079400
Total raw reads after trimming = 103922274
Total of low-quality reads was removed = 37157126
Average aligned concordantly exactly = 51.2475%
Average overall alignment rate = 91.44917%
Average GC content = 45%

Identification of Novel lncRNAs in Skeletal Muscle of Sheep

Five criteria had used to distinguish the novel lncRNAs (Alternative spliced) using pipeline (Figure S1) at the two stages (young and adult) of skeletal muscle tissue in sheep. First, we filtered 649300 transcripts with class code = j (Alternative spliced) using Cuffcompare software. The remaining transcripts (368099) had classified as class code = j (Alternative spliced). Approximately 56% of assembly transcripts were discarded by choosing class code = j. 358072 transcripts had removed by submitting the retrained transcripts (368099) for filtering length < 200bp and exon number < 2. A total of 10027 remaining transcripts had subjected to predict coding potential using two tools CPC2 (score > 0.5) (Kang et al., 2017) and PLEK (score > 0) (Li et al. 2014). We obtained 2910 coding and non-coding transcripts, only 310 transcripts had considered as a non-coding potential, and any coding transcript in one of the two tools was removed. The non-coding transcripts had submitted to remove ORF ≥ 300 aa using the TransDecoder tool (v5.5.0). We subjected 308 of the remaining non-coding transcripts to identify the novel lncRNAs (Alternative spliced) using NONCODE databases (v.5). At last, we introduced 139 potential novel lncRNAs.

Interaction Between Novel lncRNAs and Target mRNA Genes

For predicting the binding positions between the novel lncRNAs (Alternative spliced) and targeted mRNA genes, 139 sequences of novel lncRNAs (Alternative spliced) (query) with 10921 sequences of mRNA genes (target) were interacted using RIsearch software (Wenzel et al., 2012) with a threshold of the base-pairing free energy no more than -50. Our findings demonstrated that 65 novel lncRNA transcripts had targeted 263 mRNA genes (Table S1). We have revealed that three novel lncRNA transcripts, TCONS_00041386, TCONS_00050059, and TCONS_00056428, had a strong relationship with targeted mRNA genes, and five novel lncRNA transcripts TCONS_00055761, TCONS_00055762, TCONS_00055763, TCONS_00055764, and TCONS_00055770 had created complicated network correlations with targeted mRNA genes. Moreover, we noticed that six of novel lncRNA transcripts, TCONS_00050059, TCONS_00056428, TCONS_00055761, TCONS_00055762, TCONS_00055763, and TCONS_00055764, had more expression in the young than in the adult stages except for two transcripts, TCONS_00041386 and TCONS_00055770, which had less expression level at the early stage depending on values of transcript expression as fragments per kilobase per million (FPKM).

Construction of lncRNA-mRNA Network

All of 65 novel lncRNA transcripts were selected to construct the interaction network between novel lncRNAs and targeted mRNA genes using Cytoscape software v.3.7.2 (Shannon et al., 2003) (Figure S2). Our results from the regulatory network demonstrated that among 65 novel lncRNA transcripts, TCONS_00041386 connect with 48 mRNA genes, TCONS_00050059 connect with 28 mRNA genes, TCONS_00056428 connect with 20

mRNA genes, and 5 novel lncRNA transcripts (TCONS_00055761, TCONS_00055762, TCONS_00055763, TCONS_00055764 and TCONS_00055770) connect with 146 mRNA genes to construct complex network correlations. We noticed that the *BEST2* and *MFSD4B* genes connection with 18,12 novel lncRNAs, respectively, to form a strong correlation.

Discussion

Accumulating evidence has indicated that long non-coding RNAs (lncRNAs) play vital roles in differentiation, development, and human disease by regulating gene expression (Saliani et al., 2021 and 2022). The lncRNAs with multiple mechanisms have been classified into six main paradigms: R Loop, miRNA decoy or sponge, scaffolds, tripartite helix, stabilizing mRNA, and guides (Ramakrishnaiah et al., 2020). Increasing evidence indicates that lncRNAs can modulate nearly every cellular process through their association with mRNAs, DNAs, miRNAs, and proteins (Li et al., 2019; Badday Betti et al., 2022). Therefore, binding position detections and interaction analysis between novel lncRNAs and targeted mRNA, RIsearch software (Wenzel et al., 2012) were used in which free energy of base binding is no more than -50 (Yuan et al., 2020). In the present study, comprehensive RNA-seq analysis was used to identify the effect of novel lncRNAs (Alternative spliced) and their target mRNA longissimus dorsi muscle tissue samples of sheep in two functional stages.

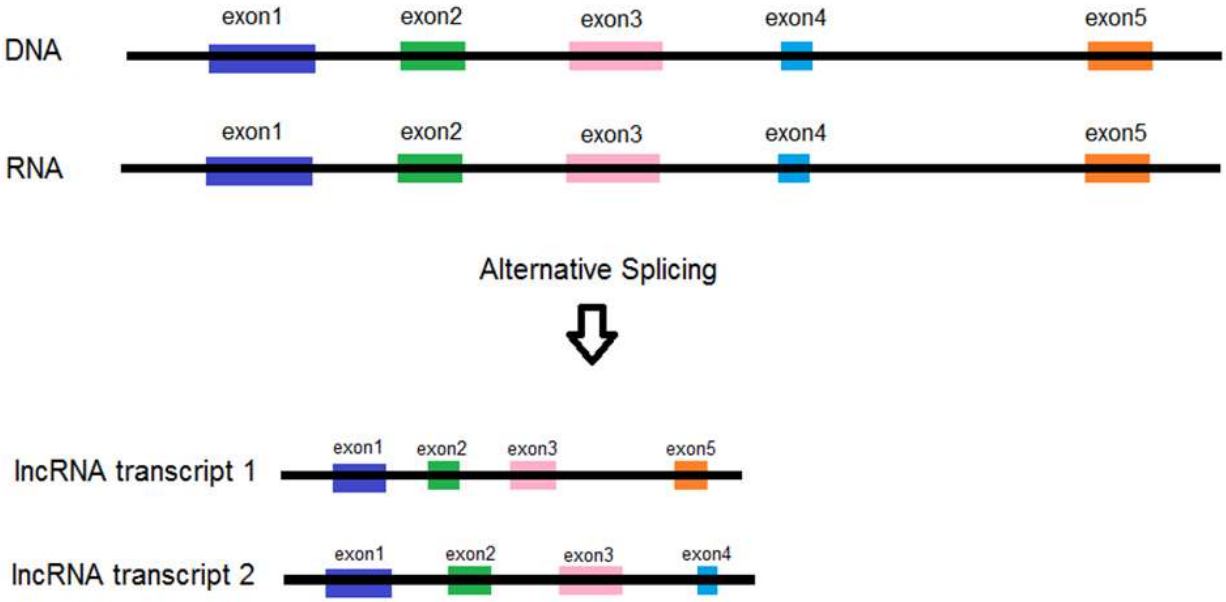

Figure 1. Schematic image of alternative splicing of lncRNA

The results implied the correlation between novel lncRNA transcripts with differential expression levels and muscle tissue in young and adult individuals. mRNA genes targeted by novel lncRNA transcripts extracted from the annotation GTF file for ovine muscle tissue were mentioned in many previous studies in which they play pivotal roles in skeletal muscle growth and development. Our results showed that 65 novel lncRNA transcripts had binding locations with 263 targeted mRNA genes (Yuan et al., 2020, Li et al., 2018 and 2019). Three novel lncRNA transcripts are strongly associated with their targeted genes. For example, TCONS_00041386 targeted 48 genes, TCONS_00050059 targeted 28 genes, and TCONS_00056428 targeted 20 genes. Clark et al. in 2017 showed that only 31 of 48 genes, 14 of 28 genes, and 9 of 20 genes, respectively, had shown differentially expressed in skeletal muscle between Texel (purebred) and T x BF (hybrid Texel x Scottish Blackface) (Clark et al., 2017). In addition, they reported that TCONS_00055769, novel lncRNA, targeted 29 genes and made a complex network, but only 19 out of 29 genes had appeared differentially expressed in skeletal muscle sheep between two breeds (Clark et al., 2017). In agreement with the previous study, TCONS_00047742, TCONS_00035416, and TCONS_00042104 (each separately) interacted with 10 genes but only 5 of 10 genes, 2 of 10 genes, and 3 of 10 genes, respectively, had demonstrated differentially expressed in sheep skeletal (Clark et al., 2017). TCONS_00042100, TCONS_00042102, and TCONS_00042103 interacted with the same 7 genes, but only 2 of 7 genes had mentioned differentially expressed in sheep skeletal muscle (Clark et al., 2017).

The other five lncRNA transcripts correlated with 146 mRNA genes and created complicated networks. For instance, TCONS_00055761 and TCONS_00055763 interacted with the same 27 genes, TCONS_00055762 interacted with 34 genes, TCONS_00055764 interacted with 30 genes, and TCONS_00055770 interacted with 28 genes, among them 18, 21, 18, and 17 genes, respectively also mentioned by Clark et al. to be differentially expressed in sheep skeletal muscle. Additionally, we observed some of these genes such as ENSOARG00000001608, targeted by TCONS_00055762, TCONS_00055770 and TCONS_00055764, ENSOARG00000016908 targeted by TCONS_00055762 and TCONS_00055764, ECI1, and ENSOARG00000015179, ANPEP, ENSOARG00000018514 targeted by TCONS_00041386, NRAP targeted by TCONS_00056428 had higher expression levels in sheep skeletal muscle (fold change (FC) ≥ 2) (Clark et al., 2017). We found the *ABL2* gene targeted by novel transcript TCONS_00055764, also reported by Yuan et al., as one of the differential expression genes in the longissimus dorsi muscle of sheep (Yuan et al., 2020). *HSP90AA1*, *CXCL14*, and *NRAP* genes targeted by novel transcripts TCONS_00041386, TCONS_00050059, and TCONS_00056428, respectively. Lobjois et al. have mentioned *HSP90AA1* gene was involved with the myogenic differentiation and cell proliferation in pig longissimus dorsi muscle (LDM) (Lobjois et al., 2008). It was found that the *CXCL14* gene had a vital role in the cell differentiation of chicken muscles (Nihashi et al., 2019). Noce et al. have shown that the *NRAP* gene was expressed in five breeds of sheep longissimus dorsi muscle (LDM) (Noce et al., 2018). Other genes such as *PCK1*, *IRX3*, *CCND3*, *COLGALT2*, *KCNN1*, *UBE2Q1*, *CCDC88C*, and *SLC25A13* have been targeted by some of the novel transcripts such as TCONS_00041386, TCONS_00050059, TCONS_00055762, TCONS_00055764, TCONS_00055770, and TCONS_00055761 reported with differential expression patterns in skeletal muscle and high and low production mutton sheep.

Our study demonstrated six novel lncRNA transcripts, including TCONS_00050059, TCONS_00056428, TCONS_00055761, TCONS_00055762, TCONS_00055763, and TCONS_00055764, had high expression levels during the early stage compared with an adult. This result agrees with the article reported by Yuan et al. in 2020, which found there are time-specific lncRNA expressions through the pregnancy and after birth stages. Furthermore, they noticed those essential modifications in skeletal muscle development through gestation and newborn stages. In conclusion, we detected three novel lncRNA transcripts (TCONS_00041386, TCONS_00050059, and TCONS_00056428) had a strong relationship with targeted mRNA genes, and five novel lncRNA transcripts (TCONS_00055761, TCONS_00055762, TCONS_00055763, TCONS_00055764, and TCONS_00055770) created complex network correlations with targeted mRNA genes. Six novel lncRNA transcripts (TCONS_00050059, TCONS_00056428, TCONS_00055761, TCONS_00055762,

TCONS_00055763, and TCONS_00055764) had high expression in the young stages than in the adult. Finally, our findings proposed that novel lncRNAs (Alternative spliced) may play a critical role in regulating sheep skeletal muscle growth and development and improving mutton sheep breeding programs. Moreover, it is important to note that finding exact regulatory functions of lncRNAs need more investigation and research.

Conflict of Interest
The authors declare that there are no conflicts of interest.

Acknowledgments
This study was supported by Ferdowsi University of Mashhad, grant number 3/47789.

Supplementary Information
Figure S1. Flow chart of the pipeline used to detect the novel lncRNAs (Alternative spliced)

Table S1. The results of the interaction between novel lncRNAs-mRNAs (Separate file as supplementary file).

Figure S2. Interaction network between novel lncRNAs and their target mRNA genes; red arrows denote lncRNAs, and green circles represent mRNAs. Lines represent the interaction between lncRNAs-mRNAs (Separate file as supplementary file).

References

Andrews S. (2010) FastQC: a quality control tool for high throughput sequence data. Available online. Retrieved May, 17: www.bioinformatics.babraham.ac.uk/projects/fastqc/.

Ballarino M., Cazzella V., D'Andrea D., Grassi L., Bisceglie L., Cipriano A., et al. (2015) Novel long noncoding RNAs (lncRNAs) in myogenesis: a miR-31 overlapping lncRNA transcript controls myoblast differentiation. Molecular and Cellular Biology, 35(4), 728-736.

Badday Betti S., Tahmoorespur M., Javadmanesh A. (2022) Identification of lncRNAs expression and their regulatory networks associated with development and growth of skeletal muscle in sheep using RNA-Seq. Agriculture and Natural Resources, 56(2): 161-174.

Bolger A. M., Lohse M. and Usadel B. (2014) Trimmomatic: a flexible trimmer for Illumina sequence data. Bioinformatics (Oxford,England), 30(15),2114–2120.

Chao T., Ji Z., Hou L., Wang J., Zhang C., Wang G., et al. (2018) Sheep skeletal muscle transcriptome analysis reveals muscle growth regulatory lncRNAs. PeerJ, 6: e4619.

Chao T., Wang G., Wang J., Liu Z., Ji Z., Hou L., et al. (2016) Identification and classification of new transcripts in dorper and small-tailed han sheep skeletal muscle transcriptomes. PLoS One, 11(7), e0159638.

Clark E. L., Bush S. J., McCulloch M. E., Farquhar I. L., Young R., Lefèvre L., et al. (2018) A High Resolution Atlas of Gene Expression in the Domestic Sheep. In Plant and Animal Genome XXVI Conference (January 13-17, 2018). PAG.

Derrien T., Johnson R., Bussotti G., Tanzer A., Djebali S., Tilgner H., et al. (2012) The GENCODE v7 catalog of human long noncoding RNAs: analysis of their gene structure, evolution, and expression. Genome Research, 22(9), 1775-1789.

Fang S., Zhang L., Guo J., Niu Y., Wu Y., Li H., et al. (2018) NONCODEV5: a comprehensive annotation database for long noncoding RNAs. Nucleic Acids Research, 46(D1), D308-D314.

Gabory A., Jammes H. and Dandolo L. (2010) The H19 locus: role of an imprinted noncoding RNA in growth and development. Bioessays, 32(6), 473-480.

Gabory A., Ripoche M. A., Le Digarcher A., Watrin F., Ziyyat A., Forné T., et al. (2009) H19 acts as a trans regulator of the imprinted gene network controlling growth in mice. Development, 136(20), 3413-3421.

Ghanipoor-Samami M., Javadmanesh A., Burns B. M., Thomsen D. A., Nattrass G. S., Estrella C., Kind K. L., et al. (2018) Atlas of tissue- and developmental stage specific gene expression for the bovine insulin-like growth factor (IGF) system. PloS one, 13(7), e0200466.

Kang Y. J., Yang D. C., Kong L., Hou M., Meng Y. Q., Wei L., et al. (2017) CPC2: a fast and accurate coding potential calculator based on sequence intrinsic features. Nucleic Acids Research, 45(W1), W12-W16.

Kim D., Langmead B. and Salzberg S. L. (2015) HISAT: a fast spliced aligner with low memory requirements. Nature Methods, 12(4), 357-360.

Kinka D. and Young J. K. (2019) Evaluating domestic sheep survival with different breeds of livestock guardian dogs. Rangeland Ecology & Management, 72(6), 923-932.

Li A., Zhang J. and Zhou Z. (2014) PLEK: a tool for predicting long noncoding RNAs and messenger RNAs based on an improved k-mer scheme. BMC Bioinformatics, 15(1), 1-10.

Li H., Handsaker B., Wysoker A., Fennell T., Ruan J., Homer N., et al. (2009) The sequence alignment/map format and SAMtools. Bioinformatics, 25(16), 2078-2079.

Li Q., Liu R., Zhao H., Di R., Lu Z., Liu E., et al. (2018) Identification and Characterization of Long Noncoding RNAs in Ovine Skeletal Muscle. Animals, 8(7), 127.

Li Z., Zhao W., Wang M. and Zhou X. (2019) The role of long noncoding RNAs in gene expression regulation, Gene Expression Profiling in Cancer. BoD – Books on Demand, pp. 1-17.

Lobjois V., Liaubet L., SanCristobal M., Glénisson J., Feve K., Rallieres J., et al. (2008) A muscle transcriptome analysis identifies positional candidate genes for a complex trait in pig. Animal Genetics, 39(2), 147-162.

Neguembor M.V., Jothi M. and Gabellini D. (2014) Long noncoding RNAs, emerging players in muscle differentiation and disease. Skeletal Muscle, 4(1): 1-12.

Nihashi Y., Umezawa K., Shinji S., Hamaguchi Y., Kobayashi H., Kono T., et al. (2019) Distinct cell proliferation, myogenic differentiation, and gene expression in skeletal muscle myoblasts of layer and broiler chickens. Scientific Reports, 9(1), 1-15.

Noce A., Cardoso T. F., Manunza A., Martínez A., Cánovas A., Pons A., et al. (2018) Expression patterns and genetic variation of the ovine skeletal muscle transcriptome of sheep from five Spanish meat breeds. Scientific Reports, 8(1), 1-7.

Pertea G. and Pertea M. (2020). GFF utilities: GffRead and GffCompare. F1000Research, 9.

Ramakrishnaiah Y., Kuhlmann L. and Tyagi S. (2020) Towards a comprehensive pipeline to identify and functionally annotate long noncoding RNA (lncRNA). Computers in Biology and Medicine: 104028.

Rashidian, Z., Dehdilani, N., Dehghani, H., Javadmanesh, A. (2020). Isolation and culturing myogenic satellite cells from ovine skeletal muscle. Iranian Journal of Veterinary Science and Technology, 12(2), 36-43.

Relaix F. and Zammit P. S. (2012) Satellite cells are essential for skeletal muscle regeneration: the cell on the edge returns centre stage. Development, 139(16), 2845-2856.

Saliani M., Mirzaiebadizi A., Javadmanesh A., Siavoshi A. and Ahmadian M.R. (2021) KRAS-related long noncoding RNAs in human cancers. Cancer Gene Therapy, 1-10.

Saliani M., Jalal R. and Javadmanesh A. 2022. Differential expression analysis of genes and long non-coding RNAs associated with KRAS mutation in colorectal cancer cells. Scientific Reports, 12: 7965.

Shannon P., Markiel A., Ozier O., Baliga N. S., Wang J. T., Ramage D., et al. (2003) Cytoscape: a software environment for integrated models of biomolecular interaction networks. Genome Research, 13(11), 2498-2504.

Trapnell C., Roberts A., Goff L., Pertea G., Kim D., Kelley D. R., et al. (2012) Differential gene and transcript expression analysis of RNA-seq experiments with TopHat and Cufflinks. Nature Protocols, 7(3), 562-578.

Trapnell C., Williams B. A., Pertea G., Mortazavi A., Kwan G., Van Baren M. J., et al. (2010) Transcript assembly and quantification by RNA-Seq reveals unannotated transcripts and isoform switching during cell differentiation. Nature Biotechnology, 28(5), 511-515.

Wenzel A., Akbaşli E. and Gorodkin J. (2012) RIsearch: fast RNA–RNA interaction search using a simplified nearest-neighbor energy model. Bioinformatics, 28(21), 2738-2746.

Yuan C., Zhang K., Yue Y., Guo T., Liu J., Niu C., et al. (2020) Analysis of dynamic and widespread lncRNA and miRNA expression in fetal sheep skeletal muscle. PeerJ, 8, e9957.

Supplementary Information:

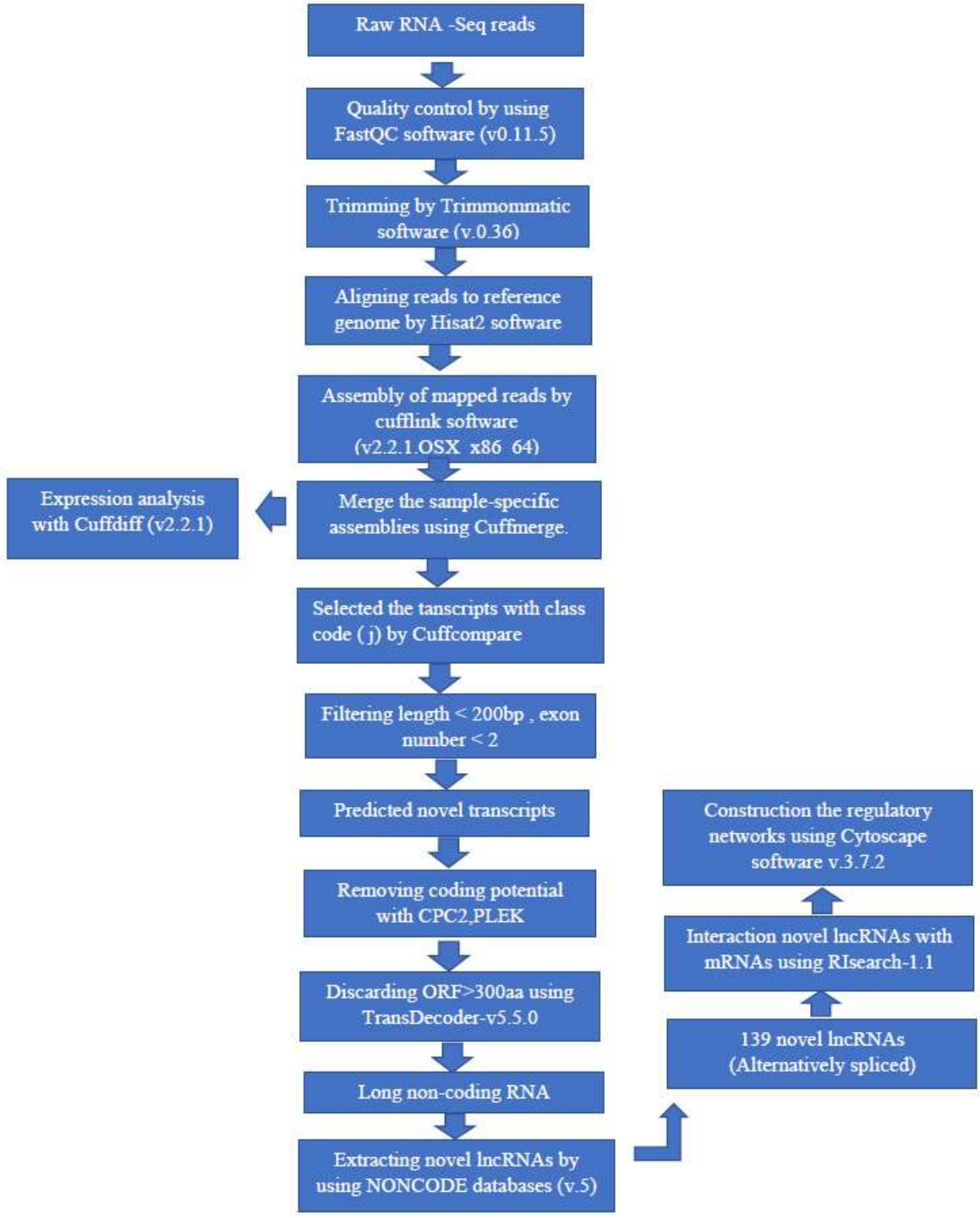

Figure S1. Flow chart for the pipeline was used to detect the novel lncRNAs (Alternative spliced)

Review / Mini-Review

LncRNAs as Regulators of the STAT3 Signaling Pathway in Cancer

Narges ZadehRashki[1¶], Zahra Shahmohammadi[1¶], ZahraSadat Damrodi[1¶], Sohrab Boozarpour [1]*, Arezou Negahdari[2], Nazanin Mansour Moshtaghi[3], Mehdi Vakilinejad[4], Shaaban Ghalandarayeshi[5]

[1]*Department of Biology, Faculty of Basic Sciences, Gonbad Kavous University, Gonbad Kavous, Iran*
[2]*Radiologist, Dr. Arezou Negahdari Ultrasound-Radiology Clinic, Gonbad Kavous, Iran*
[3]*Surgical Oncologists, Dr. Beski Hospital, Gonbad Kavous, Iran*
[4]*Pathologist, Sina Laboratory, Gonbad Kavous, Iran*
[5]*Department of Statistics and Mathematics, Faculty of Basic Sciences, Gonbad Kavous University, Gonbad Kavous, Iran*

Received 19 March 2022 Accepted 18 April 2022

Abstract

Cancer is a disorder of growth control and cell differentiation caused by the abnormal expression of multiple genes. Long non-coding RNAs (lncRNAs) are critical regulators of numerous biological processes, especially in the development of diseases. Abnormal expression of some lncRNAs causes disease, especially cancer, and disease resistance. lncRNAs may act as oncogenes or tumor suppressors and can be used as diagnostic or prognostic markers, and may also have therapeutic potential in cancer treatment. Studies show that many lncRNAs have different effects on cell activity by regulating multiple downstream targets, such as signaling pathways that are signal transducers and activators of transcription 3 (STAT3). The STAT3 signaling pathway is one of the most critical pathways in developing various diseases, including cancer, which plays a vital role in cellular processes, disease onset and progression, and stem cell regeneration by regulating its target genes. STAT3 has been proven to be an anticancer target in various contexts. Types of genes can activate the STAT3 pathway in cancer. Many lncRNAs have been identified associated with the STAT3 pathway that is upstream or downstream. Oncogenic lncRNAs, including PVT1, HOTAIRM1, and MCM3AP-AS1, increase STAT3 expression, while tumor suppressor lncRNAs, such as TSLNC8, TPTEP1, and DILC decrease STAT3 expression. These lncRNAs can affect STAT3 signaling activity through numerous molecular mechanisms, including sponge of microRNAs, transcriptional activation/inhibition, and epigenetic alterations. Numerous studies show that targeting lncRNAs and molecules associated with the STAT3 signaling pathway are promising therapeutic strategies for various cancers. This review highlighted the mechanisms of the upstream lncRNAs of the STAT3 signaling pathway.

***Keywords*:** STAT3 Transcription Factor, Genetics, Oncogenes, Tumor Suppressor, MicroRNAs

Introduction

Cancer is a genetic disease with unbalanced gene expression, disrupting the gene networks responsible for the cellular identity, growth, and natural differentiation (Cheetham et al., 2013). Numerous studies have shown that defects in the regulation of oncogenes or tumor suppressor genes play an important role in tumorigenesis and cancer progression (Guzel et al., 2020; Prensner and Chinnaiyan, 2011). With the development of modern technology, evidence of genome and transcriptome sequence has been demonstrated that the major part (70%) of gene expression products are non-coding ribonucleotides (ncRNAs) (Zhang et al., 2019b). ncRNA molecules that regulate gene expression are classified into two main groups: short and long ncRNAs (lncRNA) (Chan and Tay, 2018). Short ncRNAs include piRNAs, siRNAs, miRNAs (Sana et al., 2012). lncRNAs with over 200 ribonucleotides length are the largest class of ncRNAs. The most common lncRNAs are lincRNAs, asRNAs, pseudogenes and circRNAs (Kulczynska and Siatecka, 2016). lncRNAs, as the most important regulators, are involved in many biological processes, especially in cancer progression (Saliani et al., 2021). lncRNAs have different functional mechanisms at the epigenetic, transcriptional, and post-transcriptional levels by regulating multiple downstream targets such as chromatins, proteins, and RNAs (Figure 1) (Do and Kim, 2018). Previous evidence has shown that deregulation of lncRNA expression may lead to several disorders and diseases, including the development of various

¶ These authors contributed to this study equally.
* Corresponding author's e-mail address:
so.boozarpour@gmail.com

human tumors (Liang et al., 2019; Poursheikhani et al., 2020; Sánchez and Huarte, 2013).

A number of studies revealed that the STAT3 pathway is involved in different types of cancer (de Araujo et al., 2020; Lin et al., 2021; Yang et al., 2005). One of the important strategies to suppress cancers is targeting the STAT3 pathway (Segatto et al., 2018). STAT3 was first discovered in 1994 as a DNA binding protein activated by the EGF and IL-6 (Zhong et al., 1994). Activation of the STAT3 signaling pathway is mediated by growth factor receptors and cytokine receptors such as IL-6 receptor, and non-receptor tyrosine kinases such as EGFR, PDGFR, and SRC (Schroeder et al., 2014). STAT3 is activated through tyrosine and serine phosphorylation via upstream regulators, inducing dimerization of STAT3 molecules (Banerjee and Resat, 2016). The STAT3 activated dimer is transferred to the nucleus and, with the help of a variety of coactivator proteins, including NCOA/SRC1α, APE/Ref1, CBP, binds to regulatory regions of genes involved in different phenotypes of cancer cells (Figure 2) (Qin et al., 2019a). Some targeted genes transcribed by STAT3 include *cyclin D1*, *MYC*, *Survivin*, *SOCSs*, and *MMPs* (Carpenter and Lo, 2014; Johnson et al., 2018). Since the STAT3 signaling pathway regulation can play a pivotal role in controlling various cancers, in this article, we have reviewed the lncRNAs that are related (Figures 3 and 4, Table 1).

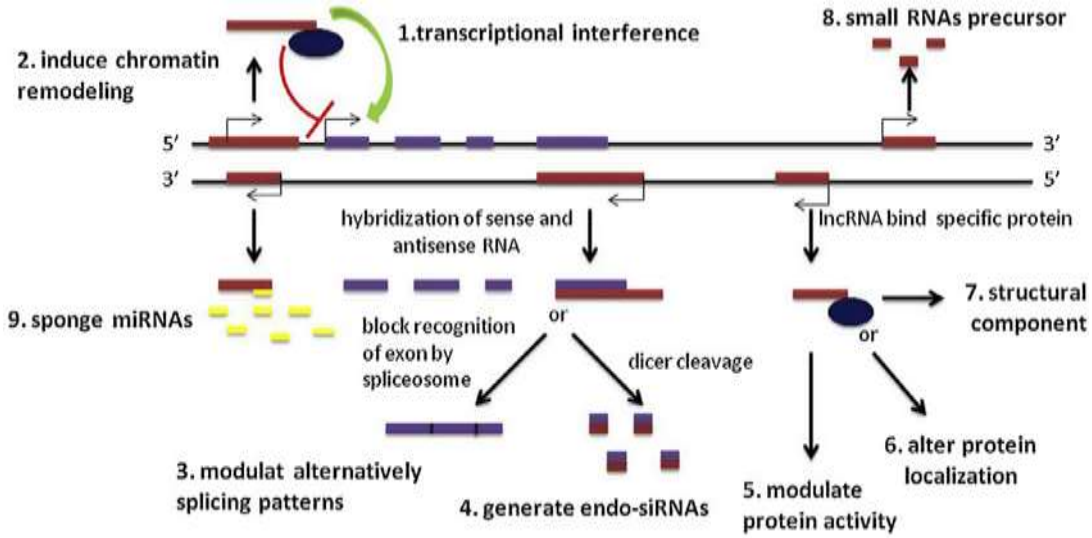

Figure 1. Examples of lncRNAs cellular functions (Shi et al., 2013). They can affect the expression of transcriptional coding genes by chromatin remodeling, negatively (1) or positively (2). Antisense transcripts can be paired with their own specific sense RNAs to alternative forms (3) or endo-siRNA linkages (4). By interacting with proteins, activity (5), their location (6) or even cellular subsets of protein complexes may be affected (7). lncRNAs may process small, single or double stranded RNAs such as endo-siRNAs or miRNAs (8). In addition, they can also act as sponges for miRNAs (9).

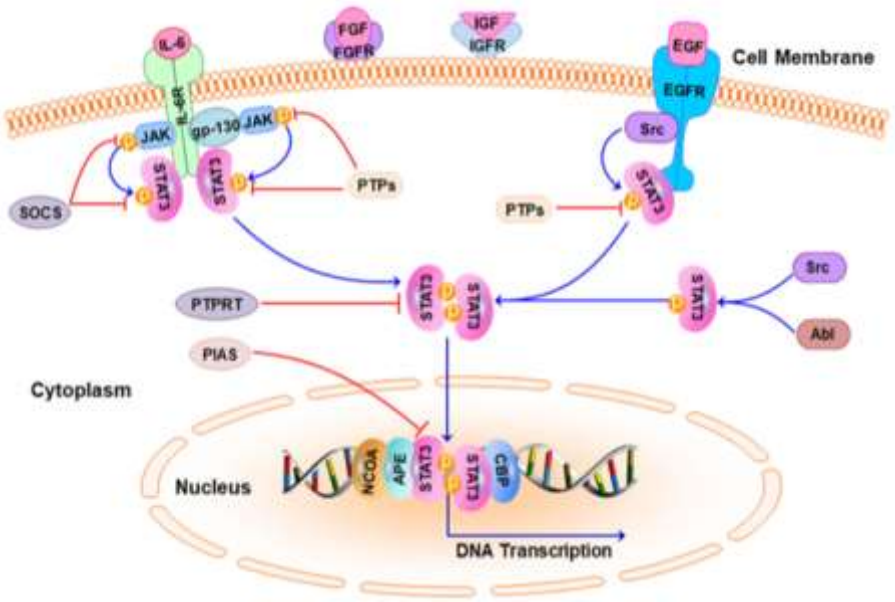

Figure 2. The STAT3 signaling pathway (Qin et al., 2019b).

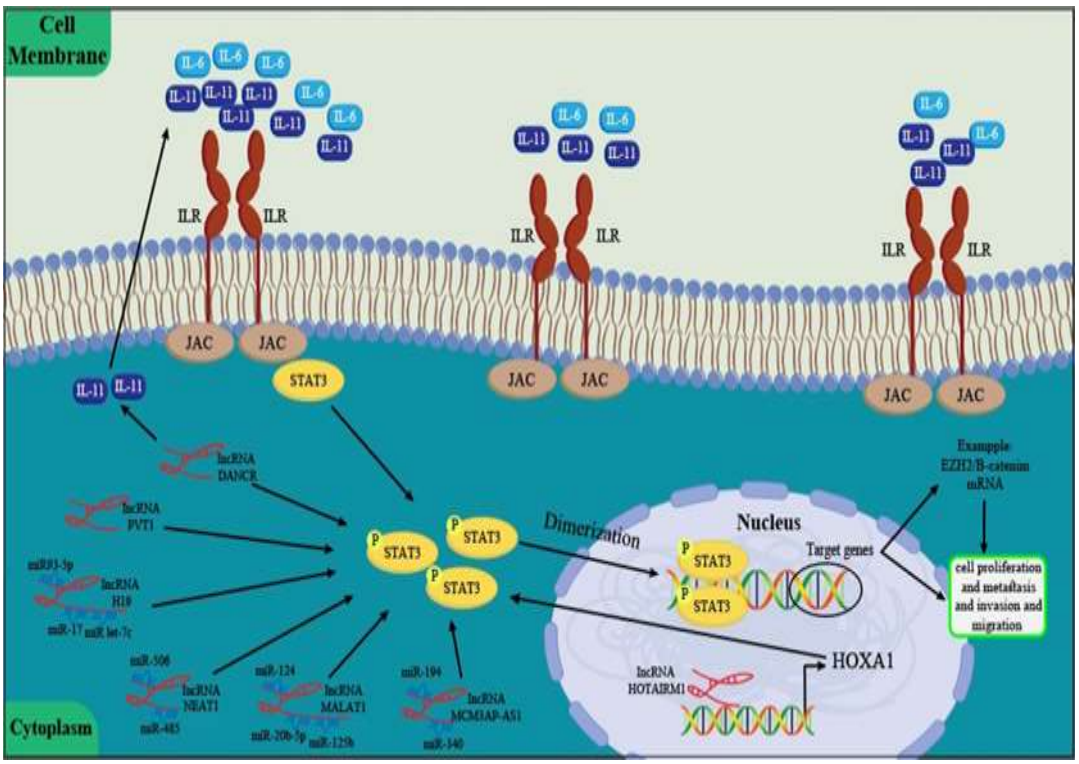

Figure 3. Oncogenic lncRNAs regulate STAT3 signaling pathway.

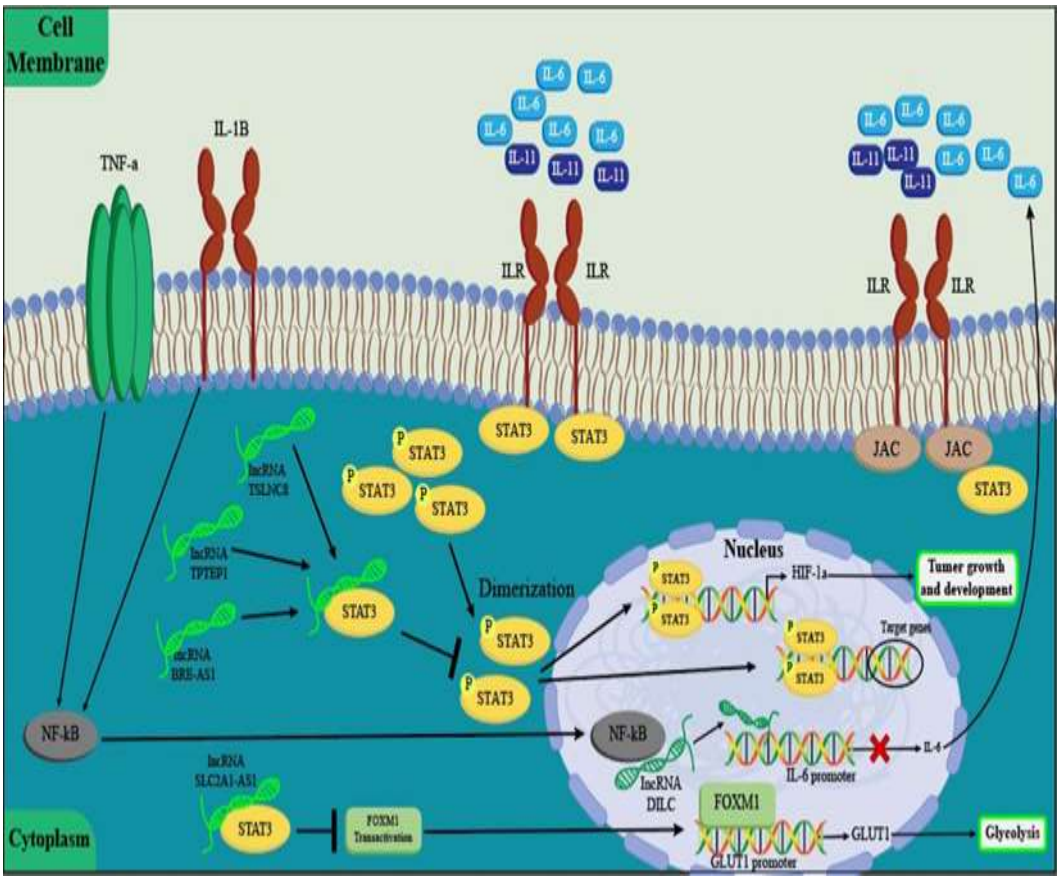

Figure 4. Tumor suppressor lncRNAs regulate STAT3 signaling pathway.

Table 1. LncRNAs that regulate STAT3 pathway

lncRNA name	Coordinate	Up or down-regulation	Type of cancer	Reference
PVT1	chr8:127794526-128187101	up-regulation	Gastric, hepatoblastoma	(Luo and Cao, 2019; Zhao et al., 2020)
MCM3AP-AS1	chr21:46228977-46259390	up-regulation	Lung, hepatocellular carcinoma (HCC)	(Li et al., 2020; Wang et al., 2019)
HOTAIRM1	chr7:27095647-27100265	up-regulation	Endometrial, breast, glioblastoma, leukemia	(Díaz-Beyá et al., 2015; Kim et al., 2020; Li et al., 2018a; Li et al., 2019c; Xia et al., 2020; Xie et al., 2021)
MALAT1	chr11:65496266-65509085	up-regulation	Retinoblastoma, Non-small-cell lung carcinoma (NSCLC), Oral squamous cell carcinoma (OSCC)	(Chang and Hu, 2018; Li et al., 2018b; Wang et al., 2020b)
NEAT1	chr11:65416581-65450093	up-regulation	Gastric, HCC	(Tan et al., 2019; Zhang et al., 2018b)

H19	chr11:1995129-2001710	up-regulation	Lung, breast, esophageal	(Chen et al., 2019a; Li et al., 2019a; Liu et al., 2019)
DANCR	chr4:52712257-52723623	up-regulation	Bladder, nasopharyngeal	(Chen et al., 2019b; Zhang et al., 2019c)
TSLNC8	chr8:29667485-29748124	down-regulation	HCC, lung	(Fan et al., 2019; Zhang et al., 2018a)
TPTEP1	chr22:16601887-16698742	down-regulation	HCC	(Ding et al., 2019)
SLC2A1-AS1	chr1:42958277-43196506	down-regulation	HCC	(Shang et al., 2020)
BRE-AS1	chr2:27889455-27891114	down-regulation	Bladder	(Zhang et al., 2020)
DILC	chr13:114239003-114295788	down-regulation	Bladder, CRC, liver	(Gu et al., 2018; Li et al., 2019b; Ma et al., 2019; Wang et al., 2016)
GAS5	chr1:173851284-173869006	down-regulation	Cervical	(Fang et al., 2020; Yao et al., 2019)

Oncogenic LncRNAs Regulate the STAT3 Signaling Pathway

LncRNA PVT1

LncRNA PVT1 is a long non-coding RNA transcribed from the human *PVT1* (plasmacytoma variant translocation 1) gene at position chromosome 8:127794526-128187101. lncRNA PVT1 is involved in various mechanisms such as protein interactions, targeting of regulatory genes, increased expression, and competing endogenous RNA (ceRNA) (Onagoruwa et al., 2020). In hepatoblastoma, lncRNA PVT1 is up-regulated and positively associated with progression and metastasis. lncRNA PVT1 activates the transcription of downstream targets involved in cell cycle progression by activating the STAT3 signaling pathway. In addition, selective inhibition of STAT3 by the Static results in loss of lncRNA PVT1 function in the pre-proliferation of hepatoblastoma cells. Due to the association of lncRNA PVT1 with hepatoblastoma malignancy and poor prognosis, it has been suggested to be used as a biomarker to improve classification and help in treatment decisions for hepatoblastoma patients (Luo and Cao, 2019). Also, lncRNA PVT1 plays an important role in regulating angiogenesis and VM formation via the STAT3 signaling pathway in gastric cancer. lncRNA PVT1 interacts directly with the STAT3 transcription activator and activates STAT3 via a stem-loop structure in the region of 850-1770. lncRNA PVT1 increases VE-cadherin, N-cadherin, and Slug proteins expression and decreases E-cadherin expression, which is significantly reversed by inhibiting STAT3. Furthermore, inhibition of STAT3 reduces the number of VM capillaries promoted by PVT1. Therefore, blocking the lncRNA PVT1/STAT3 axis can be a promising strategy in targeted therapy in gastric cancer patients (Zhao et al., 2020).

LncRNA MCM3AP-AS1

LncRNA MCM3AP-AS1 is an antisense transcript from the *MCM3AP* coding gene, located on chromosome 21:46228977-46259390, identified for the first time in lung cancer (Reymond et al., 2002; Yu et al., 2015). Many mechanisms involved in the development of cancers are affected by lncRNA MCM3AP-AS1, including cell proliferation (Yuan et al., 2016b), tumor angiogenesis (Yang et al., 2017), and cell survival (Zhang et al., 2019a). lncRNA MCM3AP-AS1 mainly functions as an oncogene; nevertheless, in some cases acts as a tumor suppressor (Zhu et al., 2019). lncRNA MCM3AP-AS1 mainly serves as a ceRNA and downregulates tumor suppressor microRNAs such as miR-340, miR-143-3P, miR-194-5P, therefore can restore the oncogenic function of an mRNA targeted molecules. In HCC, miR-340 decreases the activation of the STAT3 signaling pathway by downregulating *JAK1*, reducing the expression of Bcl-2, cyclin D1, and the MMP2 (Li et al., 2020; Yuan et al., 2017). Moreover, miR-194, as a lncRNA MCM3AP-AS1 target, directly acts on *SOCS2* gene transcripts, thereby up-regulated STAT3 signaling pathway. Targeting *SOCS2* by miR-194 reduces oncogenic kinases FLT3 and JAK2 and ultimately increases ERK and STAT3 signaling (Das et al., 2017; Wang et al., 2019).

LncRNA HOTAIRM1

LncRNA HOX antisense intergenic RNA myeloid 1 (*HOTAIRM1*) is located on chromosome 7:27095647-27100265 in the HOXA gene cluster between *HOXA1* and *HOXA2* genes (Zhang et al., 2009). lncRNA HOTAIRM1 has two spliced cytoplasmic isoforms, HM1-3 (775 nucleotides in length) and HM1-2-3 (1044 nucleotides in length), and the un-spliced form HOTAIRM1 mainly was observed in the nucleus (Hamilton et al., 2020). lncRNA HOTAIRM1 was initially identified as an important factor in granulocyte differentiation of human NB4 promyelocytic leukemia (Zhang et al., 2009). lncRNA HOTAIRM1, as an oncogenic, abnormally increases in a type of human tumors. lncRNA HOTAIRM1 and *HOXA1* gene are involved in tumorigenicity of human cancers, including endometrial (Li et al., 2019c), breast (Kim et al., 2020), glioblastoma (Xia et al., 2020; Xie et al., 2021) and leukemia (Díaz-Beyá et al., 2015). LncRNA HOTAIRM1 activates *HOXA1* gene transcription by reducing histone and DNA methylation. Thus, the local epigenetic status of the *HOXA1* gene and its expression is positively regulated by lncRNA HOTAIRM1 (Li et al., 2018a). Up-regulation of *HOXA1* in breast epithelial cancer cells increases the expression of JAK-STAT pathway components (STAT3 and 5B), leading to increased cell proliferation, survival, and oncogenicity. Therefore, lncRNA HOTAIRM1 controls the expression of JAK-STAT pathway components by regulating HOXA1 expression (Mohankumar et al., 2008).

LncRNA MALAT1

Hence lncRNA MALAT1, first characterized in non-small cell lung cancer (NSCLC), the transcripts called the lung adenocarcinoma associated with metastasis 1. lncRNA MALAT1, also known as nuclear-enriched transcript 2 (NEAT2), with 8.5 kb in length and located on chr11:65496266-65509085 (Sun and Ma, 2019). lncRNA MALAT1 plays an important role in the cell proliferation, cell death, cell cycle, migration, invasion, immunity, angiogenesis and tumorigenesis by regulating numerous signaling pathways such as MAPK/ERK (Chen et al., 2016a; Liu et al., 2018), PI3K/AKT (Dong et al., 2015), WNT/β-catenin (Liang et al., 2017), NF-κB (Zhao et al., 2016) and STAT3. miR-124 has been studied in various malignant tumors, including prostate cancer (Lashkarboloki et al., 2020), retinoblastoma (Hu et al., 2018), esophageal squamous cell carcinoma (Li et al., 2019d), and is associated with lncRNAs and STAT3. Overexpression of lncRNA MALAT1 has been shown in five human NSCLC cell lines, including A549, H23, H522, H1299, and H460. Luciferase reporter assay showed that miR-124 was targeted directly by lncRNA MALAT1 and STAT3. These results were confirmed with *in vitro* analysis in NSCLC cell lines, as the inhibition of lncRNA MALAT1 and miR-124 expression reduced and increased STAT3 expression, respectively. Therefore, the MALAT1/miR-124/STAT3 axis could be a key player in developing NSCLC (Li et al., 2018b). In addition, a positive relationship was reported between MALAT1 and STAT3 in Retinoblastoma (RB) cells. lncRNA MALAT1, by sponging miR-20b-5p, can up-regulate STAT3, increasing proliferation and decreasing apoptosis in RB cells (Wang et al., 2020b). Moreover, high expression of lncRNA MALAT1 and low expression of miR-125b were observed in OSCC cell lines, including Tca8113, SCC-25, CAL-27, and HN5 cells compared to normal human oral cell line Hs680.Tg. At the same time, lncRNA MALAT1 served as a ceRNA and modulated STAT3 expression with sponging miR-125b in OSCC in both *in vitro* and *in vivo*. So, it has been suggested that lncRNA MALAT1 plays an oncogenic role in development and progression of OSCC with a modulating miR-125b/STAT3 axis. Down-regulation of lncRNA MALAT1 induces apoptosis and inhibits cell viability of OSCC cells *in vitro*. Moreover, these findings suggest that lncRNA MALAT1 can be used as a therapeutic target in the early diagnosis and treatment of OSCC (Chang and Hu, 2018).

LncRNA NEAT1

Nuclear paraspeckle assembly transcript 1 (NEAT1) is transcribed from the familial tumor syndrome multiple endocrine neoplasia (*MEN*) type 1 gene located on chr11:65416581-65450093 (Dong et al., 2018). NEAT1 has NEAT1_S and NEAT1_L isoforms, each having a 22741 and 3735 nucleotide length, respectively, with the same transcription start site but different termination points (Ghafouri-Fard and Taheri, 2019). NEAT1 is more concentrated in the nucleus and found in the cytoplasm (van Heesch et al., 2014). Overexpression of lncRNA NEAT1 has been associated with lower survival in several cancer types, such as breast cancer (Shin et al., 2019), glioma (He et al., 2016), ovarian cancer (Chen et al., 2016b), gastric cancer (Fu et al., 2016), bladder cancer (XianGuo et al., 2016). lncRNA NEAT1 have a various role in the stimulation of tumor cells and progression by regulating growth, migration, invasion, metastasis, epithelial-mesenchymal transition, stem cell-like phenotype, chemical

resistance, and radiotherapy resistance, which demonstrates the potential of lncRNA NEAT1 as a diagnostic biomarker and a new therapeutic target (Dong et al., 2018). lncRNA NEAT1 expression is increased in human gastric cancer cells compared to normal gastric cells. Deletion of lncRNA NEAT1 induces the expression of miR-506 and inhibits STAT3. On the other hand, overexpression of lncRNA NEAT1 induces STAT3 expression by suppressing miR-506 expression (Tan et al., 2019). So, miR-506 can directly target STAT3 in GC cells, and lncRNA NEAT1, by sponging miR-506, can regulate the STAT3 pathway indirectly. Therefore, inhibition of lncRNA NEAT1 significantly reduced cell viability, migration and invasion of GC cells *in vitro* (Tan et al., 2019). Moreover, lncRNA NEAT1 serves as a ceRNA of miR-485 in HCC and regulates STAT3 by inhibiting miR-485. Since, lncRNA NEAT1/miR-485/STAT3 axis is involved in migration, invasion, and promotion of viability, it can be used as a biological marker for the diagnosis or therapy of HCC (Zhang et al., 2018b).

LncRNA H19

LncRNA H19 with 2.3 kb length, located on chromosome 11:1995129-2001710 and identified in bladder carcinoma with an oncogenic role for the first time. Nevertheless, there is a controversy about the tumor-suppressing or oncogenic action of lncRNA H19. lncRNA H19, with multiple binding sites of miRNAs, acts as a competitive endogenous RNA (ceRNA) (Alipoor et al., 2020). In esophageal cancer (EC) tissue, the expression level of lncRNA H19 has significantly increased compared to normal tissue. Deleting lncRNA H19 in EC cell lines suppresses cell proliferation, migration, and invasion but increases apoptosis. On the other hand, overexpression of lncRNA H19 in EC cell lines can significantly decrease miRNA let-7c and increase STAT3, EZH2, and β-catenin (Chen et al., 2019a). In lung cancer cells, overexpression of lncRNA H19 increases STAT3 expression via sponging miR-17 (Liu et al., 2019). By sponging miR93-5p, LncRNA H19 can increase STAT3 expression, proliferation, migration and invasion in breast cancer cells (Li et al., 2019a). lncRNA H19 has high diagnostic sensitivity and specificity in breast cancer. On the other hand, anticancer drugs targeting H19 for safer and more effective breast cancer treatment will be introduced soon (Wang et al., 2020a).

LncRNA DANCR

Differentiation Antagonizing Non-Protein Coding RNA (DANCR), which was first discovered as an epidermal cell differentiation inhibitor, is located on chr4:52712257-52723623 (Zhang et al., 2019c). lncRNA DANCR is an oncogene with various biological processes, including stem cell differentiation and cell proliferation involved in developing different types of tumors (Kretz et al., 2012; Lu et al., 2018; Yuan et al., 2016a). There is a potential relationship between the high expression of lncRNA DANCR and the progression of bladder cancer (BCa). lncRNA DANCR expression is strongly related to pathological staging, grade, and status of LN (lymph node) metastases and enhances metastatic tumor and lymph node growth in bladder cancer via activation of the IL-11-mediated JAK-STAT3 signaling pathway. Silencing lncRNA DANCR dramatically increases cell population in the G0/G1 phase while decreasing cell population in the S phase; in contrast, overexpression of lncRNA DANCR increases cell proliferation and metastasis. So, novel targeted therapies for preventing metastasis in BCa patients with overexpressed DANCR might be used as an anti-IL-11 antibody and STAT3 blocker (Chen et al., 2019b). In Nasopharyngeal carcinoma (NPC), lncRNA DANCR is overexpressed and significantly associated with STAT3 signaling pathway activation. IL-6 dramatically increases lncRNA DANCR expression in both cytoplasm and nucleus. DANCR, by interacting with STAT3, reinforces IL-6 stimulation-induced STAT3 phosphorylation. Hence. There is a positive feedback loop between STAT3 phosphorylation and lncRNA DANCR transcription. Moreover, IL-6-stimulated lncRNA DANCR indirectly binds to the JAK1 via STAT3. Overall, the interaction of lncRNA DANCR with STAT3 through reinforcement of binding JAK1 to STAT3 amplifies IL-6/JAK1/STAT3 signaling for enhancing NPC progression, which recommended a potential target for a new strategy to develop NPC therapies (Zhang et al., 2019c).

Tumor Suppressor LncRNAs Regulate the STAT3 Signaling Pathway

LncRNA TSLNC8

The lncRNA TSLNC8 is located on chr8:29667485-29748124. TSLNC8, also known as LINC00589 (Chen and Yu, 2018). lncRNA TSLNC8 plays as a tumor suppressor in some types of cancer through various processes, including suppression of cell proliferation and facilitation of apoptosis and inactivation of the IL-6/STAT3 signaling pathway. For instance, deletion of lncRNA TSLNC8 is significantly associated with malignancy of hepatocellular carcinoma (HCC). lncRNA TSLNC8 inhibits STAT3 phosphorylation and

transcriptional activity in HCC cells. TSLNC8 has a recognition site at the 748-758nt for the DNA-binding domain of STAT3. It resulted in the reduction of Y705 phosphorylation and an increase of S727 phosphorylation, contributing to the suppressive effects of lncRNA TSLNC8. TSLNC8 controls proliferation, invasion, and metastasis in HCC cells via inactivating the IL-6/STAT3 signaling pathway. lncRNA TSLNC8 may be considered a potential therapeutic target for treatment (Zhang et al., 2018a). In addition, lncRNA TSLNC8 acts as a tumor suppressor in the lung cancer-causing inhibition of HIF-1 protein, along with down-regulation of IL-6 expression and its downstream genes and STAT3 phosphorylation. TSLNC8 can suppress cell proliferation, migration, and invasion and increase apoptosis in lung cancer cells via the IL-6/STAT3/HIF-1a signaling pathways (Fan et al., 2019).

LncRNA TPTEP1

The transmembrane phosphatase with tensin homolog pseudogene 1 (TPTEP1) is a lncRNA located at chromosomal position 22:16601887-16698742 as a tumor suppressor (Source: GeneCards). lncRNA TPTEP1 has three different variants and is silenced through DNA methylation in various cancers, including kidney, liver, lung, and stomach cancers. So, lncRNA TPTEP1 is expressed when DNA demethylation and deacetylase histone inhibition occurs (Liang et al., 2010). In HCC, lncRNA TPTEP1 directly binds to STAT3 and exerts its suppressive activity by inhibiting STAT3 phosphorylation, homodimerization, and nuclear translocation. Overall, TPTEP1 inhibits the progression of hepatocellular carcinoma cells via the IL-6/STAT3 signaling pathway (Ding et al., 2019).

LncRNA SLC2A1-AS1

LncRNA SLC2A1-AS1 is located on chr1:42958277-43196506 in the human genome and is known as a tumor suppressor. lncRNA SLC2A1-AS1 decrease in HCC cell lines and tissues and associated with non-recurrent survival. lncRNA SLC2A1-AS1 can regulate the abnormal expression of GLUT1 RNA, which has potential effects on the glycolysis process in cancers. Overexpression of lncRNA SLC2A1-AS1 in the nucleus inhibited proliferation and metastasis in HCC by preventing GLUT1 transcription. A suggested molecular mechanism is SLC2A1-AS1 interacts with STAT3 to inhibit FOXM1 activation via STAT3. So, lncRNA SLC2A1-AS1 does not directly regulate the transcriptional activity of GLUT1 but inhibits FOXM1 transcription, which has previously been identified as an important transcriptional activator of the GLUT1. Inactivation of the FOXM1/GLUT1 axis was shown in HCC cells. Therefore, SLC2A1-AS1 inhibits glycolysis and progression of HCC via the STAT3/FOXM1/GLUT1 axis. These mechanisms highlight the vital role of SLC2A1-AS1 in glycolysis and HCC progression (Shang et al., 2020).

LncRNA BRE-AS1

BRE-AS1 is located on chromosome 2:27889455-27891114 as a non-coding single-stranded RNA with 1659 bp in length. Low expression of lncRNA BRE-AS1 has been shown in bladder cancer tissues. Overexpression of lncRNA BRE-AS1 via suppressing STAT3 phosphorylation reduces cell proliferation and cell cycle transition but increases cell apoptosis *in vitro* and *in vivo* (Zhang et al., 2020).

LncRNA DILC

For the first time, lncRNA DILC was recognized in liver cancer stem cells (LCSCs) by microarray and real-time PCR. The name DILC came from downregulated liver cancer stem cells. lncRNA DILC is located on chromosome 13q34 (chr13:114239003-114295788) with a 2394 bp length (Wang et al., 2016). lncRNA DILC is related to the prognosis in various human diseases, including cancers such as LCSC (Wang et al., 2016) and colorectal (Gu et al., 2018; Li et al., 2019b), bladder (Ma et al., 2019). The IL-6/STAT3 signaling pathway plays an important role in the proliferation of LCSCs; IL-6 transcription is preferentially regulated by NF-κB, which is overexpression on various stem cells. NF-κB is usually activated by extracellular inflammatory cytokines such as TNF-α and IL-1β (Hinohara et al., 2012; Kagoya et al., 2014). Overexpression of lncRNA DILC blocks induction of IL-6 transcription via TNF-α and IL-1β (NF-κB). In contrast, decreased lncRNA DILC expression increases IL-6 transcription by TNF-α and IL-1β. LncRNA DILC suppresses the proliferation of LCSCs by inhibiting the IL-6/STAT3 signaling pathway. This evidence suggests that lncRNA DILC regulates LCSCs by controlling the crosstalk between TNF-α/NF-κB and IL-6/STAT3 signaling pathways (Wang et al., 2016). Moreover, overexpression of lncRNA DILC in bladder tissue and cell line can suppress bladder cancer by inhibiting IL-6 and STAT3 (Ma et al., 2019). Also, lncRNA DILC is colorectal cancer (CRC) suppressor that can inhibit CRC cell growth and metastasis. DILC suppresses CRC cell progression by inhibiting IL-6 and STAT3 signaling

pathways and is a biomarker for the prognosis of CRC patients (Gu et al., 2018; Li et al., 2019b).

LncRNA GAS5

The lncRNA growth arrest-specific transcript 5 (GAS5), with 630 nucleotides in length, is located on chromosome 1:173851284-173869006. Decreased expression of lncRNA GAS5 has been observed in many human malignancies. Increasing its expression induces apoptosis and inhibits proliferation and metastasis in tumors (Yang et al., 2020). In cervical cancer, lncRNA GAS5 has been shown to affect STAT3 signaling. Phosphorylated-STAT3 is a transcription factor for lncRNA GAS5, which binds to the GAS5 promoter. There are two STAT3 binding sites in the miR-21 enhancer sequence, and in this way, STAT3 directly regulates miR-21 expression (Yao et al., 2019). Several studies have examined the oncogenic role of miR-21 in types of cancers, including colon cancer (Dehghan et al., 2019) and breast cancer (Esmatabadi et al., 2017; Savari et al., 2020). *PDCD4* is the target gene of miR-21 that increases sensitivity to cisplatin. Hence, it is possible that STAT3 regulation and the GAS5/miR-21/PDCD4 axis could have therapeutic potential for cisplatin-based chemotherapy and antitumor functions in cervical cancer (Fang et al., 2020).

Conclusion

The STAT3 signaling pathway is one of the most important pathways involved in types of cancer. LncRNAs can interact with signaling molecules and activate the STAT3 signaling pathway, affecting tumor onset and progression. The interaction between lncRNA, STAT3 signaling, and related molecules leads to the coordination of different cellular processes responsible for cell cycle determination, differentiation, migration, metastasis and drug resistance. Examining the mechanism of lncRNAs in STAT3 signaling helps us identify useful biomarkers for diagnosis and establish effective therapeutic targets for cancer treatment.

Acknowledgments

None.

Conflicts of Interest

The authors have no conflicts of interest to declare.

References

Alipoor B., Parvar S. N., Sabati Z., Ghaedi H. and Ghasemi H. (2020) An updated review of the H19 lncRNA in human cancer: molecular mechanism and diagnostic and therapeutic importance. Mol Biol Rep 47:6357-6374.

Banerjee K. and Resat H. (2016) Constitutive activation of STAT3 in breast cancer cells: A review. Int J Cancer 138:2570-2578.

Carpenter R. L. and Lo H. W. (2014) STAT3 Target Genes Relevant to Human Cancers. Cancers (Basel) 6:897-925.

Chan J. J. and Tay Y. (2018) Noncoding RNA:RNA Regulatory Networks in Cancer. Int J Mol Sci 19.

Chang S. M. and Hu W. W. (2018) Long non-coding RNA MALAT1 promotes oral squamous cell carcinoma development via microRNA-125b/STAT3 axis. Journal of Cellular Physiology 233:3384-3396.

Cheetham S. W., Gruhl F., Mattick J. S. and Dinger M. E. (2013) Long noncoding RNAs and the genetics of cancer. Br J Cancer 108:2419-2425.

Chen D. and Yu X. (2018) Long noncoding RNA TSLNC8 suppresses cell proliferation and metastasis and promotes cell apoptosis in human glioma. Molecular medicine reports 18:5536-5544.

Chen L., Feng P., Zhu X., He S., Duan J. and Zhou D. (2016a) Long non-coding RNA Malat1 promotes neurite outgrowth through activation of ERK/MAPK signalling pathway in N2a cells. Journal of cellular and molecular medicine 20:2102-2110.

Chen M. J., Deng J., Chen C., Hu W., Yuan Y. C. and Xia Z. K. (2019a) LncRNA H19 promotes epithelial mesenchymal transition and metastasis of esophageal cancer via STAT3/EZH2 axis. Int J Biochem Cell Biol 113:27-36.

Chen Z., Chen X., Xie R., Huang M., Dong W., Han J., Zhang J., Zhou Q., Li H., Huang J. and Lin T. (2019b) DANCR Promotes Metastasis and Proliferation in Bladder Cancer Cells by Enhancing IL-11-STAT3 Signaling and CCND1 Expression. Mol Ther 27:326-341.

Chen Z. J., Zhang Z., Xie B. B. and Zhang H. Y. (2016b) Clinical significance of up-regulated lncRNA NEAT1 in prognosis of ovarian cancer. Eur Rev Med Pharmacol Sci 20:3373-3377.

Das R., Gregory P. A., Fernandes R. C., Denis I., Wang Q., Townley S. L., Zhao S. G., Hanson A. R.,

Pickering M. A. and Armstrong H. K. (2017) MicroRNA-194 promotes prostate cancer metastasis by inhibiting SOCS2. Cancer research 77:1021-1034.

de Araujo E. D., Keseru G. M., Gunning P. T. and Moriggl R. (2020) Targeting STAT3 and STAT5 in Cancer. Cancers (Basel) 12.

Dehghan F., Boozarpour S., Torabizadeh Z. and Alijanpour S. (2019) miR-21: a promising biomarker for the early detection of colon cancer. OncoTargets and therapy 12:5601.

Díaz-Beyá M., Brunet S., Nomdedéu J., Pratcorona M., Cordeiro A., Gallardo D., Escoda L., Tormo M., Heras I. and Ribera J. M. (2015) The lincRNA HOTAIRM1, located in the HOXA genomic region, is expressed in acute myeloid leukemia, impacts prognosis in patients in the intermediate-risk cytogenetic category, and is associated with a distinctive microRNA signature. Oncotarget 6:31613.

Ding H., Liu J., Zou R., Cheng P. and Su Y. (2019) Long non-coding RNA TPTEP1 inhibits hepatocellular carcinoma progression by suppressing STAT3 phosphorylation. J Exp Clin Cancer Res 38:189.

Do H. and Kim W. (2018) Roles of Oncogenic Long Non-coding RNAs in Cancer Development. Genomics Inform 16:e18.

Dong P., Xiong Y., Yue J., Hanley S. J., Kobayashi N., Todo Y. and Watari H. (2018) Long non-coding RNA NEAT1: a novel target for diagnosis and therapy in human tumors. Frontiers in genetics 9:471.

Dong Y., Liang G., Yuan B., Yang C., Gao R. and Zhou X. (2015) MALAT1 promotes the proliferation and metastasis of osteosarcoma cells by activating the PI3K/Akt pathway. Tumor Biology 36:1477-1486.

Esmatabadi M. J. D., Farhangi B., Montazeri M., Monfared H., Sistani R. N. and Sadeghizadeh M. (2017) Up-regulation of miR-21 decreases chemotherapeutic effect of dendrosomal curcumin in breast cancer cells. Iranian journal of basic medical sciences 20:350.

Fan H., Li J., Wang J. and Hu Z. (2019) Long Non-Coding RNAs (lncRNAs) Tumor-Suppressive Role of lncRNA on Chromosome 8p12 (TSLNC8) Inhibits Tumor Metastasis and Promotes Apoptosis by Regulating Interleukin 6 (IL-6)/Signal Transducer and Activator of Transcription 3 (STAT3)/Hypoxia-Inducible Factor 1-alpha (HIF-1alpha) Signaling Pathway in Non-Small Cell Lung Cancer. Med Sci Monit 25:7624-7633.

Fang X., Zhong G., Wang Y., Lin Z., Lin R. and Yao T. (2020) Low GAS5 expression may predict poor survival and cisplatin resistance in cervical cancer. Cell death & disease 11:1-17.

Fu J. W., Kong Y. and Sun X. (2016) Long noncoding RNA NEAT1 is an unfavorable prognostic factor and regulates migration and invasion in gastric cancer. J Cancer Res Clin Oncol 142:1571-1579.

Ghafouri-Fard S. and Taheri M. (2019) Nuclear enriched abundant transcript 1 (NEAT1): a long non-coding RNA with diverse functions in tumorigenesis. Biomedicine & Pharmacotherapy 111:51-59.

Gu L. Q., Xing X. L., Cai H., Si A. F., Hu X. R., Ma Q. Y., Zheng M. L., Wang R. Y., Li H. Y. and Zhang X. P. (2018) Long non-coding RNA DILC suppresses cell proliferation and metastasis in colorectal cancer. Gene 666:18-26.

Guzel E., Okyay T. M., Yalcinkaya B., Karacaoglu S., Gocmen M. and Akcakuyu M. H. (2020) Tumor suppressor and oncogenic role of long non-coding RNAs in cancer. North Clin Istanb 7:81-86.

Hamilton M. J., Young M., Jang K., Sauer S., Neang V. E., King A. T., Girke T. and Martinez E. (2020) HOTAIRM1 lncRNA is downregulated in clear cell renal cell carcinoma and inhibits the hypoxia pathway. Cancer letters 472:50-58.

He C., Jiang B., Ma J. and Li Q. (2016) Aberrant NEAT1 expression is associated with clinical outcome in high grade glioma patients. APMIS 124:169-174.

Hinohara K., Kobayashi S., Kanauchi H., Shimizu S., Nishioka K., Tsuji E., Tada K., Umezawa K., Mori M., Ogawa T., Inoue J., Tojo A. and Gotoh N. (2012) ErbB receptor tyrosine kinase/NF-kappaB signaling controls mammosphere formation in human breast cancer. Proc Natl Acad Sci U S A 109:6584-6589.

Hu C., Liu S., Han M., Wang Y. and Xu C. (2018) RETRACTED: Knockdown of lncRNA XIST inhibits retinoblastoma progression by modulating the miR-124/STAT3 axis. Biomed Pharmacother 107:547-554.

Johnson D. E., O'Keefe R. A. and Grandis J. R. (2018) Targeting the IL-6/JAK/STAT3 signalling axis in cancer. Nat Rev Clin Oncol 15:234-248.

Kagoya Y., Yoshimi A., Kataoka K., Nakagawa M.,

Kumano K., Arai S., Kobayashi H., Saito T., Iwakura Y. and Kurokawa M. (2014) Positive feedback between NF-kappaB and TNF-alpha promotes leukemia-initiating cell capacity. J Clin Invest 124:528-542.

Kim C. Y., Oh J. H., Lee J.-Y. and Kim M. H. (2020) The LncRNA HOTAIRM1 promotes tamoxifen resistance by mediating HOXA1 expression in ER+ Breast Cancer Cells. Journal of Cancer 11:3416.

Kretz M., Webster D. E., Flockhart R. J., Lee C. S., Zehnder A., Lopez-Pajares V., Qu K., Zheng G. X., Chow J. and Kim G. E. (2012) Suppression of progenitor differentiation requires the long noncoding RNA ANCR. Genes & development 26:338-343.

Kulczynska K. and Siatecka M. (2016) A regulatory function of long non-coding RNAs in red blood cell development. Acta Biochim Pol 63:675-680.

Lashkarboloki M., Boozarpour S., Jorjani E., Sabouri H. and Fahimi M. (2020) Association Study of miR-124-a-3 Gene rs34059726 Polymorphism with Prostate Cancer in Gonbad Kavous.

Li J. P., Xiang Y., Fan L. J., Yao A., Li H. and Liao X. H. (2019a) Long noncoding RNA H19 competitively binds miR-93-5p to regulate STAT3 expression in breast cancer. J Cell Biochem 120:3137-3148.

Li Q., Dong C., Cui J., Wang Y. and Hong X. (2018a) Over-expressed lncRNA HOTAIRM1 promotes tumor growth and invasion through up-regulating HOXA1 and sequestering G9a/EZH2/Dnmts away from the HOXA1 gene in glioblastoma multiforme. Journal of Experimental & Clinical Cancer Research 37:1-15.

Li Q. G., Xu X. Q., Zhou D. Y., Jia Z. B., Yu B. F., Xu F. G. and Zhang L. (2019b) Long non-coding RNA DILC as a potentially useful biomarker for the diagnosis and prognosis of colorectal cancer. Eur Rev Med Pharmacol Sci 23:3320-3325.

Li S., Mei Z., Hu H. B. and Zhang X. (2018b) The lncRNA MALAT1 contributes to non-small cell lung cancer development via modulating miR-124/STAT3 axis. Journal of Cellular Physiology 233:6679-6688.

Li X., Pang L., Yang Z., Liu J., Li W. and Wang D. (2019c) LncRNA HOTAIRM1/HOXA1 axis promotes cell proliferation, migration and invasion in endometrial cancer. OncoTargets and therapy 12:10997.

Li X., Yu M. and Yang C. (2020) YY1-mediated overexpression of long noncoding RNA MCM3AP-AS1 accelerates angiogenesis and progression in lung cancer by targeting miR-340-5p/KPNA4 axis. J Cell Biochem 121:2258-2267.

Li Z., Qin X., Bian W., Li Y., Shan B., Yao Z. and Li S. (2019d) Exosomal lncRNA ZFAS1 regulates esophageal squamous cell carcinoma cell proliferation, invasion, migration and apoptosis via microRNA-124/STAT3 axis. J Exp Clin Cancer Res 38:477.

Liang J., Liang L., Ouyang K., Li Z. and Yi X. (2017) MALAT 1 induces tongue cancer cells' EMT and inhibits apoptosis through Wnt/β-catenin signaling pathway. Journal of oral pathology & medicine 46:98-105.

Liang M., Jia J., Chen L., Wei B., Guan Q., Ding Z., Yu J., Pang R. and He G. (2019) LncRNA MCM3AP-AS1 promotes proliferation and invasion through regulating miR-211-5p/SPARC axis in papillary thyroid cancer. Endocrine 65:318-326.

Liang Q., Ding J., Xu R., Xu Z. and Zheng S. (2010) The novel human endogenous retrovirus-related gene, psiTPTE22-HERV, is silenced by DNA methylation in cancers. Int J Cancer 127:1833-1843.

Lin W. H., Chang Y. W., Hong M. X., Hsu T. C., Lee K. C., Lin C. and Lee J. L. (2021) STAT3 phosphorylation at Ser727 and Tyr705 differentially regulates the EMT-MET switch and cancer metastasis. Oncogene 40:791-805.

Liu L., Liu L. and Lu S. (2019) lncRNA H19 promotes viability and epithelial-mesenchymal transition of lung adenocarcinoma cells by targeting miR-29b-3p and modifying STAT3. Int J Oncol 54:929-941.

Liu S., Yan G., Zhang J. and Yu L. (2018) Knockdown of long noncoding RNA (lncRNA) metastasis-associated lung adenocarcinoma transcript 1 (MALAT1) inhibits proliferation, migration, and invasion and promotes apoptosis by targeting miR-124 in retinoblastoma. Oncology research 26:581.

50- Lu Q. c., Rui Z. h., Guo Z. l., Xie W., Shan S. and Ren T. (2018) Lnc RNA-DANCR contributes to lung adenocarcinoma progression by sponging miR-496 to modulate mTOR expression. Journal of cellular and molecular medicine 22:1527-1537.

Luo Z. and Cao P. (2019) Long noncoding RNA PVT1 promotes hepatoblastoma cell proliferation through activating STAT3. Cancer Manag Res 11:8517-8527.

Ma Q. Y., Li S. Y., Li X. Z., Zhou T. F., Zhao Y. F., Liu F. L., Yu X. N., Lin J., Chen F. Y., Cao J., Xi H. J. and Li H. Y. (2019) Long non-coding RNA DILC suppresses bladder cancer cells progression. Gene 710:193-201.

Mohankumar K. M., Perry J. K., Kannan N., Kohno K., Gluckman P. D., Emerald B. S. and Lobie P. E. (2008) Transcriptional activation of signal transducer and activator of transcription (STAT) 3 and STAT5B partially mediate homeobox A1-stimulated oncogenic transformation of the immortalized human mammary epithelial cell. Endocrinology 149:2219-2229.

Onagoruwa O. T., Pal G., Ochu C. and Ogunwobi O. O. (2020) Oncogenic Role of PVT1 and Therapeutic Implications. Front Oncol 10:17.

Poursheikhani A., Abbaszadegan M. R., Nokhandani N. and Kerachian M. A. (2020) Integration analysis of long non-coding RNA (lncRNA) role in tumorigenesis of colon adenocarcinoma. BMC Med Genomics 13:108.

Prensner J. R. and Chinnaiyan A. M. (2011) The emergence of lncRNAs in cancer biology. Cancer Discov 1:391-407.

Qin J.-J., Yan L., Zhang J. and Zhang W.-D. (2019a) STAT3 as a potential therapeutic target in triple negative breast cancer: a systematic review. Journal of Experimental & Clinical Cancer Research 38:1-16.

Qin J. J., Yan L., Zhang J. and Zhang W. D. (2019b) STAT3 as a potential therapeutic target in triple negative breast cancer: a systematic review. J Exp Clin Cancer Res 38:195.

Reymond A., Camargo A. A., Deutsch S., Stevenson B. J., Parmigiani R. B., Ucla C., Bettoni F., Rossier C., Lyle R. and Guipponi M. (2002) Nineteen additional unpredicted transcripts from human chromosome 21. Genomics 79:824-832.

Saliani M., Mirzaiebadizi A., Javadmanesh A., Siavoshi A. and Ahmadian M. R. (2021) KRAS-related long noncoding RNAs in human cancers. Cancer Gene Ther.

Sana J., Faltejskova P., Svoboda M. and Slaby O. (2012) Novel classes of non-coding RNAs and cancer. J Transl Med 10:103.

Sánchez Y. and Huarte M. (2013) Long non-coding RNAs: challenges for diagnosis and therapies. Nucleic acid therapeutics 23:15-20.

Savari B., Boozarpour S., Tahmasebi-Birgani M., Sabouri H. and Hosseini S. M. (2020) Overexpression of microRNA-21 in the Serum of Breast Cancer Patients. MicroRNA 9:58-63.

Schroeder A., Herrmann A., Cherryholmes G., Kowolik C., Buettner R., Pal S., Yu H., Müller-Newen G. and Jove R. (2014) Loss of androgen receptor expression promotes a stem-like cell phenotype in prostate cancer through STAT3 signaling. Cancer research 74:1227-1237.

Segatto I., Baldassarre G. and Belletti B. (2018) STAT3 in breast cancer onset and progression: a matter of time and context. International journal of molecular sciences 19:2818.

Shang R., Wang M., Dai B., Du J., Wang J., Liu Z., Qu S., Yang X., Liu J., Xia C., Wang L., Wang D. and Li Y. (2020) Long noncoding RNA SLC2A1-AS1 regulates aerobic glycolysis and progression in hepatocellular carcinoma via inhibiting the STAT3/FOXM1/GLUT1 pathway. Mol Oncol 14:1381-1396.

Shi X., Sun M., Liu H., Yao Y. and Song Y. (2013) Long non-coding RNAs: a new frontier in the study of human diseases. Cancer Lett 339:159-166.

Shin V. Y., Chen J., Cheuk I. W., Siu M. T., Ho C. W., Wang X., Jin H. and Kwong A. (2019) Long non-coding RNA NEAT1 confers oncogenic role in triple-negative breast cancer through modulating chemoresistance and cancer stemness. Cell Death Dis 10:270.

Sun Y. and Ma L. (2019) New insights into long non-coding RNA MALAT1 in cancer and metastasis. Cancers 11:216.

Tan H. Y., Wang C., Liu G. and Zhou X. (2019) Long noncoding RNA NEAT1-modulated miR-506 regulates gastric cancer development through targeting STAT3. J Cell Biochem 120:4827-4836.

van Heesch S., van Iterson M., Jacobi J., Boymans S., Essers P. B., de Bruijn E., Hao W., MacInnes A. W., Cuppen E. and Simonis M. (2014) Extensive localization of long noncoding RNAs to the cytosol and mono-and polyribosomal complexes. Genome biology 15:1-12.

Wang J., Sun J. and Yang F. (2020a) The role of long non-coding RNA H19 in breast cancer. Oncol Lett 19:7-16.

Wang L., Zhang Y. and Xin X. (2020b) Long non-coding RNA MALAT1 aggravates human retinoblastoma by sponging miR-20b-5p to upregulate STAT3. Pathology-Research and Practice 216:152977.

Wang X., Sun W., Shen W., Xia M., Chen C., Xiang

D., Ning B., Cui X., Li H., Li X., Ding J. and Wang H. (2016) Long non-coding RNA DILC regulates liver cancer stem cells via IL-6/STAT3 axis. J Hepatol 64:1283-1294.

Wang Y., Yang L., Chen T., Liu X., Guo Y., Zhu Q., Tong X., Yang W., Xu Q., Huang D. and Tu K. (2019) A novel lncRNA MCM3AP-AS1 promotes the growth of hepatocellular carcinoma by targeting miR-194-5p/FOXA1 axis. Mol Cancer 18:28.

Xia H., Liu Y., Wang Z., Zhang W., Qi M., Qi B. and Jiang X. (2020) Long noncoding RNA HOTAIRM1 maintains tumorigenicity of glioblastoma stem-like cells through regulation of hox gene expression. Neurotherapeutics 17:754-764.

XianGuo C., ZongYao H., Jun Z., Song F., GuangYue L., LiGang Z., KaiPing Z., YangYang Z. and ChaoZhao L. (2016) Promoting progression and clinicopathological significance of NEAT1 over-expression in bladder cancer. Oncotarget 5.

Xie P., Li X., Chen R., Liu Y., Liu D., Liu W., Cui G. and Xu J. (2021) Upregulation of HOTAIRM1 increases migration and invasion by glioblastoma cells. Aging (Albany NY) 13:2348.

Yang C., Zheng J., Xue Y., Yu H., Liu X., Ma J., Liu L., Wang P., Li Z., Cai H. and Liu Y. (2017) The Effect of MCM3AP-AS1/miR-211/KLF5/AGGF1 Axis Regulating Glioblastoma Angiogenesis. Front Mol Neurosci 10:437.

Yang J., Chatterjee-Kishore M., Staugaitis S. M., Nguyen H., Schlessinger K., Levy D. E. and Stark G. R. (2005) Novel roles of unphosphorylated STAT3 in oncogenesis and transcriptional regulation. Cancer Res 65:939-947.

Yang X., Xie Z., Lei X. and Gan R. (2020) Long non-coding RNA GAS5 in human cancer. Oncology letters 20:2587-2594.

Yao T., Lu R., Zhang J., Fang X., Fan L., Huang C., Lin R. and Lin Z. (2019) Growth arrest-specific 5 attenuates cisplatin-induced apoptosis in cervical cancer by regulating STAT3 signaling via miR-21. Journal of Cellular Physiology 234:9605-9615.

Yu H., Xu Q., Liu F., Ye X., Wang J. and Meng X. (2015) Identification and validation of long noncoding RNA biomarkers in human non–small-cell lung carcinomas. Journal of thoracic oncology 10:645-654.

Yuan J., Ji H., Xiao F., Lin Z., Zhao X., Wang Z., Zhao J. and Lu J. (2017) MicroRNA-340 inhibits the proliferation and invasion of hepatocellular carcinoma cells by targeting JAK1. Biochem Biophys Res Commun 483:578-584.

Yuan S. x., Wang J., Yang F., Tao Q. f., Zhang J., Wang L. l., Yang Y., Liu H., Wang Z. g. and Xu Q. g. (2016a) Long noncoding RNA DANCR increases stemness features of hepatocellular carcinoma by derepression of CTNNB1. Hepatology 63:499-511.

Yuan Y., Cai T., Xia X., Zhang R., Chiba P. and Cai Y. (2016b) Nanoparticle delivery of anticancer drugs overcomes multidrug resistance in breast cancer. Drug Deliv 23:3350-3357.

Zhang H., Luo C. and Zhang G. (2019a) LncRNA MCM3AP-AS1 Regulates Epidermal Growth Factor Receptor and Autophagy to Promote Hepatocellular Carcinoma Metastasis by Interacting with miR-455. DNA Cell Biol 38:857-864.

Zhang J., Li Z., Liu L., Wang Q., Li S., Chen D., Hu Z., Yu T., Ding J., Li J., Yao M., Huang S., Zhao Y. and He X. (2018a) Long noncoding RNA TSLNC8 is a tumor suppressor that inactivates the interleukin-6/STAT3 signaling pathway. Hepatology 67:171-187.

Zhang L., Liu B., Deng Q. and Li J. (2020) LncRNA BRE-AS1 acts as a tumor suppressor factor in bladde r cancer via mediating STAT3. Eur. Rev. Med. Pharmacol. Sci 24:5320-5328.

Zhang T., Hu H., Yan G., Wu T., Liu S., Chen W., Ning Y. and Lu Z. (2019b) Long Non-Coding RNA and Breast Cancer. Technol Cancer Res Treat 18:1533033819843889.

Zhang X., Lian Z., Padden C., Gerstein M. B., Rozowsky J., Snyder M., Gingeras T. R., Kapranov P., Weissman S. M. and Newburger P. E. (2009) A myelopoiesis-associated regulatory intergenic noncoding RNA transcript within the human HOXA cluster. Blood 113:2526-2534.

Zhang X., Yang J., Bian Z., Shi D. and Cao Z. (2019c) Long noncoding RNA DANCR promotes nasopharyngeal carcinoma progression by interacting with STAT3, enhancing IL-6/JAK1/STAT3 signaling. Biomed Pharmacother 113:108713.

Zhang X. N., Zhou J. and Lu X. J. (2018b) The long noncoding RNA NEAT1 contributes to hepatocellular carcinoma development by sponging miR-485 and enhancing the expression of the STAT3. J Cell Physiol 233:6733-6741.

Zhao G., Su Z., Song D., Mao Y. and Mao X. (2016) The long noncoding RNA MALAT 1 regulates the lipopolysaccharide-induced inflammatory response through its interaction with NF-κB. FEBS letters

590:2884-2895.

Zhao J., Wu J., Qin Y., Zhang W., Huang G. and Qin L. (2020) LncRNA PVT1 induces aggressive vasculogenic mimicry formation through activating the STAT3/Slug axis and epithelial-to-mesenchymal transition in gastric cancer. Cell Oncol (Dordr) 43:863-876.

Zhong Z., Wen Z. and Darnell J. E., Jr. (1994) Stat3: a STAT family member activated by tyrosine phosphorylation in response to epidermal growth factor and interleukin-6. Science 264:95-98.

Zhu Y., Shi L., Zhou C., Wang Z., Yu T., Zhou J. and Yang Y. (2019) Long non-coding RNA MCM3AP-AS1 inhibits cell viability and promotes apoptosis in ovarian cancer cells by targeting miR-28-5p. Int. J. Clin. Exp. Med 12:2939-2951.

Journal of Cell and Molecular Research (2022) 13 (2), 151-155 DOI: 10.22067/JCMR.2022.75921.1033

Research Article

Appropriate Reference Gene for the Gene Expression Analysis in U87 Glioblastoma Cell Line

Mina Lashkarboloki[1], Amin Jahanbakhshi[2], Seyed Javad Mowla[1], Bahram M. Soltani[1*]

[1] *Department of Genetics, Faculty of Biological Sciences, Tarbiat Modares University, Tehran, Iran*
[2] *Stem Cell and Regenerative Medicine Research Centre, Iran University of Medical Sciences (IUMS), Tehran, Iran*

Received 19 March 2022 Accepted 22 April 2022

Abstract

Cancer is one of the most challenging diseases in the world. It is widely accepted that knowing the molecular aspects of diseases, including cancers, helps to develop methods for their therapy and diagnosis. Long non-coding RNAs (lncRANs) are a novel category of regulatory genes known to be involved in cancer incidence. The expression of these genes is said to be suitable of using in prognosis, diagnosis, targeted therapy, etc. The RT-qPCR method that is widely used for analyzing the gene expression requires the application of appropriate reference genes as the internal control. The expression status of a proper housekeeping reference gene is not supposed to change under experimental circumstances. This study aimed to find a suitable reference gene in the U87 cells after overexpression of a gene of interest. To this aim, the expression status of four common reference genes (*ACTB*, *β2M*, *GAPDH*, and *HPRT1*) was examined in the transfected U87 cells. The U87 cells were transfected with a vector overexpressing YWHAE-lncRNA and an empty vector (mock). After total RNA extraction and cDNA synthesis, RT-qPCR was applied using the aforementioned internal control genes. Data were analyzed, and their graphs were plotted in GraphPad Prism 8.2 software. *B2M* showed the most change; accordingly, *GAPDH and HPRT1* expression levels were changed about 5 and 4 times, respectively. Of the candidate genes, only the *ACTB* gene had a consistent expression level in two different modes of transfection, and therefore, it is suggested as an appropriate reference gene for the study of gene expression in the transfected U87 cell line. It is remained to be tested if *β2M*, *GAPDH*, and *HPRT1* common internal controls are specifically affected by YWHAE-lncRNA overexpression or other lncRNAs may affect their expression as well.

***Keywords*:** Long non-coding RNA, Housekeeping genes, Real-Time PCR

Introduction

Glioblastoma multiform (GBM) is the most common type of malignant tumor in the central nervous system with low survival (Louis et al., 2007). Despite many scientific and medical advances in recent decades, there is still insufficient information on molecular pathogenesis and complex intracellular biological interactions that regulate the progression of the disease (Appin et al., 2014). Therefore, it is necessary to identify critical molecular pathways involved in the development and progression of glioma to provide new biomarkers for improvement or treatment. Genetic changes initiate various biological processes, leading to many disorders and tumor formation. Many types of research have focused on the molecular differences between tumors and normal tissues (Futreal et al., 2004; Hornberg et al., 2006). Analysis of gene expression using real-time quantitative PCR is a standard approach to identifying genes with different expression levels (Akiyama et al., 2014). RT-qPCR is a highly sensitive, specific, and reproducible method for obtaining validated results (Taylor et al., 2019). Different factors such as the amount of raw material, RNA quality and quantity, cDNA synthesis efficiency can affect gene expression results in the qPCR method (Nolan et al., 2006). Therefore, real-time data must be normalized with a suitable internal control gene (Wong and Medrano, 2005; Soltanian et al., 2021). Appropriate reference genes should

*Corresponding author's e-mail address: *soltanib@modares.ac.ir*

have a consistent expression level in all samples, regardless of tissue type, growth stage, disease status, and pharmacological or biological treatments. For example, *GAPDH* is reported as a suitable reference gene in nano-curcumin-treated colorectal cancer-originated cells (Choori et al., 2018). It is widely accepted that the expression of no gene is stable in all the cellular conditions and therefore the proper candidate reference genes must be validated under each experimental condition (Dundas and Ling, 2012). Several studies introduced a set of reference genes for the study of glioma tissue, but their results were not consistent. Therefore, they suggested that in each study, a suitable reference gene should be approved (Kreth et al., 2010). In the present study, we investigated the suitability of four reference genes, *ACTB, β2M, GAPDH,* and *HPRT1*, for qPCR analysis in the human glioma U87 cell line.

Materials and Methods

Cell Culture and Transfection

The U87 cell line (ATCC: HTB-14) was provided from the the Pasteur Institute Cell Bank (Tehran, Iran) and cultured in HG-DMEM (Gibco) medium. The culture medium was supplemented with 10% fetal bovine serum (FBS) (Gibco), 100 U/mL of penicillin, 100 µg/mL of streptomycin (Sigma-Aldrich). Incubation was performed at 37 °C with 5% CO_2, and the cells with 85 to 90% confluency were equally seeded in a 24-well plate. The cells were transfected with the plasmid containing YWHAE long non-coding RNA gene, after 24 hours. Transfection was performed using TurboFect reagent (Thermo Fisher Scientific, USA) according to manufacturer protocol. PCDNA3.1 plasmid without fragment was transfected as the mock control. By using a reverse fluorescent microscope (Nikon eclipse Te2000-s, Japan) GFP signal was observed 24 hrs after transfection to measure the rate.

RNA Extraction and cDNA Synthesis

Total RNA was extracted using RiboEx (Krishgen Biosystems, India), according to the manufacturer's protocol. Agarose gel electrophoresis and NanoDrop TM 1000 (Thermo Scientific, USA) were used to measure the quality and quantity of the extracted RNA, respectively. Depending on the quantity and quality of RNAs, different volumes but the same concentration of RNAs (1µg/µL) were used for cDNA synthesis. The cDNA synthesis was performed using ExcelRT™ Reverse Transcriptase (SMOBIO, Taiwan) and Oligo $(dT)_{18}$ and Random hexamers as primers.

RT-qPCR

In order to evaluate the quality of cDNA synthesis, PCR reactions were performed in 28 cycles using *β2M, GAPDH, HPRT1,* and *ACTB* gene primers for each group of synthesized cDNAs. Then, qPCR was carried out using 50 ng concentration of cDNA, SYBR Premix Kit (TaKaRa, Japan), and specific primers for considered reference genes in StepOne™ Real-Time PCR.

Statistical Analysis

The qPCR data were analyzed according to the $2^{-\Delta\Delta Ct}$ methods. Then, GraphPad Prism software (version 6) was used to perform the t-test and draw the charts. Results with a *p*-value less than 0.05 were considered statistically significant.

Results and Discussion

Transfection

The transfection rate of U87 cells was 50% which was examined and confirmed by pEGFP-C1 as a control vector (Figure 1A). Also, to ensure the transfection efficiency, the expression of the lnc-YWHAE gene was investigated by qPCR in overexpression construct and empty construct (mock). The results showed that lnc-YWHAE expression in overexpressed cells increased 43,000 times (CT 32 reduced to CT 16) compared to the control cells (Figure 1B).

RNA Extraction and cDNA Synthesis

Assessment of the quality of RNA by agarose gel electrophoresis and NanoDrop showed that RNA extraction from each sample has an acceptable quality, but these RNAs are not of the same quantity (Figure S1). However, RNA with a final concentration of 1 µg was used for cDNA synthesis. After cDNAs were synthesized, to confirm their quality, PCR reactions were performed in 28 cycles for the *β2M* gene. The agarose gel electrophoresis showed that the cDNAs had been synthesized with good quality, but their quantity is different from each other (Figure S2).

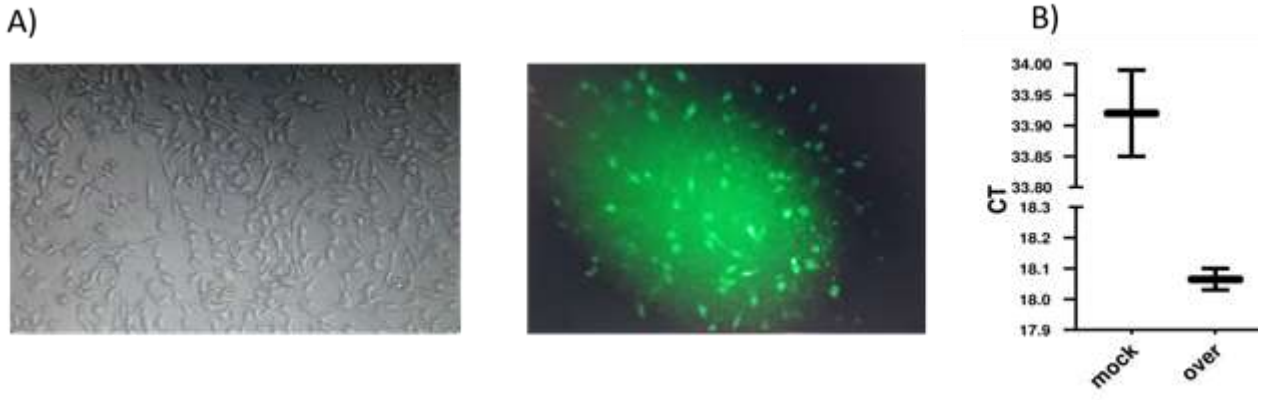

Figure 1. The transfection rate. A) Fluorescent microscope image shows that the structure transfers to the u87 cell line. B) To confirm transfection, lnc-YWHAE expression was measured in controlled and over-expressed cells. Lnc-YWHAE CT was reduced to 18 in overexpressed samples.

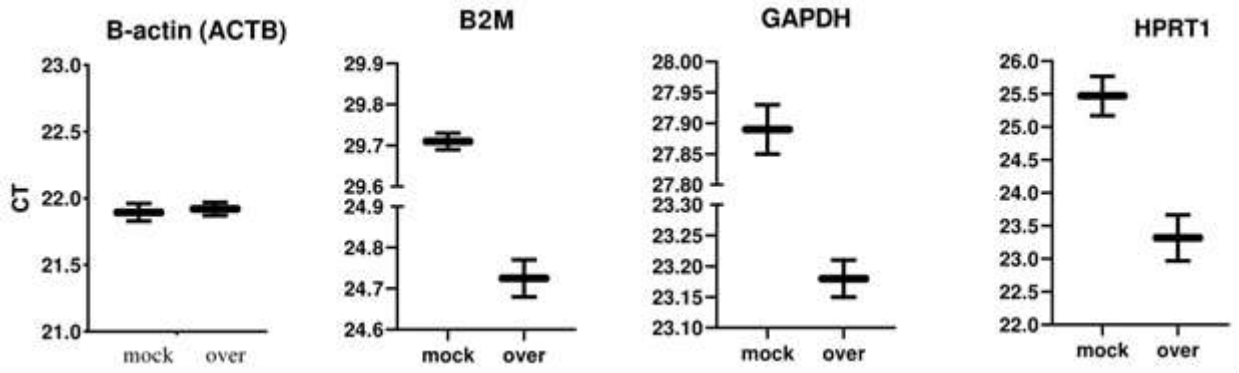

Figure 2. Ct of the reference gene. RT-qPCR results show that the expression of all housekeeping genes except *B-actin* (*ACTB*) changes after overexpression of the target gene.

RT-qPCR

One ng of cDNA synthesized was used in the qPCR reaction for four typical reference genes *ACTB*, *β2M*, *GAPDH*, and *HPRT1*. Specific amplification was confirmed by a single peak melting curve diagram (Figure S3). Results showed that Ct values of *β2M*, *GAPDH*, and *HPRT1* genes in sample 1 (U87 transfected with YWHAE long non-coding RNA) and sample 2 (U87 transfected with empty construct) alter, but for *ACTB*, the threshold cycles are very close and almost identical (Figure 2). Moreover, statistical analysis revealed that if the *ACTB* gene is used as a reference gene, *β2M*, *GAPDH*, and *HPRT1* gene expression will alter after the transfection.

Recent studies on glioma introduced various genes as internal controls. The *GAPDH*, *RPL13A*, *CYC1*, and *ACTB* were used as the housekeeping genes in real-time PCR data analysis on glioma tissue samples (Grube et al., 2015; Röhn et al., 2018). One of the effective factors in gene expression is the process of tumor progression. The *GAPDH*, *IPO8*, *RPL13A*, *SDHA*, and *TBP* genes were suitable internal controls that did not change in different grades (II-IV) of human astrocytoma, and *TBP* and *IPO8* were the most stable of them (Kreth et al., 2010; Gabriele et al., 2018). But in another study, the *RPL13A* and *TBP* were stable in all of the samples and ideal for analyzing gene expression in glioblastoma, whereas other genes, such as *GAPDH* and *β2M*, were not suitable due to their changes in RNA expression levels (Aithal and Rajeswari, 2015). Some studies reported that *HPART* is a suitable reference gene, while others do not (Kreth et al., 2010; Valente et al., 2014; Aithal and Rajeswari, 2015). However, the effects of *in vitro* manipulation of cells, such as drug treatment or gene transfection, on the conditions are very variable.

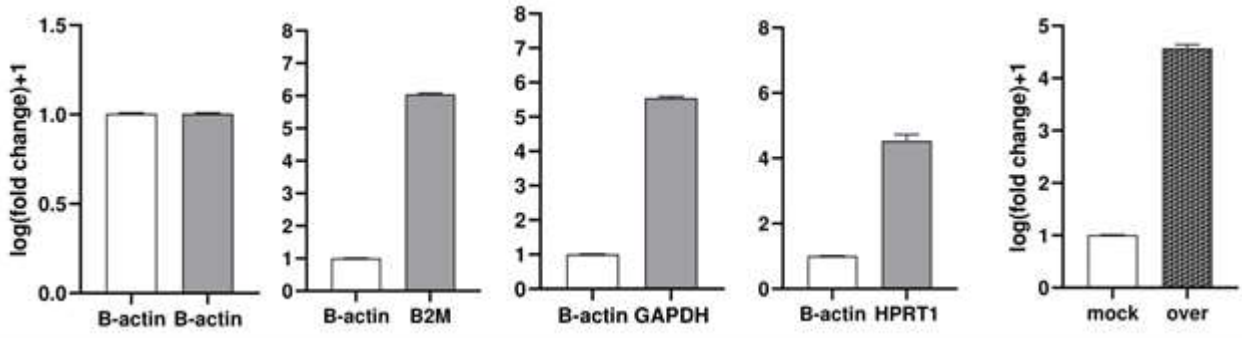

Figure 3. Lnc-YWHAE normalization after selection of the suitable internal control. A) Altered expression of all the internal control genes except β-actin after normalization with internal control of β-actin. B) Measurement of lnc-YWHAE expression level after normalization with β-actin shows the overexpression of this gene after transfection.

After transfection of long non-coding RNAs, such as *HOTAIRM1*, *SUMO1P3*, and *AC003092.1*, to the U87 cell line and their overexpression, *GAPDH* has been used for normalization (Xu et al., 2018; Lin et al., 2020; Lou et al., 2020). But in the other study, *ACTB* was selected as a reference in the U87 cell line (Li et al., 2020; Nie et al., 2015; Jung et al., 2013). Also, in other glioma cell lines, U251 and A172, *GAPDH* has been used (Liu et al., 2017; Wang et al., 2019). So, in different studies, the appropriate reference genes are different.

Our study showed that in order to select reliable reference genes, the specific conditions of each experiment must be considered. In order to achieve this possibility, first ,the quantity and quality of RNAs were determined, and then, cDNA synthesis was performed. After examining the quality of synthesized cDNAs by 28-cycle RT-PCR, the real-time-qPCR reaction was performed. Among the four genes, only *ACTB* expression did not change and was constant under different cell transfection conditions, while other genes, *β2M*, *GAPDH*, and *HPRT1*, were not stable (Figure 3A). Overexpression of YWHAE long non-coding RNA affects most internal control gene expression. Many studies have used a typical housekeeping gene as a reference gene, but our results show that in addition to using experiences, specific conditions of the test, type of samples, cell lines, and gene structure transfected into cells must be considered. For this purpose, before starting the analysis of RT-qPCR data, a suitable reference gene should be selected.

In this study, we first showed that YWHAE long non-coding RNA has the ability to change the expression of some internal control genes and then introduced *ACTB* as an appropriate reference gene for the normalization of genes expression and measured lnc-YWHAE expression level that increased $\log_2$ fold change 5 compared to the control sample (figure 3B).

Conflict of Interest

The authors have no conflicts of interest to declare.

Acknowledge

The authors would like to thank 4402 lab members in TMU for their support.

References

Aithal M. and Rajeswari N. (2015) Validation of housekeeping genes for gene expression analysis in glioblastoma using quantitative real-time polymerase chain reaction. Brain Tumor Research and Treatment 3(1): 24–29.

Akiyama Y., Komiyama M., Miyata H., Yagoto M., Ashizawa T., Iizuka A., et al. (2014) Novel cancer-testis antigen expression on glioma cell lines derived from high-grade glioma patients. Oncology Reports 31:1683– 1690.

Appin C. L. and Brat D. J. (2014) Molecular genetics of gliomas. Cancer Journal 20:66–72.

Choori M., Boozarpour S., Moradi A. and Jorjani E. (2018) Investigation of POU5F1 and NANOG gene expression in colon cancer cell line (Caco-2) treated by dendrosomal nano-curcumin. Cellular and Molecular Researches (Iranian Journal of Biology) 31(3):292-301.

Dundas J. and Ling M. (2012) Reference genes for measuring mRNA expression. Theory in Biosciences 131:215–223.

Futreal P. A., Coin L., Marshall M., Down T., Hubbard T., Wooster R., et al. (2004) A census of human cancer genes. Nature Reviews Cancer 4(3):177–83.

Gabriele R., Arend K., Boris K., Pantelis S., Roland G. and Marco T. (2018) ACTB and SDHA are suitable endogenous reference genes for gene expression studies in human astrocytomas using quantitative RT-PCR. Technology in Cancer Research & Treatment 17:1-6.

Grube S., Go¨ttig T., Freitag D., Ewald C., Kalff R. and Walter J. (2015) Selection of suitable reference genes for expression analysis in human glioma using RT-Qpcr. Journal of Neurooncology 123:35–42.

Hornberg J. J., Bruggeman F. J., Westerhoff H. V. and Lankelma J. (2006) Cancer: a systems biology disease. Biosystems 83(2–3):81–90.

Jung T. Y., Choi Y. D., Kim Y. H., Lee J. J., Kim H. S., Kim J. S., et al. (2013) Immunological characterization of glioblastoma cells for immunotherapy. Anticancer Research 33(6):2525-33.

Kreth S., Heyn J., Grau S., Kretzschmar H. A., Egensperger R. and Kreth F. W. (2010) Identification of valid endogenous control genes for determining gene expression in human glioma. Neuro-Oncology 12:570–579.

Li Y., Liu Y., Zhu H., Chen X., Tian M., Wei Y., et al. (2020) N-acetylglucosaminyltransferase I promotes glioma cell proliferation and migration through increasing the stability of the glucose transporter GLUT1. FEBS Letters 594(2):358-366.

Lin Y. H., Guo L., Yan F., Dou Z. Q., Yu Q. and Chen G. (2020) Long non-coding RNA HOTAIRM1 promotes proliferation and inhibits apoptosis of glioma cells by regulating the miR-873-5p/ZEB2 axis. Chinese Medical Journal 133(2):174-182.

Liu T., Zhang T., Zhou F., Wang J., Zhai X., Mu N., et al. (2017) Identification of genes and pathways potentially related to PHF20 by gene expression profile analysis of glioblastoma U87 cell line. Cancer Cell International 17: 87.

Lou J. Y., Luo J., Yang S. C., Ding G. F., Liao W., Zhou R. X., et al. (2020) Long non-coding RNA SUMO1P3 promotes glioma progression via the Wnt/β-catenin pathway. European Review for Medical and Pharmacological Sciences 24(18):9571-9580.

Louis D. N., Ohgaki H., Wiestler O. D., Cavenee W. K., Burger P. C., Jouvet A., et al. (2007) The 2007 WHO classification of tumors of the central nervous system. Acta Neuropathology 114:97–109.

Nie Q. M., Lin Y. Y., Yang X., Shen L., Guo L. M., Que S. L., et al. (2015) IDH1R^{132}H decreases the proliferation of U87 glioma cells through upregulation of microRNA-128a. Molecular Medicine Reports 12(5):6695-701.

Nolan T., Hands R. E. and Bustin S. A. (2006) Quantification of mRNA using real-time RT-PCR. Nature Protocols 1:1559–1582.

Röhn G., Koch A., Krischek B., Stavrinou P., Goldbrunner R. and Timmer M. (2018) ACTB and SDHA are suitable endogenous reference genes for gene expression studies in human astrocytomas using quantitative RT-PCR. Technology in Cancer Research & Treatment 1:17.

Soltanian S., and Sheikhbahaei M. (2021) Identification of suitable housekeeping genes for quantitative gene expression analysis during retinoic acid-induced differentiation of embryonal carcinoma NCCIT cells. Journal of Cell and Molecular Research 12(2):104-10.

Taylor S. C., Nadeau K., Abbasi M., Lachance C., Nguyen M. and Fenrich J. (2019) The ultimate qPCR experiment: producing publication quality, reproducible data the first time. Trends in Biotechnology 37(7):761-774.

Valente V., Teixeira S. A., Neder L., Okamoto O. K., Oba-Shinjo S. M., Marie S. K., et al. (2014) Selection of suitable housekeeping genes for expression analysis in glioblastoma using quantitative RT-PCR. Annals of Neurosciences 21(2):62-3.

Wang Z., Chen N., Yang J., Wang Q. and Li A. (2019) Microarray gene profiling analysis of glioblastoma cell line U87 reveals suppression of the FANCD2/Fanconi anemia pathway by the combination of Y15 and temozolomide. Archives of Medical Science 15(4):1035-1046.

Wong M. L. and Medrano J. F. (2005) Real-time PCR for mRNA quantitation. Biotechniques 39:75–85.

Xu N., Liu B., Lian C., Doycheva D. M., Fu Z., Liu Y., et al. (2018) Long noncoding RNA AC003092.1 promotes temozolomide chemosensitivity through miR-195/TFPI-2 signaling modulation in glioblastoma. Cell Death 19(12):1139.

Supplementary Information:

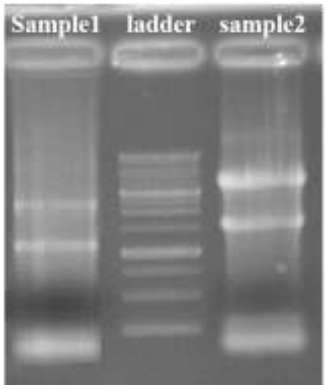

Figure S1. RNA samples on agarose gel, show differences in RNA quality.

Figure S2. PCR products on agarose, show the difference in the quality of the cDNAs.

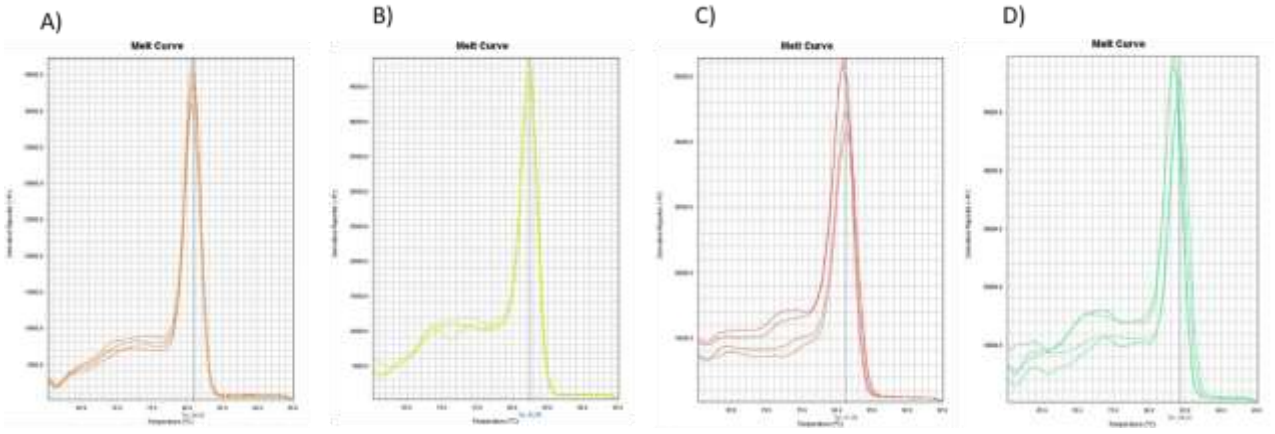

Figure S3. Melting curve diagram. Melting curve for internal control genes. A) B2M; B) GAPDH; C) ACTB; D) HPRT1.

Scientific Reviewers

MANUSCRIPT PREPARATION

Manuscripts should be prepared in accordance with the uniform requirements for Manuscript's Submission to **"Journal of Cell and Molecular Research".**

Language: Papers should be in English (either British or American spelling). The past tense should be used throughout the results description, and the present tense in referring to previously established and generally accepted results. Authors who are unsure of correct English usage should have their manuscript checked by somebody who is proficient in the language; manuscripts that are deficient in this respect may be returned to the author for revision before scientific review.

Typing: Manuscripts must be typewritten in a font size of at least 12 points, double-spaced (including References, Tables and Figure legends) with wide margins (2.5 cm from all sides) on one side of the paper. The beginning of each new paragraph must be clearly indicated by indentation. All pages should be numbered consecutively at the bottom starting with the title page.

Length: The length of research articles should be restricted to ten printed pages. Short communication should not exceed five pages of manuscript, including references, figures and tables. Letters should be 400-500 words having 7-10 references, one figure or table if necessary. Commentaries and news should also be 800-1000 words having 7-10 references and one figure or table if necessary.

Types of Manuscript: JCMR is accepting original research paper, short communication reports, invited reviews, letters to editor, biographies of scientific reviewers, commentaries and news.

Statement of Human and Animal Rights: Author's should declare regulatory statement regarding the experiments using animals, human cells/tissues that all in vivo experiments have been performed according to the guidelines (explained by WHO, international animal rights federations or your respective institute) to use animals in their research work.

Conflict of Interest Statement: Authors or corresponding author should declare statement of conflict of interest at the last of manuscript.

Manuscript Evaluation Time: All submitted manuscripts will be evaluated and reviewed according to following evaluation schedule.
Pre-Editorial Evaluation: All submitted manuscripts, right after their submission to JCMR will be evaluation by Editors for being according to the journal scope and format. This evaluation can take 2-7 days of submission.
Reviewer's Evaluation: Selected manuscripts after pre-editorial evaluation will be sent to minimum two blind reviewers assigned by Editor-in-Chief. This process may take 21-27 days.
Post Editorial Evaluation: After receiving reviewer's comments, editors evaluate the manuscripts considering the comments and decide their first decision. This process takes 3-5 days and then authors are informed regarding the editorial decision.

GENERAL ARRANGEMENT OF PAPERS

Title: In the first page, papers should be headed by a concise and informative title. The title should be followed by the authors' full first names, middle initials and last names and by names and addresses of

laboratories where the work was carried out. Identify the affiliations of all authors and their institutions, departments or organization by use of Arabic numbers (1, 2, 3, etc.).

Footnotes: The name and full postal address, telephone, fax and E-mail number of corresponding author should be provided in a footnote.

Abbreviations: The Journal publishes a standard abbreviation list at the front of every issue. These standard abbreviations do not need to be spelled out within paper. However, non-standard and undefined abbreviations used five or more times should be listed in the footnote. Abbreviations should be defined where first mentioned in the text. Do not use abbreviations in the title or in the Abstract. However, they can be used in Figures and Tables with explanation in the Figure legend or in a footnote to the Table.

Abstract: In second page, abstract should follow the title (no authors' name) in structured format of not more than 250 words and must be able to stand independently and should state the Background, Methods, Results and Conclusion. Write the abstract in third person. References should not be cited and abbreviations should be avoided.

Keywords: A list of three to five keywords for indexing should be included at bottom of the abstract. Introduction should contain a description of the problem under investigation and a brief survey of the existing literature on the subject.

Materials and Methods: Sufficient details must be provided to allow the work to be repeated. Correct chemical names should be given and strains of organisms should be specified. Suppliers of materials need only be mentioned if this may affect the results. Use System International (SI) units and symbols.

Results: This section should describe concisely the rationale of the investigation and its outcomes. Data should not be repeated in both a Table and a Figure. Tables and Figures should be selected to illustrate specific points. Do not tabulate or illustrate points that can be adequately and concisely described in the text.

Discussion: This should not simply recapitulate the Results. It should relate results to previous work and interpret them. Combined Results and Discussion sections are encouraged when appropriate.

Acknowledgments: This optional part should include a statement thanking those who assisted substantially with work relevant to the study. Grant support should be included in this section.

References: References should be numbered and written in alphabetical order. Only published, "in press" papers, and books may be cited in the reference list (see the examples below). References to work "in press" must be accompanied by a copy of acceptance letter from the journal. References should not be given to personal communications, unpublished data, manuscripts in preparation, letters, company publications, patents pending, and URLs for websites. Abstracts of papers presented at meetings are not permissible. These references should appear as parenthetical expressions in the text, e.g. (unpublished data). Few example of referencing patterns are given as follows:

Examples of text references:

Cite a source written by one author: (Kikuchi, 2014)

Cite a source written by two authors: (Rinn and Chang, 2012)

Cite a source written by three or more authors: (Mead et al., 2015)

Examples of end references:

Bongso A., Lee E. H. and Brenner S. (2005) Stem cells from bench to bedside. World Scientific Publishing Co. Singapore, 38-55 pp.

Kikuchi K. (2014) Advances in understanding the mechanism of zebrafish heart regeneration. Stem Cell Research 13:542-555.

Irfan-Maqsood M. (2013) Stem Cells of Epidermis: A Critical Introduction. Journal of Cell and Molecular Research 5:1, 1-2.

(6 authors:) Mead B., Berry M., Logan A., Scott R. A., Leadbeater W. and Scheven B. A. (2015) Stem cell treatment of degenerative eye disease. Stem Cell Research 14:243-257.

Rinn J. L. and Chang H. Y. (2012) Genome regulation by long noncoding RNAs. Annual Review of Biochemistry 81:1-9.

Note: When citing more than six authors, give the name of the first six authors and abbreviate the others to et al.

(more than 6 authors:) Vaculik C., Schuster C., Bauer W., Iram N., Pfisterer K., Kramer G., et al. (2012) Human dermis harbors distinct mesenchymal stromal cell subsets. Journal of Investigative Dermatology 132:563-574.

Tables and Figures: Tables and Figures should be numbered (1, 2, 3, etc.) as they appear in the text. Figures should preferably be the size intended for publication. Tables and Figures should be carefully marked. Legends should be typed single-spaced separately from the figures. Photographs must be originals of high quality. Photocopies are not acceptable. Those wishing to submit color photographs should contact the Editor regarding charges.

JCMR Open Access Policy: Journal of Cell and Molecular Research follows the terms outlined by the Creative Common's Attribution-Only license (CC-BY) to be the standard terms for Open Access. Creative Commons License.

Note: All manuscripts submitted to JCMR are tracked by using "iThenticate" or "small tools" for possible plagiarism before acceptance to JCMR.

Table of Contents

Journal of Cell and Molecular Research

Volume 13, Number 2, (Winter) 2022